University of Sheffield

The Role of Leaf Structure in Rice Photosynthetic Performance

By:

Saranrat Wang

A thesis submitted in partial fulfilment of the requirements for the degree of Doctor of Philosophy The University of Sheffield

School of Biosciences

December 2022

Abstract

Improving the efficiency of photosynthesis has been identified as a major aim in plant biology. As a result of previous work, a model of photosynthesis has been developed which incorporates the cellular anatomy of the leaf. Analysis of the model suggests that leaf cell size plays an important role in photosynthesis, particularly in how photosynthesis responds to an increase in CO_2 level.

In Chapter 2, I aim to test the hypothesis that the change of cell size and shape alters photosynthesis by analysing a series of transgenic plants with altered leaf cell size. I have identified a series of transgenic rice plants (*JL* lines) and characterised their leaf anatomy, revealing variation in mesophyll and bundle sheath cell size. Interestingly, two lines; *JL4* and *JL27* showed a difference of lobing formation in mesophyll cells. Chlorophyll fluorescence-gas exchange analysis indicated that these line were impaired in photosynthesis.

In addition, the results from *JL* lines presented an unexpected relationship between mesophyll cell shape (cell lobing) and stomatal characteristics. This observation was followed up using transgenic rice plants with altered stomatal density. *osEPF1_oe* lines (low stomata number) and *osEPFL9_oe* lines (high stomata numbers) were used to analyse a potential link between stomatal function and the internal cell structure of the leaf. This work suggested that the degree of mesophyll lobing in transgenic rice is altered in response to the environment, which supports a link between the degree of cell lobing and gas diffusion through stomata.

In Chapter 3, I investigated the process of mesophyll cell lobing in rice, with the aim of identifying the earliest stage of mesophyll cell lobing, using rice leaf 6th of IR64 as a model for this study. The results indicated that the initiation of cell lobing occurred at an early stage of leaf development (P3/P4 stage) of leaf length less than 20 mm. This is similar to the stage when stomata differentiation occurs. This work supports the idea that MC lobing is regulated by stomatal function during leaf development.

In Chapter 4, I used another approach to test the idea from Chapter 2 that mesophyll cell lobing in rice is modulated by stomatal function. Using a series of rice plants gene-edited in the HT1 gene (which are expected to show abnormal stomatal opening to CO_2 level, I investigated whether abnormal stomatal function in this mutant also led to altered mesophyll cell structure. The results indicated that mesophyll cell shape (lobiness) is responsive to stomata conductance and that increased gas flux could lead to increased cell lobing. Unexpectedly, the ht1 mutations also influenced leaf structure in many aspects complicating the interpretation of these data.

In conclusion, my research indicates that altered gas flux via stomata can affect mesophyll cell shape in rice. This adds to previous work in the area indicating that stomatal conductance can influence cell size and separation in the leaf mesophyll. However, there is still a lack of evidence to explain the mechanism by which stomatal function could lead to these changes, which needs to be explored in future research. For future work, it might also be interesting to further study mesophyll cell size and shape using 3D imaging techniques and compare it with the 2D imaging data reported in my work . In addition it would be interesting to explore the metabolic changes occurring as the mesophyll cells change size and shape, exploring the link to photosynthetic function and gas exchange. Overall, my results support a co-ordinated link between mesophyll cell size and shape, stomatal function and photosynthesis.

Collaborations and Publication

The majority of the work in this thesis is my own work. However, there are some data samples and analytical tools I obtained from my colleagues.

For data

The previous data of *JL* lines in Fig 2.5 was taken from Dr. Jennifer Sloan (University of Sheffield)

For seed samples

All the samples I used to investigated were from Dr. Naomi Cox (*JL* rice seeds), Emily Harrison (*osEPF1_oe* and *osEPFL9_oe*), Dr. Jennifer Sloan (IR64) and ShanShan Wang (HT1 mutant rice seeds). All University of Sheffield.

For analytical tools

R codes and the script for data analysis was improved and created by Dr. Jennifer Sloan (University of Sheffield).

Acknowledgements

List of Abbreviations

A	CO_2 Assimilation Rate
ATP	Adenosine triphosphate
BSC/ BS cell	Bundle Sheath Cell
C_i	Intercellular CO_2 concentration
CO_2	Carbon dioxide
EtOH	Ethanol
G_s	Stomatal conductance
G_{smax}	Maximum stomatal conductance
G3P	1,3-Bisphosphoglycerate
HT1	High temperature 1 gene
IV	The interveinal distance between two minor veins
J_{max}	The maximum rate of electron transport
JL	The transgenic rice plants from Jane Langdale' laboratory
LM	Light microscope
L_{gc}	The guard cell length (µm)
L_p	The pore length (µm)
MC	Mesophyll Cell
NADPH	Nicotinamide adenine dinucleotide phosphate hydrogen
OsEPF1_oe	The overexpress gene of EPIDERMAL PATTERNING FACTOR 1
OsEPFL9_oe	The overexpress gene of EPIDERMAL PATTERNING FACTOR-like 9
P (X), X= 1, 2, 3, …	Plastochron stage 1, 2…
PSI	Photosystem 1
PSII	Photosystem 2
RuBP	Ribulose 1,5-bisphosphate
SAM	Shoot apical meristem

SEM	Scanning electron microscope
SD	Stomata density
TS	Transverse direction
TPU	Triose phosphate utilization
V_{cmax}	The maximum rate of carboxylation
W_{gc}	The guard cell width (μm)
W_s	The stomatal width (μm)
Z	Longitudinal direction

Contents

Chapter 1 The role of leaf structure in rice photosynthetic performance

Chapter 2 Mesophyll and bundle sheath cell size influence photosynthetic performance in rice

Chapter 3 The development of lobing in rice mesophyll cells

Chapter 4 How do stomata influence mesophyll cell lobing?

Chapter 5 Final discussion

List of figures

List of Tables

Chapter 1

The role of leaf structure in rice photosynthetic performance

1.1 Introduction

Rice belongs to the family; *Poaceae*, Genus; *Oryza*. There are two main cultivated species which are widely grown; *Oryza sativa* or Asian rice and *Oryza glaberrima* or African rice. Despite China's recognition as one of the domestication centers for Asian cultivated rice and the acknowledgment of common wild rice (*O. rufipogon*) as the progenitor of *O. sativa*, there is still ongoing debate regarding the number of domestication events and the precise geographic origin of Asian cultivated rice in China (Wei et al.,2012). *O. glaberrima* originated from *Oryza barthii* as an ancestor rice in African countries, which was grown by people who lived at the bend of the Niger River more than 2000 years ago (Linares 2002; Hu et al.,2018).

Rice is an important staple crop for consumption worldwide, especially Asian countries such as China, India, Bangladish and Thailand (Watson et al. 2014). More than 3 billion of people consume rice as the main dietary energy supply and it is also used as part of social rituals and festivals which people celebrate after harvesting (Chaudhari et al. 2018; Ahuja et al. 2006). Over the last 50 years, a large number of people have been confronted with food shortage because of a lack of farmland, environmental change, and a rapid rise in global population (Zhu et al. 2010). Among these problems, changes in environmental factors, i.e. temperature, light intensity and atmospheric CO_2 level have had a high impact on crop productivity and security (Ainsworth et al.2005; Lee et al. 2009). In the mid-20th century, the green revolution led to increase agricultural production, which was achieved by using new technologies to develop plants in terms of fertilization and disease prevention. By doing this, the crops that were developed as a result of these efforts demonstrated significant progress when compared to traditionally grown crops in the area. These advancements included higher yields, consistent productivity, adaptability to different regions, shorter growing seasons, enhanced resistance to diseases and pests, ability to withstand challenging environmental conditions like drought and flooding, and improved quality of the harvested grains. (Wu and Butz, 2004; Zhu et al., 2010; Long et al., 2015).

As the global population increases and more people migrate to cities, the land that was sufficient to produce enough rice for 27 individuals in 2010 will now need to sustain 43 people by 2050. To address this challenge, rice yields will have to be raised by 50% compared to the levels in 2010 (Hibberd et al.,2008). There is thus a need to find new ways to increase rice yield. One potential solution is improving the efficiency of photosynthesis by introducing 'C4' traits into rice, which could enhance photosynthetic efficiency by 50%, while also improving nitrogen and water use efficiency (Mitchell and Sheehy, 2006;Kajala et. al.,2011). After decades of study, the mechanism by which plants respond to increased CO_2 levels remains unclear but it involves changes in both physical (structural) and biological (biochemical) features. At the physical level, plants respond to high CO_2 levels by changing leaf structure. This process generally occurs during the early stages of leaf development when cells in the leaf are still going through cell division and differentiation. As a consequence, the structure of the leaf is changed permanently and cannot easily be reversed by later changes in environmental factors. With respect to the influence that these structural changes have on photosynthesis, the concept of mesophyll (g_m) and stomatal (g_s) conductance are key. These conductances are used to measure the ease of CO_2 diffusion from the atmosphere through stomata to the site of CO_2 fixation into the Calvin-Benson cycle via Rubisco. At the biochemical level, high CO_2 levels lead to changes in metabolic pathways. Thus, the level and activity of many enzymes involved in carbon assimilation are changed rapidly (minutes to days). These metabolic change can occur in all parts of the leaf at most stages of development, and are generally reversible (Terashima et al. 2011; Tholen et al. 2011; Tholen et al. 2012).

However, understanding the relative roles of leaf structure and biochemistry in photosynthesis remains a major challenge in plant biology, and trying to predict how the various potential combinations would influence plant performance under various future CO_2 environments is a daunting enterprise. In the following sections I provide an overview of rice plant morphology and anatomy, with a focus on leaf structure and development. I then provide a summary of the metabolic processes of photosynthesis, and a review of our understanding of how leaf structure influences photosynthetic performance. This then leads onto an outline of the main aims and objectives of this thesis.

1.2.   General background

1.2.1. The morphology of rice plant

O. sativa is a diploid species with 24 chromosomes and the genetic code AA (Kwon et al.2006). It is a type of rice plant that grows as an annual grass. The plant has round, hollow, jointed stems, with flat and sessile leaf blades. It produces a terminal panicle, and under favourable conditions, it can grow for more than one year. Like other species in the Oryza tribe, rice thrives in aquatic environments (Chang and Bardenas, 1965). The description here primarily applies to the widely found *O. sativa* L., but it can also be used to describe the African cultivated species *O. glaberrima* (2n = 24). O. *glaberrima* differs from O. sativa mainly in the absence of secondary branches on the main branches of the panicle, as well as minor variations in hairiness on the lemmas and the length of the ligule (Futakuchi et al.,2012). O. *glaberrima* is strictly an annual plant. The morphology of rice can be divided into its seedling appearance, vegetative structures (roots, stems, and leaves), and reproductive phases (panicles and spikelet) as shown in Fig.1.1.
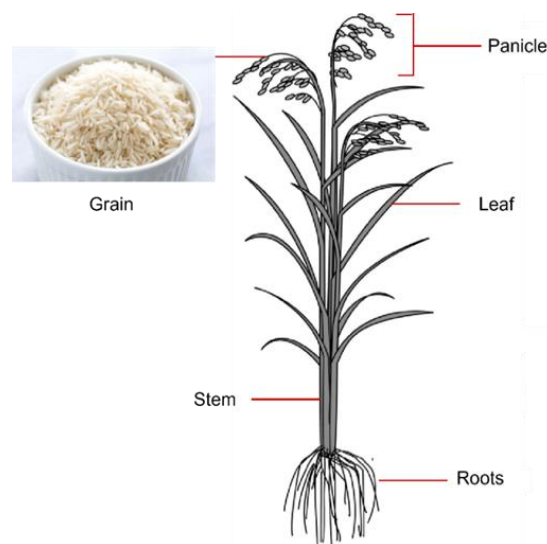
Figure.1.1 The structure of rice can be categorized into three parts: the appearance of the seedling, the vegetative components (roots, stems, and leaves), and the reproductive stages (panicles and spikelets). This picture is modified from Itoh et al. (2005).

1.2.1.1. Seedling Structure

Rice grains without dormancy start germinating immediately after ripening, while dormant varieties require a rest period before germination (Sohn et al.,2021). Freshly harvested samples of dormant varieties need specific treatments like heat or mechanical dehulling to break dormancy (Gilbert, 2000). In well-drained soil, the coleorhiza, which surrounds the radicle, emerges first during germination. In submerged conditions, the coleoptile appears before the coleorhiza. Shortly after, the primary seminal root (radicle) breaks through the coleorhiza, followed by two or more secondary seminal roots that develop lateral roots. With time, the seminal roots are replaced by adventitious roots. The coleoptile, which encloses the young leaves, emerges as a tapered cylinder and can have colours ranging from colourless to pale green, green, or pale purple to purple. The mesocotyl refers to the elongated axis between the coleoptile and the point where the root and culm join. As the mesocotyl elongates, the coleoptile is lifted above the ground. Eventually, the coleoptile breaks open at the tip, enabling the emergence of the initial "primary" leaf. This primary leaf is green, cylindrical in shape, and does not have a blade. The following leaf then undergoes differentiation, forming a sheath, blade, ligule, and auricles (Chang and Bardenas,1965).

1.2.1.2. Vegetative Organs

The rice plant can vary in size, with certain dwarf mutants reaching heights of only 3 to 4 meters and floating varieties surpassing 7 meters. However, most commercially cultivated rice varieties typically fall within the range of 1 to 2 meters in height. The plant's vegetative components consist of roots, culms (stems), and leaves. A tiller is a branch of the plant that carries the culm, leaves, roots, and occasionally a panicle (Chang and Bardenas,1965).

1.2.1.3. Roots

The roots of rice plants grow and develop below the surface of the soil. The root architecture consists of embryonic and post-embryonic roots with five different types, namely, the radicle, the embryonic and postembryonic crown roots (nodal roots), the

small lateral roots and the large lateral roots (Hochholdinger and Feix, 1998). The radicle is the part of embryonic plant which develops to be a primary root. The embryonic crown roots come out of coleoptilar node after 3 days of germination (Hochholdinger and Feix, 1998; Martin and Harris, 1976).

Each thin branching root is generated from the stem and gather to form fibrous, containing root hairs and rootlets which anchor, support a plant to the ground. The root acts to absorb water and nutrients from the soil, and store food. At the germination stage, the embryonic roots grow out of the seed. These roots are replaced by the secondary adventitious roots produced from nodes of the young culm which spread out under the ground to strengthen a rice plant (Steffens and Rasmussen 2016; Rebouillat et al., 2009).

1.2.1.4. Stem

The stem is composed of two major parts; nodes and internodes. In general, a node act as a joint to connect between two regions of the culm and contains a bud which can develop into branches, leaves or flowers of the plant (Crang et al., 2018). In rice, each node contains one bud and young leaf that can grow into a tiller or shoot. The mature internodes are hollow and grooved with a smooth surface. The length of internodes varies. The lower internodes are shorter and thicker than the upper ones, acting in deep water to support the stem above water (Boon et al. 2008). The main function of the stem is to deliver water and nutrient from the soil to the plant and bring the air from atmosphere to the root (McElrone et al., 2013).

1.2.1.5. Leaves

Leaves are the essential organ containing the enzymatic and light harvesting machinery required for photosynthesis, fixing carbon into the sugar which is vital for plant growth and development (Bielczynski et al., 2017; Oguchi et al., 2003). Rice leaves grow alternatively on the stem. Each node contains the leaf blade, the expanded part of a leaf which links to a node by the leaf sheath to enclose a culm. There are pairs of small ear-like auricles at the base of the blade leaf, and ligules located above auricles at every internode, which are characteristic for rice (Conklin et

al., 2019). The uppermost leaf below the panicle consists of a shortened flag leaf which is thought to be an important energy source via photosynthesis during the reproductive process (Rahman et al. 2013). Leave structure and development will be covered in more detail later in this chapter.

1.2.1.6. Floral organs

The reproductive parts of the rice plant are altered shoots. The topmost shoot of the rice plant forms a determinate inflorescence known as the panicle. The panicle is composed of individual units called spikelets, which are attached to the branched panicle by pedicels. Each spikelet consists of two sterile lemmas, the rachilla, and the floret. The floret of the rice plant is made up of the lemma, palea, and the enclosed flower. Within the flower, there are six stamens and a pistil, and the perianth is represented by the lodicules (Chang and Bardenas,1965).

1.2.1.7. Panicle

The panicle of the rice plant grows on the uppermost part of the stem, which is sometimes mistakenly referred to as a peduncle. The length of the panicle and the portion of the stem that extends beyond the flag leaf sheath determine the extent to which the panicle protrudes. Different rice varieties have varying levels of panicle extension. The solid node between the upper stem section and the panicle axis is called the panicle base. It typically doesn't have a leaf or dormant bud, but it can generate the first 1-4 branches of the panicle. The panicle base often appears as a ring of fine hairs and serves as a point of reference for measuring the length of the stem and panicle. The region surrounding the panicle base is known as the neck (Chang and Bardenas,1965).

The main axis of the rice panicle, known as the panicle axis or rachis, extends from the panicle base to the top. It is hollow except at the nodes where the panicle branches emerge. The swellings at these junctions are called panicle pulvini. The panicle follows a branching pattern called racemose, where each node on the main axis produces primary branches, and each primary branch carries secondary branches (Li et

al.,2021). The secondary branches hold the spikelets on stalks. The primary branches can be arranged singly or in pairs. Each rice varieties has different lengths, shapes, and angles of the primary branches, as well as the weight and density (number of spikelets per unit length) of the panicle (Wopereis et al., 2009).

1.2.1.8. Spikelet

The spikelet is a rice flower composed two layers of floral petals; outer (lemma) and inner (Palea) layers. Inside the flower contains 6 stamens and a pistil as the reproductive organs. Each stamen consist of two-celled anthers with pollen or sperm and a filament. The pistil contains the ovary, style and stigma. Rice is a self-pollinating crop (autogamous) in which pollen is delivered to the stigma in the same flower, then the gametes transferred to the ovary for fertilization (Wopereis et al., 2009).

1.2.2. The stage of rice plant development

The optimum temperature to grow rice is approximately 25 to 35℃, with higher or lower temperatures affecting the crop yield (Ghadirnezhad and Fallah, 2014; Nishad et ai., 2018). A suitable environment (especially temperature and moisture) is needed to activate the rice growth cycle which starts from fertilization and embryo development. Rice development consists of 4 major phases: embryo, vegetative, reproductive, and ripening phases.

1.2.2.1. Embryo

Rice embryos have unique characteristics compared to other monocot and dicot embryos. They already possess several foliage leaves before entering dormancy and germination, indicating a reversal of the usual sequence of developmental stages. This suggests that grasses, including rice, are heterochronic mutants (Asai et al.,2002; Itoh et al.,2005). Rice embryos also exhibit complex structures, such as the scutellum, coleoptile, radicle, epiblast, and SAM (Yang et al.,2013). The scutellum, similar to cotyledons in other plants, which plays a vital role in gene expression during the maturation process. Pollination in rice occurs simultaneously with flower opening, followed by fertilization a few hours later. This synchronous pollination allows for

efficient production of non-chimeric mutants by mutating a large number of zygotes (Itoh et al.,2005).

After pollination, the zygote undergoes cell divisions to form a globular embryo. Around four days after pollination, the first morphogenetic events take place, including the development of the shoot apical meristem, coleoptile primordium, and radicle primordium. The first leaf primordium becomes recognizable around five days after pollination, and the rice embryo completes its morphological development shortly after the formation of the third leaf primordium. The subsequent processes involve maturation and dormancy. It is a logical approach to categorize the development of embryos by identifying distinct stages based on specific morphogenetic events as shown in Itoh, J.I. (2005).

Seed dormancy is a built-in trait of seeds that determines the precise environmental conditions necessary for them to germinate. It is controlled by genetic factors, but the surrounding environment also has a notable impact, partly through the plant hormones abscisic acid and gibberellins. After being dispersed, the dormancy level of a seed can change over time due to the conditions in its surrounding environment, in addition to the influence of the environment during its initial development (Finch-Savage and Leubner-Metzger, 2006). Then, Rice germination takes place in an appropriate environment when the initial shoots and roots begin to appear from the seed, initiating the growth of the rice plant (Dunand and Saichuk, 2009).

1.2.2.2. Vegetative phase

The vegetative phase begins from germination through seedling and tillering stages (Moldenhauer and Slaton, 2001). In the stage of seed germination (Fig.1.2), seed dormancy is broken and then the radicle emerge out of the seed. The small roots grow and extend continuously to from the dense root network underground in the seedling stage (Dunand and Saichuk, 2009). The tillering phase starts when the first tiller appears from the bud on the internode. The numbers of tillers depends on genetic background, nutrients and environment. The vegetative stage can take from around 21 days to more than 10 months before transition to the reproductive stage (Wopereis et al.,2008).

1.2.2.3. Reproductive phase

The reproductive phase consists of 3 main sub-stages including panicle initiation, heading and flowering (Fig.1.2). This phase initiates when the first panicle comes out of the base of the tiller. The panicle is enclosed by the leaf sheath which can function in food storage. When more than 80% of panicles emerge from the leaf sheath (the heading sub-stage), anthers are generated from the spikelet on the panicle and the plant enters the flowering stage. During flowering, wind or insects transfer pollen from the anthers to the stigma and ovary, respectively for fertilization (Wopereis et al., 2008).

1.2.2.4. Ripening phase

The ripening phase lasts approximately 20-35 days, and last from flowering to full maturity stage. This stage is characterised by grain filling, which is dependent on temperature, nutrition and water availability. Rice maturity is reached when the opaque endosperm is hard as shown in Fig.1.2 (Wopereis et al., 2008).
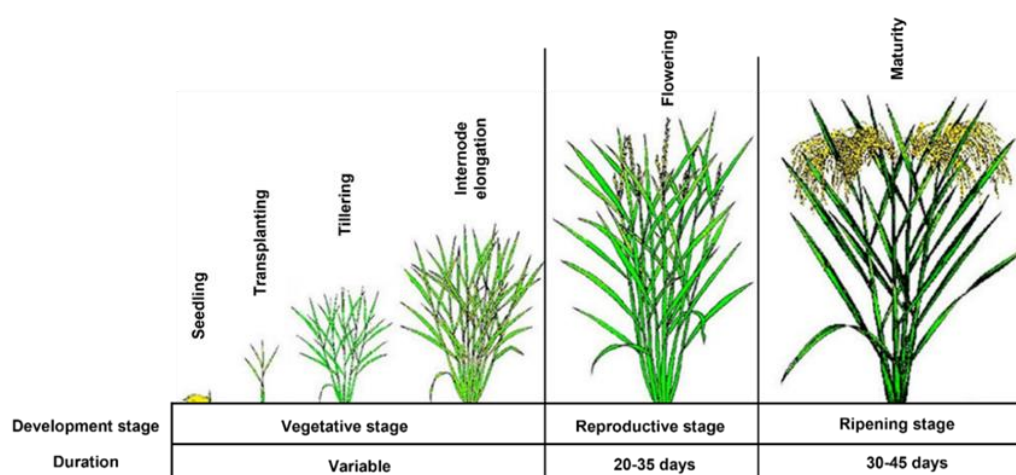
Figure 1.2. Rice development is divided to 3 stages, including vegetative, reproductive and maturity stages. The vegetative phase begins from germination until panicle initiation, which take time around a month before develop to reproductive (20-35 days) and maturity stages (30-45 days), respectively. This image is modified from Vo 2022.

1.2.3. Photosynthesis

Photosynthesis is an essential process which occurs in the green, chloroplast containing parts of the plants (e.g., stem, unripe fruits and leaves). Among these organs, leaves the play the most important role in photosynthesis (Dima et al., 2006; Cocaliadis et al., 2014; Ying et al., 2018)

In photosynthetic process, the energy from sunlight is changed to chemical energy which is eventually stored in the plant in the form of sugars and other organic molecules as food supply for plants. Light is absorbed only at particular wavelengths (red and blue) leading to the non-absorbed wavelengths providing the typical green colour of photosynthetic tissues (Vernon et al. 1965; Liu and Iersel 2021). Although typical of plants, the photosynthetic process is found in other photoautotroph organisms including algae, some unicellular protists and some prokaryotes. The basic chemical reaction of photosynthesis is:

$$6CO_2 \quad + \quad 6H_2O \quad \xrightarrow[\text{Water}]{\text{Sunlight}} \quad C_6H_{12}O_6 \quad + \quad 6O_2$$

Carbondioxide $\qquad$ Water $\qquad\qquad\qquad$ Sugar $\qquad$ Oxygen
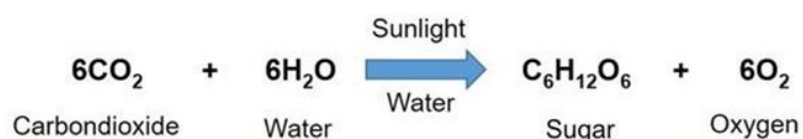
This process can be described as two separate but linked sub-processes: a light-dependent (light reaction) reaction by which light energy is used to generate chemical energy and reducing power (ATP and NADPH) with O2 released by the photolysis of water (Sudhakar and Mamat, 2019) and a light-independent reaction (dark reaction) in which the chemical energy formed in the light-dependent reaction is used to fix carbon (CO_2) into sugar (Lopez and Barclay, 2017; Yahia et al., 2019). These sub-processes are described below.

1.2.3.1. The light-dependent reaction

The light-dependent reaction uses sunlight with the wavelength of around 400-700 nm to generate chemical energy in the form of ATP and NADPH. The initial absorption of light involves a number of different types of pigments, including chlorophyll a, chlorophyll b and various carotenoids located on the thylakoid membrane inside the chloroplast. Chlorophyll a and chlorophyll b are essential pigments found in most

green plants, which absorb violet to blue and orange to red spectrums of light, as shown in Fig. 1.3. Carotenoids generally absorb light in the blue-green and violet region, extending the range of light that can be used to drive photosynthesis. Chlorophyll pigments are found in the light-harvesting complexes which surround the reaction centre protein, forming a photosystem (PS). There are two types of PS system namely, photosystem II (PSII) and photosystem I (PSI), which absorb the light at a wavelength 680 (P680) and 700 (P700) nm, respectively. Working together in the Z-scheme, P680 and P700 molecules help to absorb a greater range of light wavelength for photosynthesis (Taiz et al. 2015).
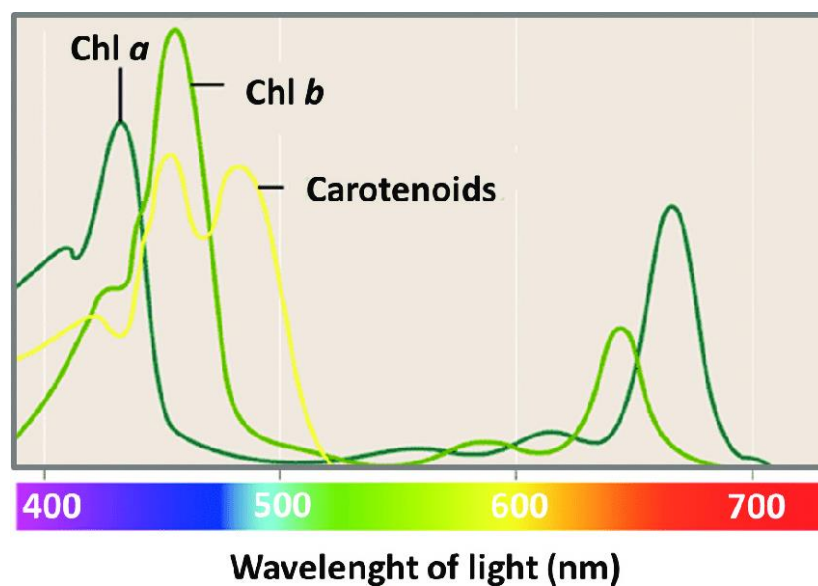
Figure 1.3. The absorption of light spectrums, chlorophyll a and b can absorb violet to blue light and orange to red light. Chlorophyll a absorbs the light at wavelength around 430 and 660 nm, while chlorophyll b absorbs at wavelength about 460 and 630 nm. Carotenoid absorb violet, blue and green region at wavelength about 450 and 500 nm (Aboonajmi and Faridi 2016).

PSII is the first step in the light reaction (Fig. 1.4). The chlorophyll pigments in PSII capture photons of light, raising the energy level of electrons in the pigment molecules. Via sequential gain and loss of energy, the energy is transferred within the light harvesting complex, channelling the energy towards the chlorophyll a molecules at the heart of the complex. These molecules can activate P680 electrons to rise up from the ground state (low energy level) to an excited state (high energy

level). When a P680 molecule loses an electron, the energy is used to hydrolyse (split) a molecule of water into an oxygen atom and two protons and electrons. An electron is transported to the P680 molecule to replace the lost electron and the oxygen atom instantly binds to another oxygen atom to structure oxygen molecule (O_2). This process of photolysis is at the heart of the light-dependent reaction. Each excited electron from the primary acceptor of PSII then move to a neighbouring PSI via an electron transport chain, generating a proton gradient via the energy lost from the excited electron as it passes along the chain. The electron transport chain consists of a sequence of electron carriers; plastoquinone (Pq), Cytochrome complex and Plastocyanin protein (Pc) (Caffarri et al., 2014; Rochaix , 2011; Rohr and Nicholson, 2021).

At PS1, light energy is again harvested and is used at the P700 site to re-energise the electron received from PSII. The excited electron from PSI is then transferred to Ferredoxin (Fd), before it is delivered to NADP+ by NADP+ reductase to produce NADPH (2e- per NADPH). During the light-dependent reaction a proton gradient is generated across the thylakoid membrane. This gradient is utilised via ATP synthase to generate ATP. Thus, at the end of the light-dependent ractions, ATP and NADPH are provided as the energy source for the light-independent reaction in the next step of photosynthesis (Lodish et al. 2000; Shimakawa and Miyake 2018).
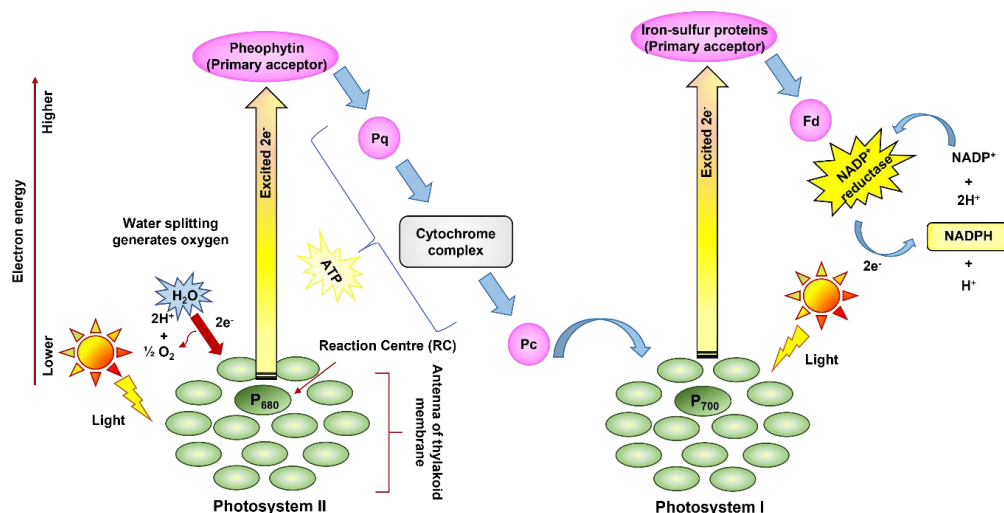
Figure 1.4. The light reaction of photosynthesis occurred in thylakoid membrane. There are two types of photosystem (PS); PSI and PSII. Each PS has its own reaction centre to absorb different light wavelengths, 680 nm for PSII and 700 nm for PSI. When the reaction centre

absorbs light, electrons are excited and transferred to an electron acceptor via an electron transport chain. Via this process ATP and NADPH are produced which are used as the energy source for the light-independent reactions. The figure is adapted from photosynthesis article (Bassham and Lambers 2021).

1.2.3.2. The light-independent reaction (dark reaction)

The light-independent reaction (dark reaction) of photosynthesis is the process where the energy (ATP and NADPH) from the light reactions is utilized for carbohydrate synthesis via a complex enzymatic pathway known as Calvin-Benson cycle, as presented in Fig.1.5. There are three major steps in this process that occur in the stroma inside a chloroplast (Yahia et al., 2019).
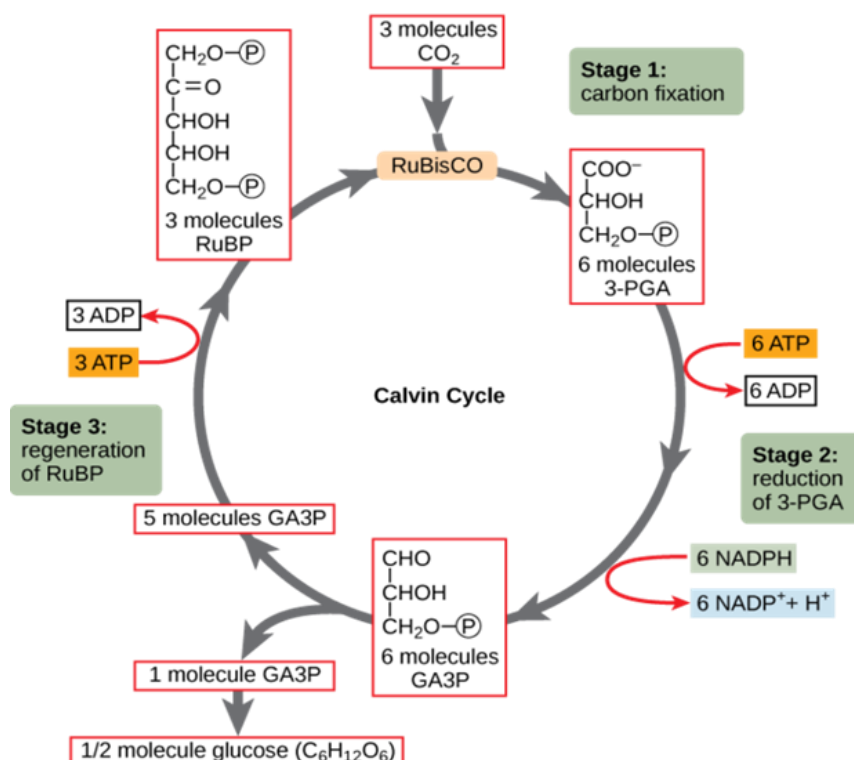
Figure 1.5. The figure shows Calvin cycle occurred in chloroplast (stroma), which consists of three steps; carbon fixation, reduction and regeneration of RuBP. CO_2 is captured by Rubisco enzyme and then converse to 3-PGA. After that, 3-PGA is reduced to 1,3-Bisphosphoglycerate (G3P) as sugar product by phosphoglycerate kinase using ATP and NADPH in the second step. In the last step, some G3P molecules regenerated to RuBP as a substrate in the cycle (Biology Libretexts, 2022).

The first step is carbon fixation. When CO_2 from atmosphere enters in the chloroplast, ribulose-1, 5-bisphosphate carboxylase (Rubisco) fixes CO_2 and catalyses the conversion of ribulose-1, 5-bisphosphate, (RuBP, 5 carbon atoms) to 3-phosphoglycerate, (3-PGA, a 3-carbon compound) per a molecule of CO_2. The second step is reduction. Phosphoglycerate kinase adds the phosphate group from ATP to each 3-PGA, so 3-PGA is changed to 1,3-Bisphosphoglycerate . Then two electrons from NADPH reduce the carboxyl group of 1,3-Bisphosphoglycerate to an aldehyde group of glyceraldehyde-3-phosphate (G3P). Three molecules of CO_2 produce six molecules of G3P. Only one molecule of G3P is the product of the Calvin cycle, with the others being recycled to regenerate the RuBP acceptor in the third step, called the regeneration of RuBP (Lopez et al., 2017;Taiz et al. 2015).

However, the Rubisco enzyme also binds with O_2 and can oxygenase RuBP to form 3-PGA and Phosphoglycerate (a 2C metabolite). This process is termed photorespiration and severely limits the efficiency of photosynthesis.

1.3. C4 adaptations to combat photorespiration

Photorespiration greatly decreases the efficiency of photosynthesis. Consequently, there have been evolutionary changes in some plants, which limits the process of photosynthesis. Most notable are those plants which use C4 photosynthesis. Most plants capture CO_2 directly via Rubisco to generate 3C sugars- defined as C3 photosynthesis. In C4 plants, the initial fixation of CO_2 does not occur via Rubisco, rather via another enzyme (PEP carboxylase) leading to an initial 4C product, thus termed C4 photosynthesis. PEP carboxylase does not fix O_2, thus photorespiration is blocked. The initial C4 product is then transported to a specific ring of cells around the vascular tissue, the bundle sheath cells. CO_2 is released from the C4 metabolite, leading to a high concentration of CO_2 in these cells. Rubisco is expressed in the BSCs, so that it is exposed to a much higher CO_2 concentration than in C3 plants, greatly decreasing the process of photorespiration. These differences are highlighted in Fig. 1.6 and described in more detail below.

C4 plants contains two types of photosynthetic cells; MCs and BS cells. In the mesophyll cells. atmospheric CO_2 is added to the three-carbon molecule of

phosphoenolpyruvate (PEP) by the enzyme PEP carboxylase and consequently changed to a four carbon molecule of oxaloacetate (OAA). Then, the four-carbon molecule is transferred to BS cells through plasmodesmata to the next step of photosynthesis. In this step, OAA (4C) releases CO_2 before regenerating PEP (3C) to receive CO_2 in mesophyll cell again as a cycle. Meanwhile, CO_2 released from OAA is captured by Rubisco in the Calvin-Benson cycle to generate sugar. In C3 plants, photosynthesis occurs only in MCs containing Rubisco to fix CO_2 from the air. Due to C4 leaf anatomy and biochemistry, BS cells in C4 plants attain a higher concentration of CO_2, decreasing photorespiration and thus increasing the photosynthetic efficiency compared with C3 plants (Wopereis et al., 2008).

C4 photosynthesis requires spatial separation of biochemistry and is associated not only with changes in the expression of genes encoding specific enzymes, it is also associated with changes in the patterns of cells within the leaf. A leaf can be considered to be made up of three fundamental cell types: veins (V), mesophyll (M) and bundle sheath (BS). In C4 leaves the number of M cells between veins is greatly restricted, leading to a cell pattern of V-BS-M-M-BS-V. This allows metabolites to be delivered rapidly to the bundle sheath cells from the mesophyll cells (Feldman et al. 2017; Sage et al.2014; Wang et al. 2017). In contrast, C3 plants generally have many more M cells, leading to a cell pattern defined by V-BS-M-(M)n -BS-V pattern of cell arrangement where n >2 (Slewinski et al 2012) as shown in Fig. 1.7. Due to the larger number of mesophyll cells, the interveinal distance between veins tends to be longer in C3 than C4 plants.

The recognition that C4 photosynthesis requires a particular pattern of cell types has led to efforts to manipulate cell patterning in C3 plants as part of programs aimed at engineering C4 photosynthesis into C3 plants, including rice. For example, a research project linked to the C4 rice consortium (Hibberd et al. 2008) has reported on a series of transgenic rice plants overexpressing a range of transcription factors from maize proposed to play a role in the acquisition of the specific vascular differentiation pattern linked to C4 photosynthesis (Wang et al. 2017). Although overall leaf phenotype was little altered (i.e., C4 leaf structure was not obtained), a number of these lines appeared to have altered mesophyll size (analysed further in Chapter 2 of this thesis). These

novel genetic resources provide useful tools to test ideas on the relationship of leaf structure and photosynthetic function.

A. C₃Photosynthesis   **B. C₄Photosynthesis**
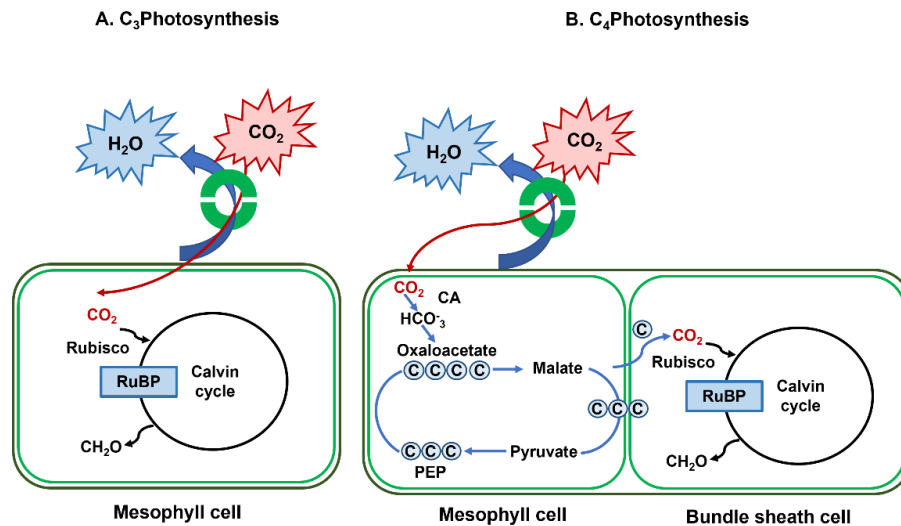
Figure 1.6. The diagram of light-independent reaction of C3 and C4 photosynthesis represents the difference of light-independent reaction between C3 (A) and C4 plants (B). In C3, the Calvin cycle is occurred in a mesophyll cells. CO_2 is fixed by Rubisco and catalysed RUBP to the first 3 carbon compound (G3P). In the other hand, CO_2 from atmosphere is fixed by PEPC and catalysed PEP to the first 4 carbon product (OAA or malate) in MCs before being transferred to BS cell, which concentrate CO_2 level around Rubisco enzyme in Calvin cycle.
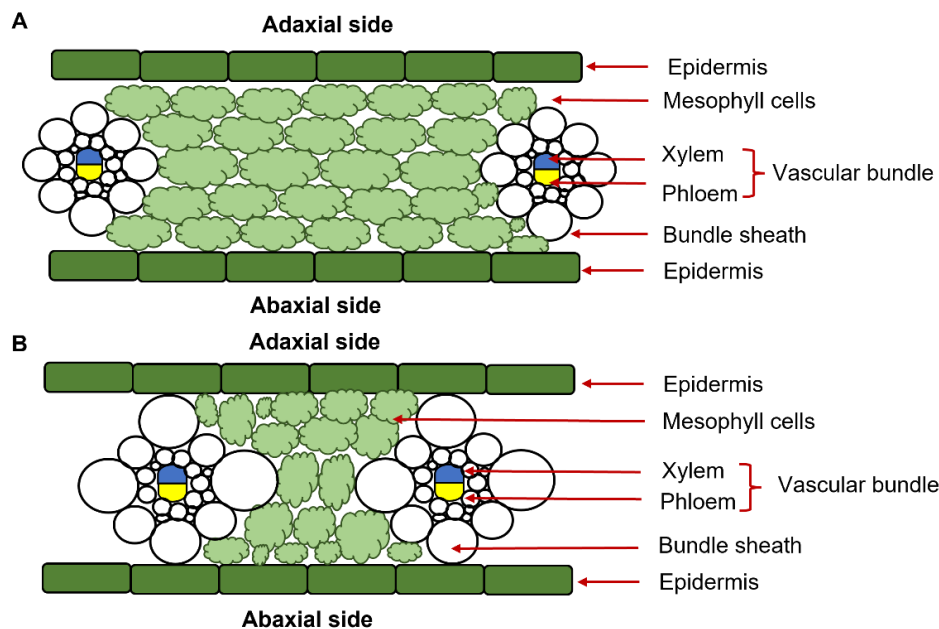
Figure 1.7. C3 plants such as rice consist of a single photosynthetic cell type (mesophyll cells). More than 4 MCs locate between two minor veins, which causes the vein spacing is wider when compared to C4 plants (A). A figure B shows Kranz anatomy in C4 plant contains two photosynthetic cell types; mesophyll and bundle sheath cells. BS cells are close together. The interveinal distance between two minor veins is short.

1.4. The study of leaf structure and photosynthesis

The biochemical processes of photosynthesis described above occur within the chloroplasts (Alberts et al., 2002). These organelles are embedded at some distance from the initial incidence of the substrates (CO_2 and light) required for photosynthesis. It is thus likely that the physical structures surrounding the chloroplasts within a leaf must, to some extent, limit the process of photosynthesis. The identity of these structural elements and their relative importance for photosynthesis have been the subject of extensive investigation over many years, leading to a number of important observations and conclusions on leaf structure/function in relation to photosynthesis, and how it responds to altered environmental conditions (Terashima et al., 2011).

Two main approaches to unravelling this problem have been taken. Firstly, investigators have performed large scale measurements on multiple leaf structural features in a range of related or unrelated species, then performed various correlation analyses to identify potential links between traits and photosynthetic performance. (Wright et al., 2004, Terashima et al., 2011, Giuliani et al., 2013). This has led to the successful identification of a number of structural parameters relevant to photosynthetic performance, including, for example, exposed mesophyll cell surface area (S_{mes}), the packing and positioning of plastids along the plasma membrane and the thickness of the mesophyll cell wall. However, such correlative approaches can only provide limited mechanistic evidence on how the identified trait is linked to the output.

Therefore, the causal relationship of any single structural parameter to the overall photosynthetic performance of a leaf remains open to discussion. The situation is made more complicated by the fact that the combinations of different anatomical and biochemical features within a leaf tend to interact to determine the final leaf photosynthetic rate. For example, leaf structural features influence both CO_2 diffusion and light environments inside a leaf, and the distribution of enzymes across a leaf can greatly influence the CO_2 microclimate, all of which influence overall photosynthetic performance.

To tackle these difficulties, some researchers have taken a more mechanistic approach in which the cellular structure of a leaf is used as a basis for computational modelling, with quantitative estimates of structure and biochemistry used to investigate whether the integrated activity of multiple cells in a virtual leaf can be used to simulate leaf photosynthetic function. Developing such models has been a focus of efforts for many years (Zhu et al., 2013, Ho et al., 2015, Xiao et al., 2016, Xiao and Zhu, 2017a, Xiao and Zhu, 2017b). Recently the Fleming lab has collaborated with the Zhu lab in Shanghai to develop a new model of rice photosynthesis, *eLeaf* (Yi et al., 2022). This model incorporates a range of rice leaf structural elements at the whole leaf, cellular and sub-cellular level, with each virtual cell modelled to perform photosynthesis according to a range of CO_2 and light levels. One of the outputs of this model is that carbon assimilation rate is positively linked to mesophyll cell size and negatively linked to bundle sheath cell size, which I will describe more details in the next chapter.

In summary, although many studies have identified elements of leaf structure which influence photosynthetic performance, experimental testing of these relationships has been limited. Recent modelling approaches have also identified potential functional relationships and the increasing availability of transgenic rice is providing genetic resources to test some of these hypotheses.

Chapter 2

Mesophyll and bundle sheath cell size influence photosynthetic performance in rice

2.1. Introduction

2.1.1. Change of leaf cell structure influences to photosynthetic performance

The primary function of the leaf is to capture CO_2 by photosynthesis, providing the material and energy for plant growth and reproduction (Wright et al., 2004; Wang et al., 2019). The site of CO_2 fixation is located in the chloroplasts dispersed randomly along the MC wall, which are themselves located mainly in mesophyll cells (Shieh et al.,1982; Maai et al., 2011). The mesophyll cells are patterned in space to generate the 3-dimensional object, the leaf, which has to absorb light energy and allow the diffusion of CO_2 from the external environment into the leaf and to the photosynthetic cells.

Once CO_2 has passed through the stomata, it enters a complex pathway of airways that lead to the expose mesophyll surfaces across which gas diffusion must occur. The area of cell for diffusion is thought to play a major role in limiting the flux of CO_2 into the mesophyll cells (Flexas et al., 2012), and thus the flux of CO_2 available for fixation in the chloroplasts, which tend to align themselves along the exposed mesophyll cell wall (John and Caemmerer, 1996, Dengler and Nelson,1999; Nadal and Flexas, 2018;). Huge efforts have been devoted to measuring anatomical features and their proxies, such as the proportion of surface area (A) of mesophyll cell exposed to intercellular air space (A_{mes}) per unit leaf area (A/ Ames), leaf thickness, cell wall, and the CO_2 permeabilities of cell membranes, and correlating them to photosynthesis in different leaves (Roderick et al, 1999; Flexas et al., 2012). These correlations serve eco-physiological studies well, but they cannot be used to mechanistically define the contribution of different anatomical/biochemical factors to the observed variations of photosynthetic rates among different leaves.

An alternative is to take a more mechanistic, bottom-up approach in which the cellular (and sub-cellular) structure of a leaf is used as the basis for computational modelling,

with quantitative estimates of structure and biochemistry used to investigate whether the integrated activity of multiple cells in a virtual leaf can be used to simulate leaf photosynthetic function (Ho et al., 2016; Xiao et al., 2016; Earles et al., 2019). This approach is computationally challenging and, as with all models, requires a number of assumptions to be made. However, if the model successfully captures an element of measured reality, it provides evidence that the proposed mechanism is at least to some extent correct. In addition, once validated these models can allow quantitative dissection of the process under study, assigning values (and thus relative importance) to the different elements comprising the model. Finally, such models are open to the exploration of parameter space in a way which is experimentally very difficult and time-consuming, allowing a more rapid evaluation of hypotheses and setting the scene for targeted experimentation to test interesting or surprising ideas arising from the model.

As a part of a BBSRC-funded project involving the collaboration of researchers at the University of Nottingham, the Institute of Plant Physiology and Ecology, CAS, Shanghai and the University of Sheffield, a 3D spatial model of photosynthesis has been developed to predict the photosynthetic rate under different light and CO_2 concentrations focusing on leaf anatomical and biochemical properties. This model, eLeaf, comprises 4 main modules. These are a 3D geometry module which captures major elements of leaf anatomy at both supra- and sub-cellular resolution; a light module which simulates the heterogeneous internal light environment inside the leaf; a CO_2 diffusion module which simulates gas flux within a leaf; and a metabolism module which captures the main biochemical processes involved in photosynthesis. This model, which has been accepted for publication (Yi et al., 2022) allows for the dissection of the model components to quantify their relative influence on photosynthetic performance under different external conditions of CO_2 and light.

The outcome of these calculations suggests that photosynthetic metabolism makes a major contribution (c. 75%) to the change in CO_2 assimilation rate measured when rice plants are grown under elevated CO_2 role, whereas about 25% of the change observed can be related to the structural changes observed in the leaf. Looking at the relative contribution of the different structural factors, one of the predictions of the model is that an increased size of mesophyll cells and a decreased size of bundle sheath cells may improve the efficiency of CO_2 assimilation under elevated levels of

CO_2 (Yi et al., 2022). However, functional data to support this hypothesis is not yet available.

2.1.2. Novel genetic resources to investigate rice leaf structure/function relationships to improve the crop yield

Photosynthesis has been identified as important trait with a view to increasing crop yield. In 1999, John Sheehy and colleagues from the International Rice Research Institute (IRRI) proposed an idea to radically improve photosynthesis in rice. This grass plant has C3 photosynthesis, which is an inherently inefficient process due to the process of photorespiration. A number of plants have evolved an alternative form of photosynthesis, termed C4 photosynthesis, which leads to a decrease in photorespiration (Sheehy et al. 2000; Sage and Zhu, 2011). Although it has evolved many times, the transition from C3 to C4 requires a number of changes in both leaf biochemistry and leaf structure. The C4 rice consortium has been established with the aim of transforming rice to a C4 photosynthetic state which will automatically lead to a very significant increase in crop yield (Mitchell and Sheehy, 2006). For example, there is evidence that if a C4 photosynthetic system can be inserted into C3 plants, the yield might be raised more than 50% with an increase of nitrogen (N) and water use efficiency (WUE) (Hibberd et al., 2008; Wang et al., 2016).

The C4 rice project has taken a number of approaches to tackling the challenge. One of these has been to identify the genes encoding the key enzymes required for C4 photosynthesis and to stack them into rice. For example, the process of introducing C4 photosynthesis into C3 rice (*Oryza sativa*) requires the installation of a biochemical mechanism that will concentrate CO_2 in modified bundle sheath cells at the carboxylation site. A quadruple line of rice was created, consisting of four core C4 photosynthetic enzymes derived from the NADP-malic enzyme subtype. These enzymes, namely ZmPEPC, ZmNADP-MDH, ZmNADP-ME, and ZmPPDK, were introduced to the rice line, resulting in elevated enzyme activity and minor physical alterations , but overall did not have any notable effects on the plant's photosynthetic rate (Lin et al., 2020).

Another approach has been to identify key transcription factors that might be introduced into rice leading to a suite of changes favouring a C4 type photosynthesis (rather than the sequential stacking of individual genes) (Wang et al., 2017). In particular, a focus has been made on identifying transcription factors that might alter rice leaf anatomy to create the leaf structure required for C4 photosynthesis to work, for example decreasing the number of mesophyll cells between vascular bundles, and altering the bundle sheath cell structure and ultrastructure (chloroplast differentiation).

These studies have shown that the SHORT ROOT(SHR) and SCARECROW (SCR) genes are expressed in the process of procambium development and vascular differentiation in *Arabidopsis* (Helariutta et al., 2000; Moshe,and Brady, 2022). The misexpression of these genes leads to altered aspects of leaf differentiation reminiscent of C4 anatomy. Similarly, the GOLDEN 2-LIKE transcription factor genes (GLKs) have been shown to play major roles in chloroplast development and chloroplast production. Thus, GLK1 plays a role in the differentiation of bundle sheath (BS) cells and GLK2 in the differentiation of mesophyll cells in C4 plants (Rossini et al., 2001; Wang et al., 2016). These studies have highlighted that SHR, SCR and GLKs are interesting genes that shed light on the route from C3 to C4 photosynthesis. However, other genes need to be identified to allow engineering of the appropriate anatomy to allow C4 photosynthesis in rice.

One example of such a study was performed by Peng Wang and colleagues from the University of Oxford. In an attempt to identify genes controlling leaf structure in C4 plants, they generated over 50 independent transgenic rice lines overexpressing individual transcription factors implicated in the development of Kranz anatomy in maize. This was done on both the *Kitaake* and *IR64* rice backgrounds. These "*JL*" lines were characterised for C4 like traits (Wang et al., 2016). Although the study does not report on any major change in leaf structure consistent with a more C4-like anatomy, there did appear to be changes in both mesophyll and bundle sheath cell size in some of the lines (analysed in more detail in the "Results" section of this chapter). These genetic resources provide a novel pool to explore the potential role of altered mesophyll and bundle sheath cell size in photosynthesis

2.1.3. The improvement of stomatal properties influences the crop yield

Another important event that occurs during photosynthesis is transpiration. The leaf must lose water by pulling water up from the roots before being evaporated from the aerial parts of plants such as leaf, stem and flower. (Gan et al., 2019; Maylani et al., 2019). The loss of water must be controlled since if too much water is lost, the plant risks death. Therefore there are various trade-offs in leaf structure which allow the leaf to balance gaining of carbon (via photosynthesis) and loss of water (McDowell et al. 2008). Depending on the environment and the life strategy of the plant, different leaf structures might be viewed as optimal, leading to the vast range of leaf form and cellular architecture. Despite these different pressures on the details of leaf structure, some generalities can be observed. For example, all leaves have controllable micropores on their surface, the stomata. Although there are some differences in stomatal structure between grasses and other plants, the vast wealth of data supports the hypothesis that the density and size of stomata plays a major role in controlling gas flux into and out of the leaf (Bertolino et al., 2019; Caine et al., 2019).

The genes manipulate the stomatal development and spacing are EPIDERMAL PATTERNING FACTOR (EPF) family such as EPF1, EPF2 and EPFL9/STOMAGEN , which generally found in *Arabidopsis thaliana* (Hunt and Gray et al.2009; Vatén and Bergmann et al.2012). These genes encode small peptides competitively bind to transmembrane receptor leucine-rich repeat receptor like kinases (LRR-RLKs), ERECTA family (ERf) receptor kinases (RKs) and ERECTA-LIKE (ERL) 1 and/or ERL2. The reaction is regulated by the receptor-like protein (RLP) TOO MANY MOUTHS (TMM) (Zoulias et al. 2018). EPF1 and EPF2 genes function as a negative regulator of stomatal development, while EPFL9/STOMAGEN acts as a positive regulator to enhance stomatal development. In rice plants, The epidermal patterning factor (*EPF1*) has been overexpressed to produce the low stomate *osEPF1_oeW* (weak phenotype) and *osEPF1_oeS* (strong phenotype) lines (Caine et al. 2019), whereas the overexpressed *EPFL9* (*osEPFL9_oe*) results in the high stomata density (Caine et al 2019). Low numbers of stomata generates the reduction of pore areas that is better able to preserve the water, so plants could survive especially under a long-term droughts, helping to improve yields Caine et al 2019.

Our previous work has shown that altered stomatal function such as stomatal density and stomatal conductance (g_s) leads to altered leaf porosity (Lundgren et al., 2019), which related to the altered mesophyll cell size/shape in wheat (Wilson et al, 2021). Also, in my research, the result of the *JL* transgenic rice plants (*JL4A3, JL4A6* and *JL27B4*) has indicated that mesophyll shape (lobiness) is regulated by gas flux through stomata as was the degree of MC lobing. In this chapter, *osEPF1_oe osEPFL9_oe* rice plants are used to further investigate the link of stomatal conductance and cell lobing.

2.2. Hypothesis

1. The size and shape of mesophyll cells leaves influence photosynthetic performance in rice.
2. The size and shape of mesophyll cells in rice is influence by gas flux into and out of the leaf via stomata.

2.3. Aims

The main aim of this chapter is to test the hypothesis raised by a previously generated computational model that mesophyll and bundle sheath cell size play a role in setting photosynthetic performance in rice.

To achieve this aim I have the following objectives:

1. To characterize a series of available transgenic rice lines to investigate whether they showed variation in mesophyll and/or bundle sheath cell size.

2. To use selected lines in a combined structural and physiological analysis to investigate whether altered mesophyll and/or bundle sheath cell size led to altered photosynthetic performance

2.4. Materials and methods

2.4.1. Rice plant varieties

2.4.1.1. *JL* transgenic rice plant

The *Kitaake cultivar (ssp. japonica)* as a control and Transgenic rice (JL) seeds (T2 generation); *JL4, 13, 15, 27* and *34* were screened and propagated by Dr. Naomi Cox and Dr. Jen Sloan from Flemming's laboratory, The University of Sheffield. *JL4* and *27* (T3) were then selected for further investigation as a model of this study . The A and B designations indicate independent transgenic lines containing the designated construct.

2.4.1.2. *OsEPF1_oeW* and *osEPF1_oeS* rice plants

The overexpressed *EPF1 (oe W and S)* with low stomatal density and IR64 seeds, T3 generation were obtained from Dr. Robert S. Caine from Grey's laboratory, The University of Sheffield. The stomatal numbers were reduced to ~50% and ~80 in *osEPF1_oeW* (medium reduction) and *osEPF1_oeS* (severe reduction) respectively (Cain et al. 2019).

2.4.1.3. *OsEPFL9_oe2* and *osEPFL9_oe3* rice plants

The overexpressed *EPFL9 (oe2 and 3)* with high stomatal density and IR64 seeds T3 generation were provided from Dr. Ligia T. Bertolino from Grey's laboratory, The University of Sheffield. Both transgenic lines contained an increase of stomatal numbers, ~70% in *osEPFL9_oe2* and ~120% in *osEPFL9_oe3* (Bertolino et al.2022).

2.4.2. Seed germination

All transgenic rice seeds and IR64 as a control were germinated on a filter paper in petri dishes filled with 15 ml of water and put in the controlled-environmental growth chamber (Conviron, Winnipeg, MB, Canada) for 7 days under the conditions as follow;

420 ppm of CO_2 level, 1000 µmol m−2 s−1 of photosynthetically active radiation (PAR), 28°C of 12-hour day light, 24°C of 12-hour dark and 60% of relative humidity for 7 day.

2.4.3. Plant growth

After a week, young rice plants were grown in 1L pot (Diameter top: 13.5 cm, Height: 11.7 cm) with soil and fertilizer. The recipe of mixed soil was 71% of Kettering Loam (Boughton, UK), 23.5% of John Innes no.3 (Leicester, UK), 5% of silica sand, 0.5% of Osmocote® (a slow-released fertiliser, Ipswich, UK) by volume in pots. Plants were grown in the controlled-environmental growth chamber with the same condition as seed germination and watered every 2 or 3 days. A 7-day-old rice leaf 1st was collected for genotyping. Then, a leaf 6 (21 to 28 days) was measured gas exchange 21 to 28 before being cut to observe leaf structure and stomatal properties.

2.4.4. PCR genotyping

To screen the transgenic rice plants, a young first rice leaf (~1 cm) of JL4, 13, 15, 27 and 34 (T2) was cut at the middle of a leaf after a week of growing to extract DNA. A leaf portion was transferred to a 1.5 ml of microcentrifuge tube and frozen in liquid nitrogen. Then, A frozen leaf was homogenized with a pestle in 500 µl of Shorty buffer (0.4 M LiCl, 25 mM EDTA, 0.2 M Tris-HCL pH 9.0, and 1% (w/v) SDS) before being centrifuged at 13000 revolutions per minute (rpm) for 10 mins. The supernatant was transferred to a fresh tube containing 350 µl of isopropanol for precipitation, mixed by inversion and centrifuged at the maximum speed (13000 rpm) for 10 mins at room temperature. The visible pellet was washed with 70% EtOH and centrifuged at the same speed for 10 mins. The liquid was poured off and the pellet air-dried for 15-20 mins on the bench before being dissolved in 200 µl of TE buffer (with shaking) for 30 mins.

After that, 4 µl of the dissolved DNA sample was taken and added in 21 µl of the PCR master mix (Invitrogen™ 5M Sodium Chloride (NaCl) with RNase-free (Fisher Scientific, Leicestershire, UK), specific primers (Merck KGaA, Dorset, UK),

deoxynucleotide triphosphate mix, dNTPs (Promega, WI, USA), Taq DNA polymerase and standard Taq Buffer, M0273 (BioLabs, Ipswich, UK)) to make a final volume to 25 µl before being performed PCR to confirm the presence of DNA. The PCR conditions were as follows; initial activation of Taq DNA polymerase at 95℃ for 5 minutes, then 35 cycles of denaturation at 95℃ for 30 seconds, following by annealing temperature at 55 C for 40 seconds, extension at 68℃, 40 seconds for *JL4, JL13, JL15 and JL34* and at 68℃, 90 seconds for *JL27*. The final extension is at 68℃ for 5 minutes. Samples were hold at 4℃ after finished. The details of each PCR primers with annealing temperature were shown in Table 2.1.

The PCR product solution was mixed with 10 µl of 5x DNA loading dye (Bioline Ltd., London, UK). 10 µl of the sample solution was taken to run on 1% (w/v) agarose gel containing Ethidium bromide (6 µl of lab stock solution per 100 mL gel) paralleled with HyperLadder TM 1 kb as a molecular weight marker (Bioline Ltd., London, UK), 100v/mAmp for 60-90 mins. The gel image was captured by gel documentary machine.

2.4.5. Rice growth of *JL* lines for screening

JL transgenic seeds were germinated on a filter paper in petri dishes filled with 15 ml of water and put in a growth chamber (Conviron, Winnipeg, MB,Canada) for 7 days under the conditions as follow; 420 ppm of CO_2 level, 1000 µmol m^{-2} s^{-1} of photosynthetically active radiation (PAR), 28˚C of 12-hour light, 24˚C of 12-hour dark and 60% of relative humidity. Then, all plants were grown in 1L pot (Diameter top: 13.5cm, Height: 11.7cm) with soil and fertilizer. The recipe of mixed soil was 71% of Kettering Loam (Boughton, UK), 23.5% of John Innes no.3 (Leicester, UK), 5% of silica sand, 0.5% of Osmocote® (a slow-released fertiliser, Ipswich, UK) by volume in pots After that, plants were grown in the controlled-environmental growth chamber with the same condition as germination and watered every 2 or 3 days. A mature leaf 6 of each rice plants aged 21 to 28 days old were analysed gas exchange by Licor 6800. The leaf portion (1 cm) of each leaf 6 was collected to do further investigation of leaf structural measurement in the next step. After 3-4 weeks, a mature leaf 6 was collected to do further experiments. After 28 days, the fertilizer was added every week until seeding.

Table 2.1. PCR primers and predicted size of amplified fragment

Lab ID	Gene ID	Type of genes	Primer name	Sequence (5'-3')	Annealing Temp(°C)	Amplicon size (bp)
JL 4	GRMZM2 G045883	cDNA	JL 4-3	Fw: CCATGCCGCCTTCCTACAC Rv: ATATCGGCGAGTATCTCGTTCA	55	532
JL 13	AC215201 3_FG008	Genomic DNA	JPF15/ 22 RT	Fw: AGATGGCATCGTCGTCTCCG Rv: ACCGTGAGTCCGATGTCGTC	55	202
JL 15	GRMZM2 G016477	cDNA	JL 15-3	Fw: CGCAACGAGTTCTCTCAGGT Rv: GGCAACAGAGGCTGGTATGT	55	1119
JL 27	GRMZM5 G893117	Genomic DNA	PW 71	Fw: GGGGACAAGTTTGTACAAAAA AGCAGGCTATGATGATGATGA GCGGTCGAG Rv: GGGGACCACTTTGTACAAGAA AGCTGGGTTCGTCGATGAAAT GCCGGAG	55	1232
JL 34	GRMZM2 G377217	cDNA	PW 80 RT	Fw: CAACCGAACAACAAGCCTTT Rv: CACTACAGCTGGGCATGAAA	55	205

2.4.6. Gas exchange measurement

To measure the photosynthetic performance, the gas exchange was analysed by a Licor 6800 (LI-COR Inc., 476 Lincoln, NE, USA). This machine was a portable machine combined with the analytical system of chlorophyll A, which consisted of two measurement systems including gas exchange and fluorescence yield (ΦF).

First, a machine was used to analyse gas exchange inside a leaf. The uptake of CO_2 and release of H_2O vapor across a leaf were detected by a high precision infrared gas analysers (IRGAs). The other leaf physiological parameters such as g_s and C_i. were also calculated (Saathoff and Welles, 2021) Second, the ΦF, the re-emission of photons from chlorophyll was also quantified to generate the information about the light reactions of photosynthesis (the quantum yield of photosystem II, $\Phi PSII$, electron transport rate, ETR) and other reactions such as non-photochemical quenching, NPQ

(Meeker et al.,2021). These data were detected in real-time measurement system. This two integral systems could provide a more complete picture of photosynthesis in term of plant physiology than using either technique alone.

To performed the experiments, a middle area of 21-28 day-old rice leaf 6 was measured leaf width and recorded in the machine. A leaf sample was acclimated in an IRGA chamber at 400 ppm of CO_2, 60% RH, light 2000 PAR, and 10000 rpm of fan speed for 20-30 minutes. The blue light fluoresce was also set up at 10% of total PAR to prevent the stomatal closure. Then CO_2 assimilation rate (A), stomatal conductance (g_s), internal CO_2 concentration inside a leaf (C_i) and PhiPSII were measured under different CO_2 levels started from 400, 300, 250, 200, 150, 100, 50, and 400 ppm as the first step. After the first step, a leaf was acclimated again before doing the second step of analysis by adjusting the conditions to 400, 500, 700, 800, 900, 1000, 1200, and 1500 ppm. A leaf was exposed to each CO_2 concentration and left data stabilization for around 1-3 minutes for the first step and 3-5 minutes for the second step of measurement. The IRGA was set to automatically match (always match) to adjust CO_2 value between sample and reference to be equal.

For more understanding, CO_2 assimilation (A) rate was plotted versus C_i value on A/Ci curve fitting utility version 2.0 (R) in Microsoft Excel file in the photosynthetic model as presented in Sharkey et al. (2007). Three more parameters; a maximum rate of Rubisco carboxylation (V_{cmax}), a maximum rate of electron transport (J_{max}), triose and Triose phosphate use (TPU) were calculated to observe the limitation of A rate in biochemical reactions occurred during photosynthesis. The parameters were calculated by the equations as shown in Sharkey et al. (2007).

2.4.7. The measurement of stomatal characteristics

To measure the stomatal density, the stomatal anatomy and maximal stomatal conductance (g_{smax}), the precise leaf impression was generated by applying the vinyl polysiloxane, VPS (ImpressPLUS Wash, Perfection Plus Ltd, Hants, UK) on the middle length of a rice leaf 6 (~1 cm of adaxial surface), wait around 1-2 minutes to allow VPS solidified before remove. The clear nail vanish was then applied on the imprint and left

it dried at RT. After drying, the nail varnish impression was peeled off and mounted onto a slide under a cover slip.

was

Images of leaf impression was observed under a light microscope (Olympus BX51 microscope). The stomatal features and g_{smax} were calculated as shown in Caine et al. (2019) on 20 stomata per plant (five per field of view) from six biological replicates. The Fiji image J script was used to count the stomatal numbers in 2 mm^2 area and also measure some parameters of stomatal features such as guard cell length (L_{gc}), guard cell width (W_g), stomatal width (W_s), and pore length (L_p) as shown in Fig. 2.1 to calculate the estimated complex area and estimated guard cell area. The anatomical g_{smax} was then calculated by using the equation from Dow et al. (2014) in Fig. 2.2.

L_{gc} = The guard cell length (µm)

L_p = The pore length (µm)

W_{gc} = The guard cell width (µm)

W_s = The stomatal width (µm)
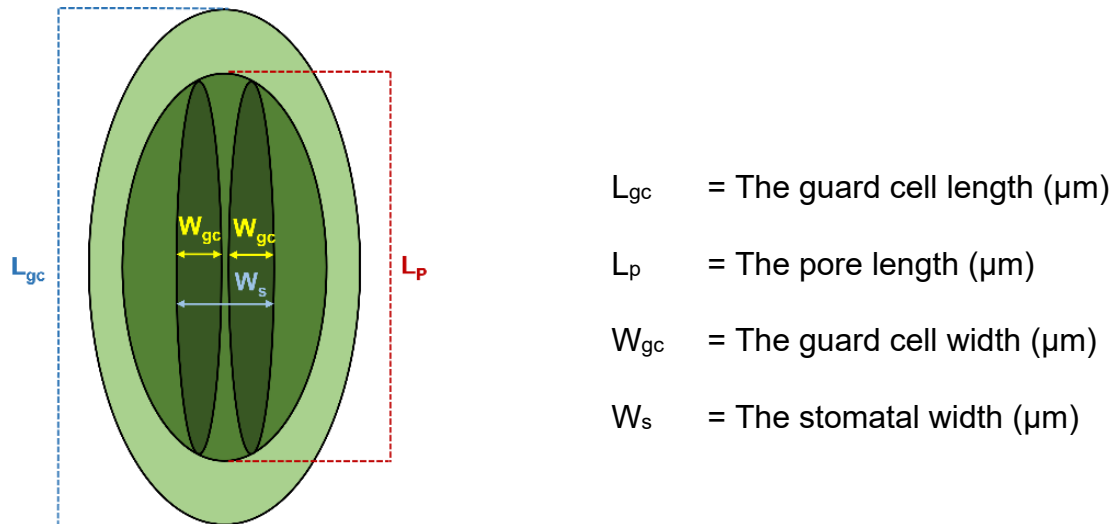
Figure 2.1. The image of an imprint of a rice leaf (adaxial side) was taken to measure stomatal characteristics under a light microscope at 40X. 4 parameters of stomatal characteristics; guard cell width (W_{gc}), guard cell length (L_{gc}), stomatal width (W_s) and pore length (L_p) were measured by Fiji image J as shown in the picture.

Estimated stomatal complex area	$= \pi . L_{gc} . \frac{1}{2} L_{gc}$

(1)

Estimated total area of guard cell	$= \pi . L_{gc} . \frac{1}{2} W_{gc}$

(2)

$$\text{Mean maximum stomatal pore area } (a_{max}) \quad = \pi . L_p . \tfrac{1}{2} L_p \qquad (3)$$

$$\text{Anatomical } g_{smax} = d . D . a_{max} / (v . (L_p + (\pi/2) . \sqrt{(a_{max}/\pi)))} \qquad (4)$$

D   = The diffusivity of water in air at 28°C (m^2s^{-1})

d   = Stomatal density (mm^2)

v   = The molar volume of air at 28°C (m^3mol^{-3})

L_p = The pore length (µm)

π = The mathematical constant (estimated 3.142)

Figure 2.2. After the measurement of stomatal structure, 4 values including stomatal density, $W_{gc,}$ L_{gc}, $W_{s,}$ and L_p from Fiji image were used to estimate stomatal complex area, total area of guard cell, maximum stomatal pore area and anatomical g_{smax} by using the formulas as represented in (1) to (4). The values of D and v in (4) were around 2.4699 x 10^{-4} m^2s^{-1} and 0.24807528 m^3mol^{-3} respectively.

2.4.8. Rice leaf histology

To study leaf anatomy, A rice 6th leaf was cut (~1 cm) as represented in Fig.2.3A, and put in a tube containing 500 µl of fixative solution; 1:3 Ethanol (EtOH): Acetic Anhydride, then vacuum-infiltrated leaf for 1 hour and left at room temperature (RT) overnight. After 24 hours, a leaf was transferred to 1:1 absolute EtOH: Technovit base liquid without hardener, vacuum infiltrated and left at RT for 24 hours before being transferred to 100% Technovit base liquid (no hardener) and placed on an orbital shaker at 4°C at RT for 1 week. A Leaf sample was then transferred to Technovit 1 solution which contained 1 g Hardener 1 per 100 ml Technovit base liquid, shook 4°C overnight.

To embedded sample, the infiltrated leaf was cut in the transverse (TS) direction or or longitudinal (Z) sections as shown in Fig. 2.3B-C. In my research, only TS sections were used for further investigation. All sections were stained in 3 ml of Technovit 1with

hardener 1 mixed with a pinch of neutral red dye for 5 minutes. Blot and dry on tissue paper before placing in 280 µl Technovit 1 with hardener 1 mixed with Hardener 2 (ratio 1:15) in an Eppendorf lid as shown in Fig. 2.3D-F. To prepare 1 ml, 62.5 µl of Hardener 2 was added in 937.5 µl of Technovit 1. The sample was left at RT until it stayed upright (around 2 hours), then transferred to 37 °C overnight to allow it completely polymerize.
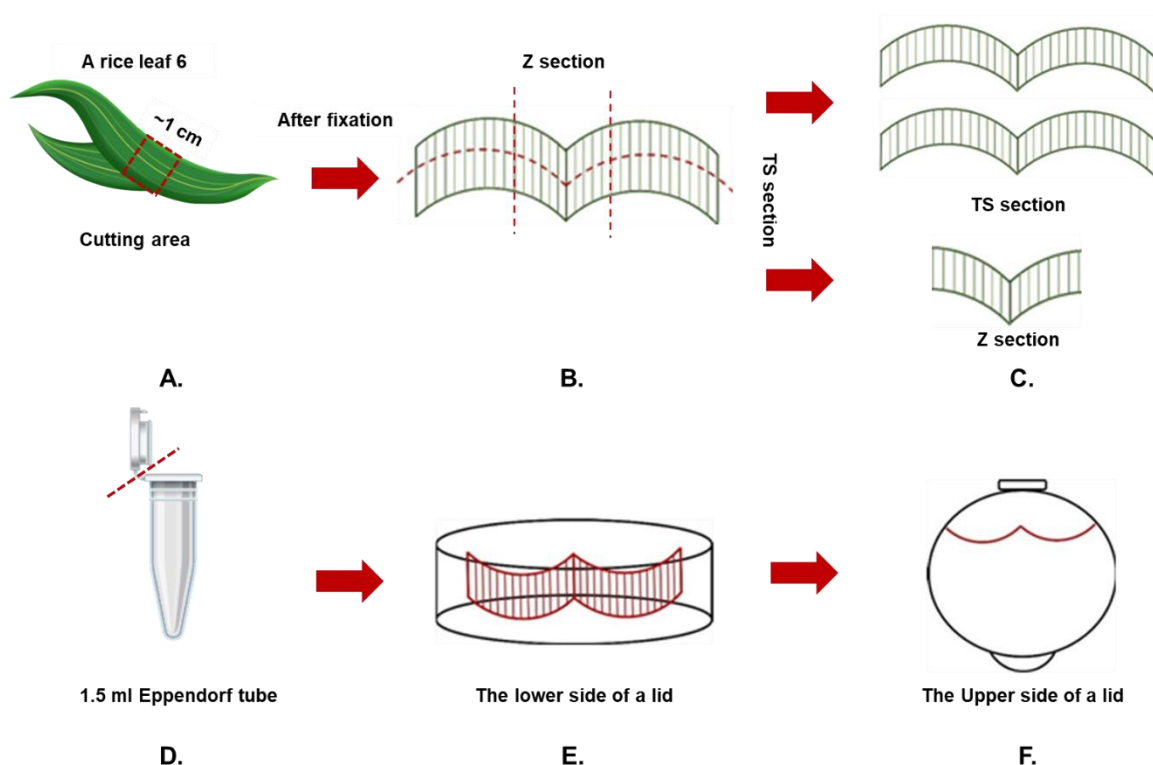
Figure 2.3. In the embedding step of a leaf preparation, a rice leaf 6 of each *JL* lines aged 21 to 28 day was cut at the middle region (~1 cm) for infiltration in fixative solution overnight (A). Then, a leaf sample was transversely cut at the middle position (TS) or vertically cut (Z). But this study focused on only TS section, which provided to two pieces of leaves (B). One of them was used for embedding step and another one was kept in 70% EtOH at 4 °C as spare (C). A lid of 1.5 ml Eppendorf tube was removed (D). An embedded TS leaf was placed vertically in an Eppendorf lid contained Technovit 1 with hardener 1 and hardener 2 (E). Sample was leaned against side of a lid to make it stayed upright (F).

After that, a sample was mounted on to a histobloc by using 2 to 3 parts of Technovit 3040 powder mixed with 1 part of 3040 liquid. The mixture solution was poured at the hold in the centre of a histoblock and placed embedding leaf on a histobloc immediately, left at RT for around 30 minutes. Before sectioning, the half of resin

(without sample) on a histoblock was cut and removed. The rest of resin was trimmed and sectioned at the thickness of 12 and 8 µm respectively by Leica RM2245 Microtome. A piece of leaf section (8 µm) was collected every 8 cuts (the total is 6 pieces per sample). Each sections was then floated on the surface of the water and pulled out by using a cover slip. Dried it on a hot plate at 60°C for around 1 hour. Stained the sample with 0.05% (w/v) toluidine blue O in 1% (w/v) borax for 25 to 30 seconds, rinsed with water by leaving a small drop on top of the sample for 10 minutes to destain and rinsed again before dried it at 60°C for 30 mins.

The cell architecture inside a leaf was firstly observed under epi-fluorescence microscope (Olympus BX51) at 4X modification and the middle areas of both left and right sides of a leaf section were selected for further investigate (Fig. 2.4). The modification was then adjusted to 40X to capture images of leaf structure. 6 anatomical parameters; bundle sheath cell (BS) area, mesophyll cell (MC) area in 5 layers (Fig. 2.5), the degree of MC lobiness, MC circularity, the interveinal distance (IV) between two minor veins, and leaf thickness were calculated by using the scripts of Fiji image J developed by a member in Fleming's laboratory. The formulas were shown in Fig. 2.6 R studio was used to calculated statistic.
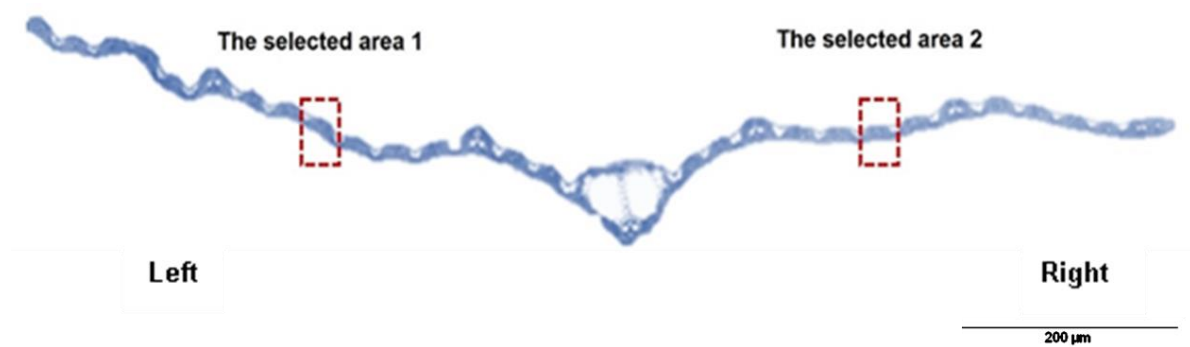
Figure 2.4. The picture showed the selected areas of leaf section. A section (8 μm) of rice leaf 6 was stained with 0.05% (w/v) toluidine blue with 1% (w/v) borax and observed under the epi-fluorescence microscope (Olympus BX51) at 4X. At this modification, two regions were selected at the middle areas of both left and right sides of a leaf section as showed in red rectangular shapes for leaf anatomical analysis.
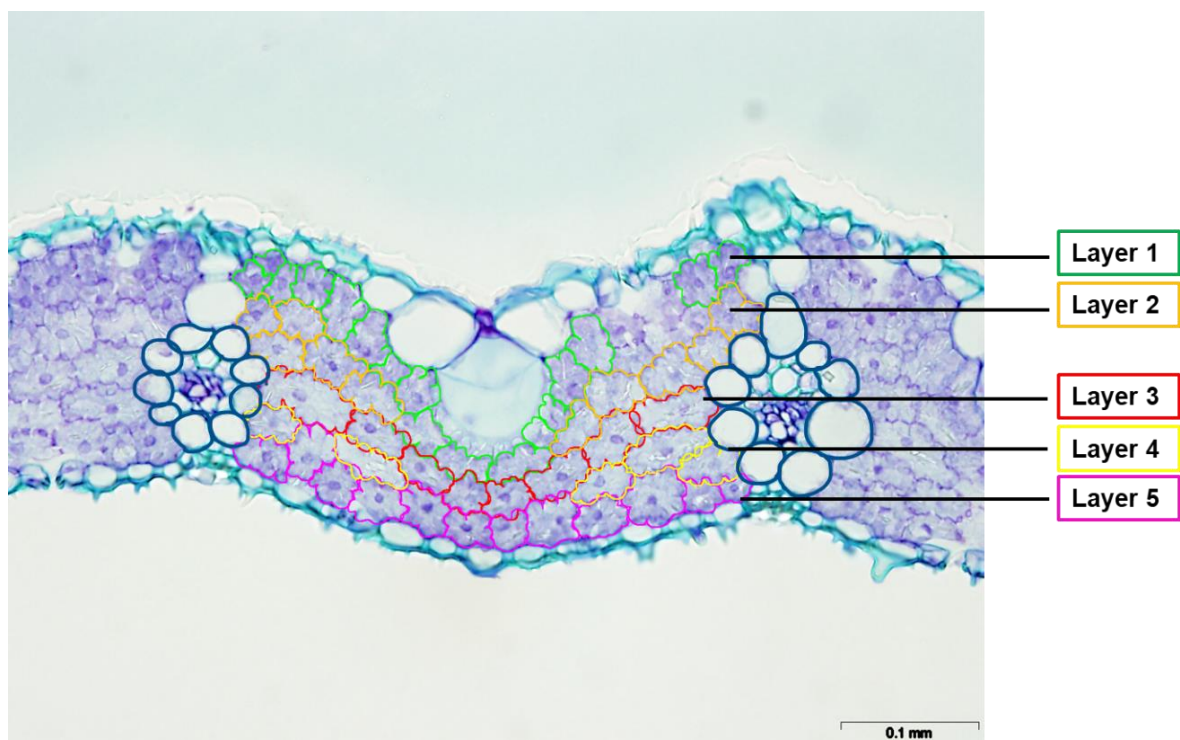
Figure 2.5. Before being analysed mesophyll cell size and shape, MCs were separated to 5 layers from layer 1 to 5. Cells in layer 1, 3 and 5 were firstly identified because they were easily to observe. MCs in layer 1 were close to the upper epidermis (adaxial surface), in layer 3 were at the middle of a leaf potion, and layer 5 was near the lower epidermis of a leaf. The rest of MCs were categorized to layer 2 (between layer 1 and 3) and 4 (between layer 3 and 5).
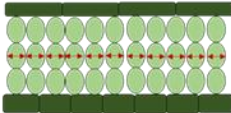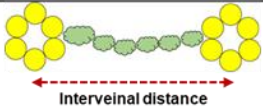
Leaf structural parameters	Pictures	Calculation
1. BS area (size)		The value of pixel of BS area
2. MC area (size)		The value of pixel of MC area
3. MC cell width		The width of MC cells at the middle layer (layer 3)
4. MC Lobiness		$\dfrac{\text{The pixel of MC perimeter}}{\text{The convex hull of MC perimeter}}$
5. MC circularity		The value of pixel of MC circularity
6. IV distance	Interveinal distance	IV distance between 2 minor veins
7. Leaf thickness	Leaf thickness	2 areas of leaf thickness were measured

Figure 2.6. This picture displayed the formular which was used in the FIJI image J script to analyse leaf anatomical characteristics by using the script of Fiji Image J. For TS section, BS and MC area were calculated from the pixel area which was the real size of the cell (green colour). MS lobing was measured from the ratio of a pixel perimeter, a boundary of MC (red line) to a convex hull perimeter acted as an elastic band to circle around the cell (blue line). MC circularity value was analysed to observe the roundness of a cell. The IV distance and leaf thickness was also calculated as shown in 6 and 7. For LS section, MC cell width was calculated from the width of cells at the middle layer which was performed only in the screening of *JL* transgenic lines.

2.5. Results

2.5.1. The screening of *JL* lines

2.5.1.1. Analysis of five selected *JL* lines (*JL*4, 13, 15, 27, and 34)

Some of transgenic rice lines provided by the group of Jane Langdale (University of Oxford) were grown for the initial analysis in this study. A rice leaf 6 of each *JL* lines were sectioned in longitudinal (Z) direction to estimate mesophyll cell width as showed in Fig. 2.7.

The result showed the variations of mesophyll cell width among *JL* rice plants. It was noteworthy that among the *JL* lines, *JL13* and *JL15* rice leaves had smaller mesophyll cell widths compared to the other lines (Kruskal-Wallis test, $p<0.05$, Dunn's multiple comparison). Additionally, the ratio between mesophyll cell (MC) size and bundle sheath cell (BSC) size was calculated and presented in Fig. 2.8. The data revealed that *JL27* exhibited the lowest MC/BS width ratio, while *JL4* had the highest ratio (Kruskal-Wallis test, $p < 0.05$, Dunn's multiple comparison).

According to the Wang study (Wang et al 2016), *JL34*, which contained ZmWKRY, stood out as a particularly small plant with very small, non-lobed mesophyll cells. While *JL34* did not display in the graphs, it was possible that the inserted maize gene in the plants could still have an impact on leaf features such as mesophyll cell size, shape, or other structural parameters.

Based on the results from Fig.2.7, Fig.2.8 and data from the Wang study (Wang et al 2016), Five transgenic *Kitaake* lines (*JL4, 13, 15, 27*, and *34*) were selected for analysis in this research. The maize genes inserted in these transgenic rice lines encoded a variety of protein functions related to signal transduction or transcription (MYB-interacting factors, basic helix–loop–helix (bHLH) transcription factors, leucine-rich repeat receptor-like protein kinases, WRKY genes) implicated in plant growth and development represented in Table 2.2. In the next step, the selected *JL* lines were propagated for further investigation.
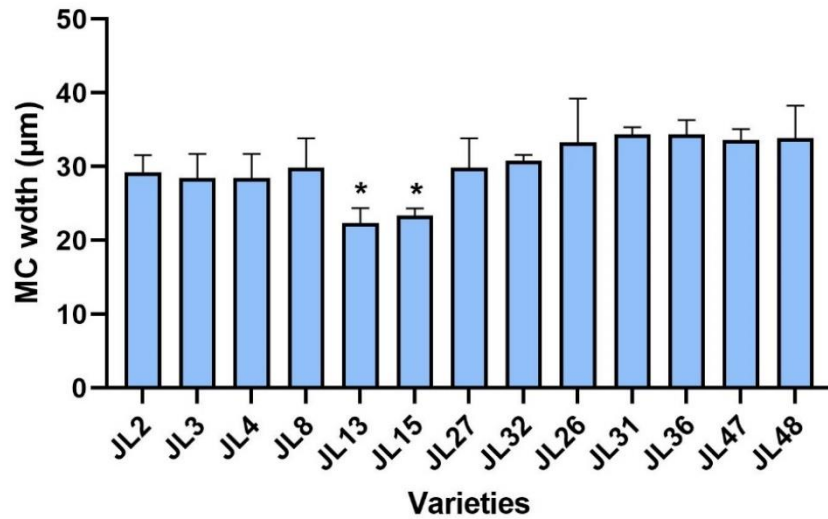
Figure 2.7. The study analyzed several transgenic *JL* lines that carried different maize gene constructs, and observed a variation in mesophyll cell width/size ranging from 29 to around 40 μm. Among these lines, *JL13* and *JL15* showed a significant difference in mesophyll cell width compared to the other lines (as determined by the Kruskal-Wallis test with Dunn's multiple comparison test, $p < 0.05$).
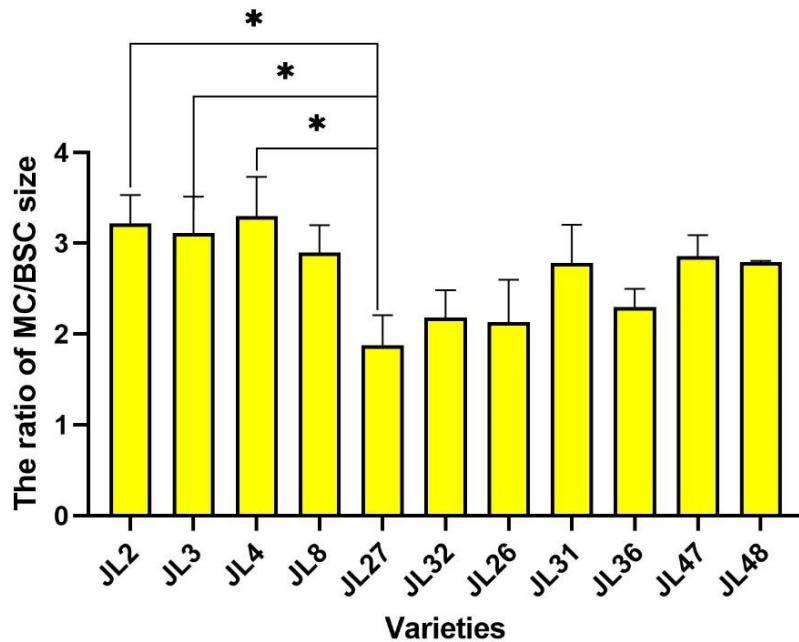
Figure 2.8. The study examined multiple transgenic *JL* lines that contained distinct maize gene constructs, observing the MC/BSC width ratio (size). According to the Kruskal-Wallis test and Dunn's multiple comparison test ($p < 0.05$), *JL4* and *JL27* demonstrated the highest and lowest ratios, respectively, relative to the other lines.

Table 2.2. The candidate genes inserted in *Kitaake* rice

Lab ID	Gene ID	Gene Family	Rice variety	Phenotype in overexpression line
JL4	GRMZM2G045883	bHLH (ZmSPL1)	Kitaake	Normal
JL13	AC215201.3_FG008	bHLH	Kitaake	Normal
JL15	GRMZM2G016477	LRR kinase	Kitaake	Normal
JL27	GRMZM5G893117	Growth regulating factor	Kitaake	Normal
JL34	GRMZM2G377217	WRKY (ZmWRKY12)	Kitaake	Normal

2.5.1.2. Confirmation of the genotype of 5 *JL* lines

To confirm the *JL* transgenic rice plants, DNA genotyping of *JL4, JL13, JL15, JL27* and *JL34* were performed. A 7 day-old of a young rice leaf 1th from each plants were collected for DNA extraction. In this experiment, A 1kb Hyper-ladderTM was used as the molecular weight marker, with nuclease-free water added to PCR reactions instead of rice DNA to act as a negative control. For each line, seed from two independent transformation events were analysed, indicated as *JL*(XAi) and JL(XBi). X and i represented the *JL* number and plant number respectively. The results were shown in Fig. 2.9.

The analysis identified 4 plants of *JL4* line; *JL4A3; JL4A6; JL4B1: JL4B4* containing the bHLH insert sized 532 bp (Fig. 2.9A). There were 3 plants from JL13A (JL13A1, *JL13A3* and *JL13A5*) and 4 plants in *JL13B* (*JL13B1, JL13B2, JL13B5,* and JL13B6) which contained bHLH gene (202 bp) as shown in Fig. 2.9B. Only one plant with LRR kinase gene sized 1119 bp found in JL15 line (Fig. 2.9C). In addition, There were 6 plants with GRF gene (1232 bp) for *JL27* lines; *JL27A2, JL27A3, JL27A4, JL27B3, JL27B4,* and *JL27B6* (Fig. 2.9D) and 5 plants from *JL34* transgenic rice plants carrying WRKY gene sized 205 bp as represented in Fig. 2.9E.

The results of genotyping clearly showed that the lines were not homozygous and were segregating for the transformed sequences. Seeds were collected for analysis in subsequent generations, but since the lines reflected overexpression constructs, I analyzed leaves from the same lines shown in Fig. 2.9 to investigate whether there was any correlation with presence of the transgene and leaf phenotype focusing on

mesophyll and bundle sheath cell size, as suggested by our analysis of the original published data. In this analysis, segregating non-transgenic plants from *JL15* were used as a control to account for changes in form that might have occurred simply due to the transformation/regeneration procedure. In this way, an initial paired dataset was generated to explore the initial hypothesis.
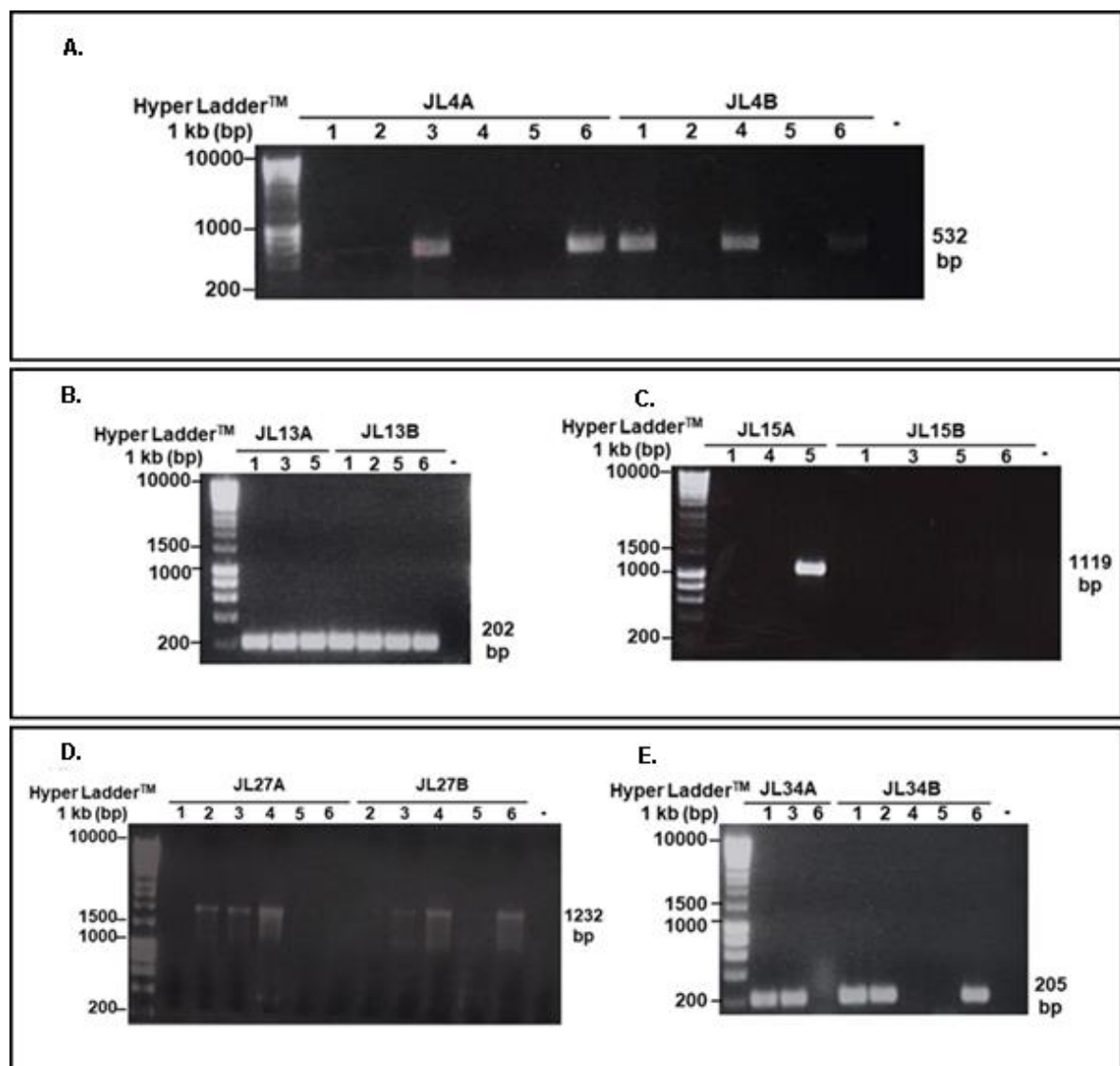
Figure 2.9. 1% agarose gels from RT-PCR show the transgenic plants that contain different transcription factor genes. There are 23 plants contained transcription factor genes; 4 plants from *JL4* (A), 7 plants from *JL13* (B), 1 plant from *JL15* (C), 6 plants from *JL27* and 5 from *JL34* (D). Each *JL* rice plants contained the different maize gene which might alter photosynthesis as shown in Table 2.2.

2.5.1.3. The leaf structure of *JL4, JL13,JL27* and *JL34*

28 day-old of rice leaf 6 were sectioned by Technovit technique. 6 anatomical parameters were quantified to allow comparison of the different lines. These parameters were BS area, MC area, the ratio of MC and BS cell area, the degree of MC lobing, MC circularity, and the interveinal (IV) distance between two minor veins to screen a series of transgenic rice plants to observe the variation in rice leaf anatomy, focusing on BS size, MC size and shape. The non-transgenic rice plants of *JL15* were selected as control, which illustrated from Fig. 2.10-2.15.

From Fig 2.10, the bundle sheath cell area showed a spread in mean value from approximately 30 μm^2 in *JL4B*, plant number 6, to 70 μm^2 in *JL34B*, plant no.2. Interestingly, the control line samples showed some of the smallest bundle sheath cells with most of the transgenic lines showing larger bundle sheath cells. Line 34B showed the largest bundle sheath cells but this was not significantly different from that observed in the controls (Kruskal-Wallis test, p =0.0628). On the other hand, MC area of *JL* lines was different from a control line (Fig. 2.11, Kruskal-Wallis test, p = 0.0326) and varied ranging from around 110 μm^2 in *JL4A*, plant no.3 (*JL4A3*) to almost 200 μm^2 in *JL27A*, plant no.3 (*JL27A3*), with no difference between the JL lines. When the ratio of mesophyll cell size to bundle sheath cell size was calculated, a large degree of variation was observed, for example, line *JL27A3* displaying relatively large bundle sheath cells relative to mesophyll cells. Statistical analysis did not reveal any significant difference between any of the samples for any of the parameters measured in Fig. 2.12 Kruskal-Wallis test (p = 0.3323).

With respect to the degree of lobing (lobiness) was calculated by the ratio of MC perimeter to convex hull of MC perimeter to investigate MC shape. The calculation of this parameter is displayed in Fig. 2.6 A small value of lobiness indicated the less lobing of mesophyll cells. The result from Fig. 2.13 showed the difference between JL lines and control with a large variation between the different lines (Kruskal-Wallis test, p = 0.0061). Notably, mesophyll cells in line *JL4A* seemed to be higher lobed than the control lines, whereas cells in line *JL13B* appeared to have a lower lobing value. However, MC shape (lobiness and circularity) did not change among *JL* lines and control. (Fig. 2.14, Kruskal-Wallis test, P = 0.0563).

Assessment of interveinal distance (Fig. 2.15, Kruskal-Wallis test, p = 0.0910) indicated that although there was some variance in this parameter between the various transgenic lines, the mean values appeared comparable to those measured in the control line. Replicate number restricted statistical analysis, but only a few plants seemed to have values distinct from the control (e.g., line *JL4B*, plant no.1 or *JL4B1* , *JL27A* plant no.3 or *JL27A3*).

Due to the limited replicate number and the spread of values recorded, the results from the measurement of leaf anatomical structures showed no difference between transgenic rice plants and a control plant. Interestingly, the MC lobing value of some *JL* lines such as *JL4A* and *JL27B* seemed different from a control. So, the lines showing the more extreme range in cell lobing might be interesting candidates
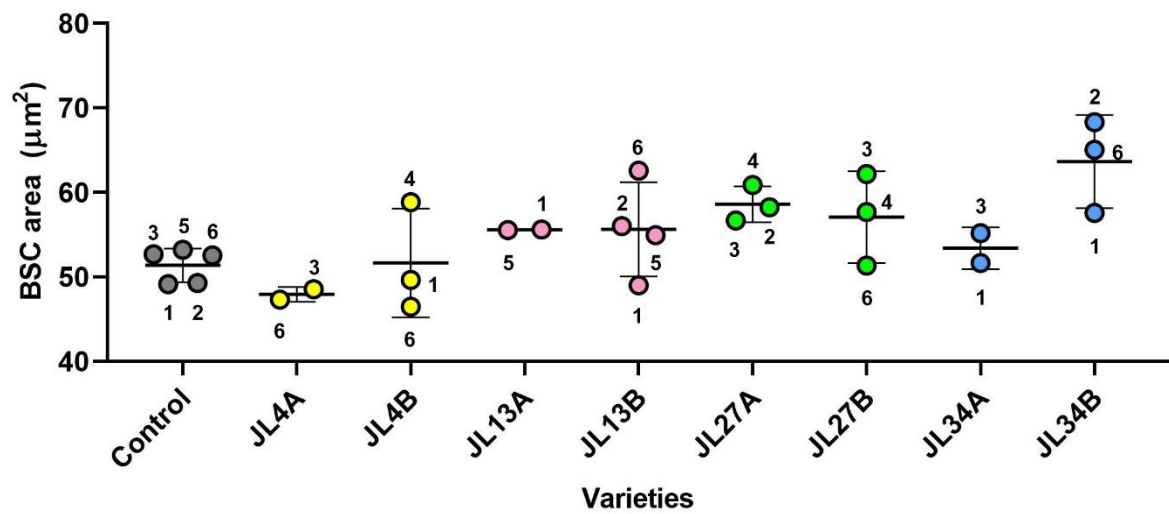
Figure 2.10. The data from rice leaf 6 of 8 transgenic rice plants (28 days old) were analysed the average of BS area by Fiji image J script (BS pixel area) and showed in a scatter plot with mean (horizontal bar) and SD (error bar). The individual dots and numbers represented the replication number of each varieties. Statistical analysis was calculated by Kruskal-Wallis test (p = 0.0628).
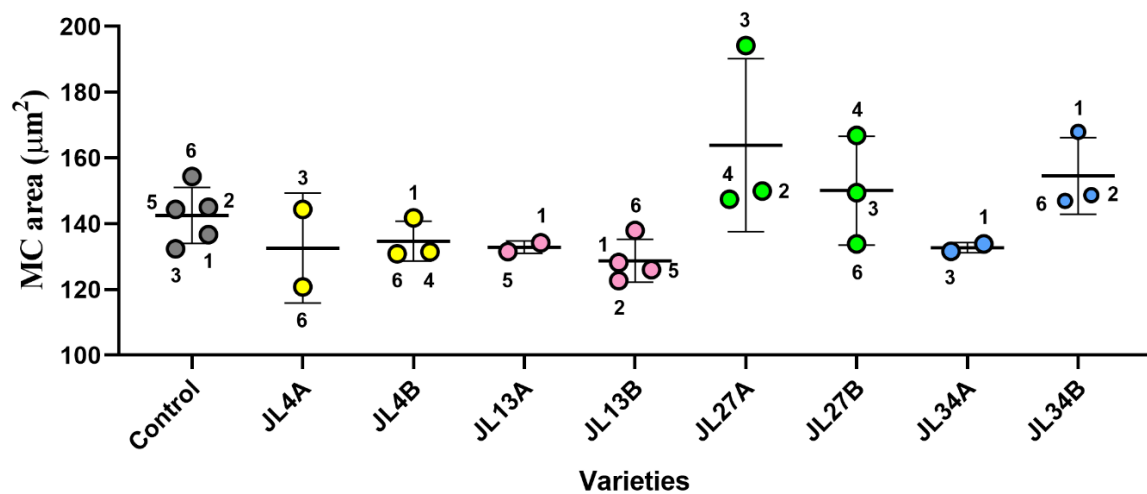
Figure 2.11. The study gathered data from the rice leaf 6 of transgenic *JL* rice plants that were 28 days old, and used Fiji image J script to measure the MC area of cells in layer 3. This data was displayed in a scatter plot that featured horizontal bars to indicate the mean and error bars to show the standard deviation (SD). Each data point and corresponding number on the plot represented the replication number of a particular rice variety. Statistical analysis was analysed by Kruskal-Wallis test. (p = 0.0326).
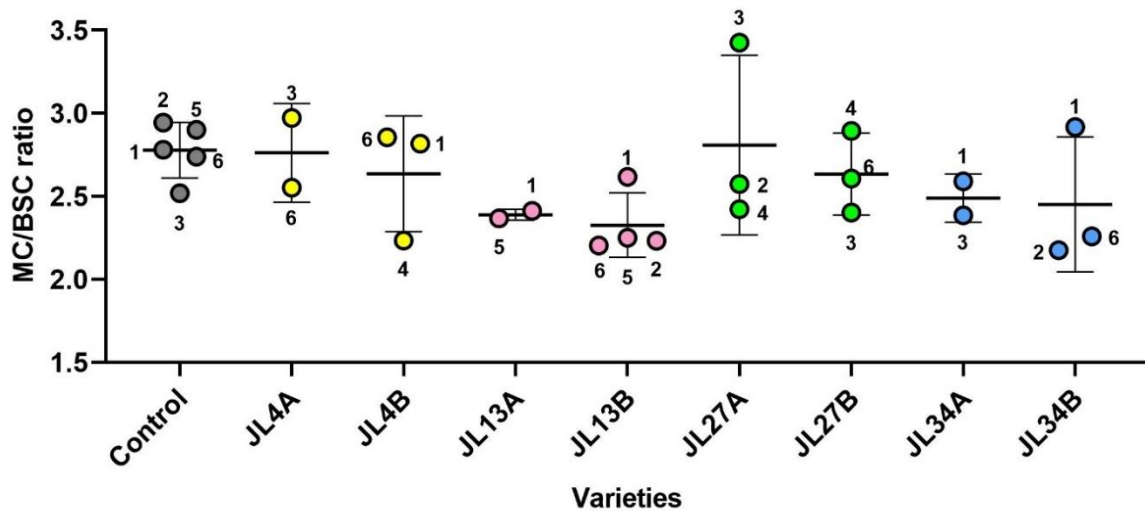
Figure 2.12. The ratio of MC/ BSC area of selected *JL* lines (28 day old of leaf 6) was calculated by mesophyll pixel area divided by bundle sheath pixel area as shown in Fig.6. The data were plotted on scatter plot with mean and SD values, which displayed in horizontal and error bar respectively. The replication number also displayed on the plot in dots with different colours. Kruskal–Wallis with p = 0.3323.
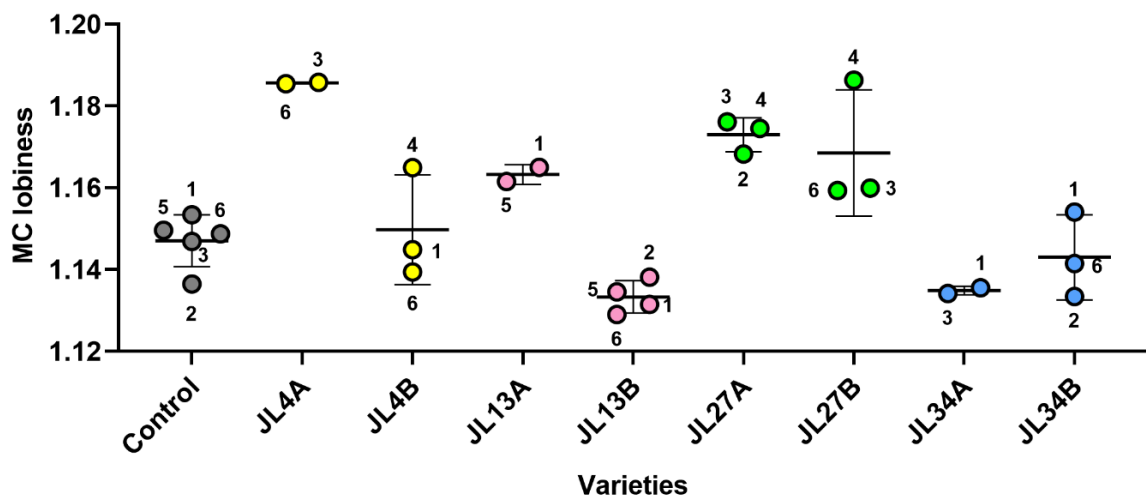
Figure 2.13. A 28-day old of *JL* rice leaf 6 was measured MC lobiness by FIJI image J script by using the formular as shown in Fig. 2.6 (the division of MC pixel perimeter and MC convex hull perimeter). All Mesophyll cells located at layer 3 between two minor veins were calculated and plotted on the scatter plot. The higher value showed the more degree of cell lobing. Mean, SD and replication number (dots with different colours) displayed in the plot. Kruskal–Wallis, one-way ANOVA was performed with p = 0.0061.
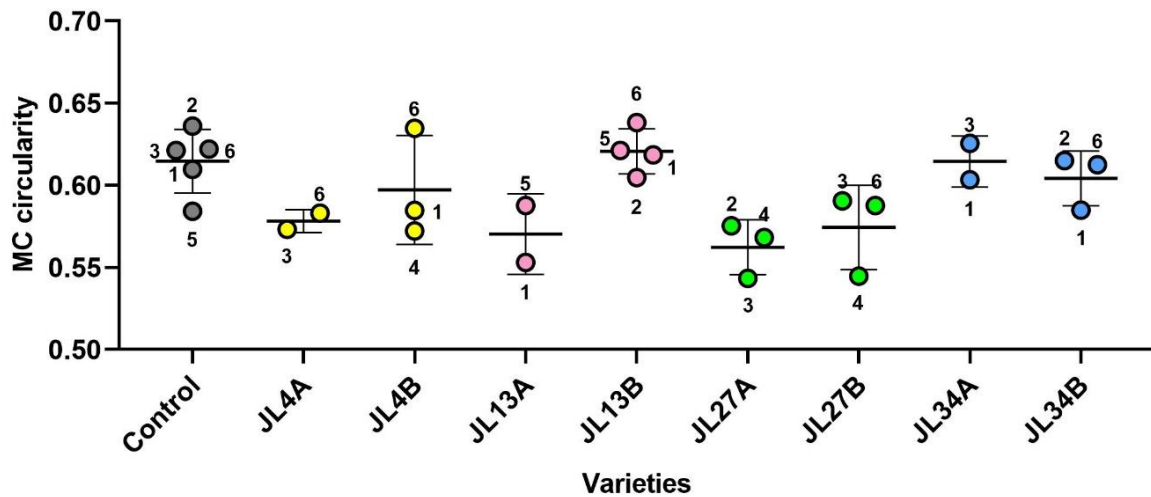
Figure 2.14. The data represented the measurement of mesophyll circularity of *JL* lines from each rice leaf 6 (28 days old). MC circularity was measured by the pixel of cell circularity at layer 3 by using Fiji image J script to observe the cell roundness. The data was showed in a scatter plot with mean (horizontal bar) and SD (error bar). Less value described an increase cell circularity. The individual dots and numbers represented the replication number of each varieties. Statistical analysis was calculated by Kruskal-Wallis test with Dunn's multiple comparisons (p = 0.0563).
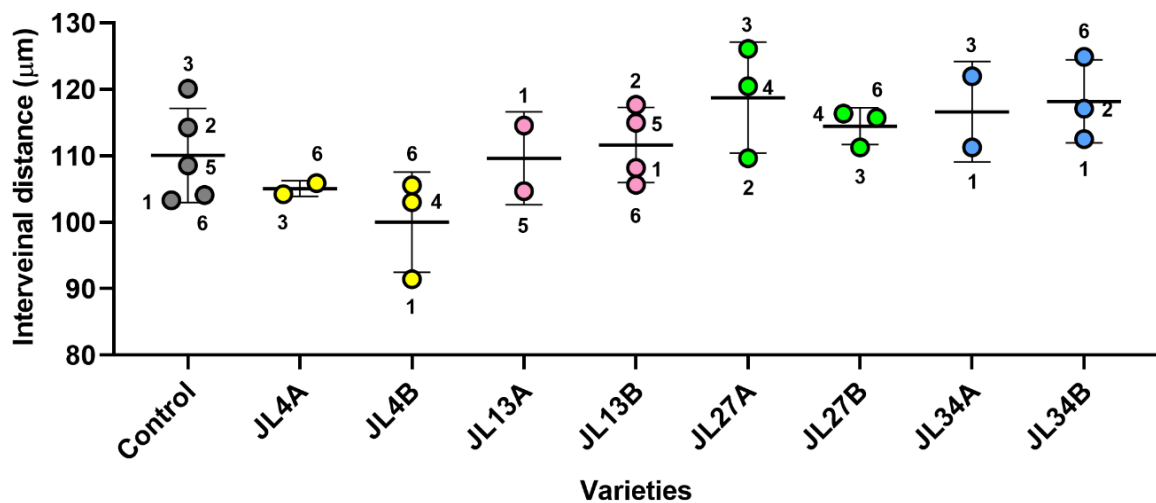
Figure 2.15. The target area of interveinal distance between two minor veins of JL-rice plants and a control (28 days old) was analysed and showed in the individual scatter plot with mean and SD. Each dot and number on the scatter plot indicated the replication number for each variety. Statistical analysis was calculated by Kruskal-Wallis test with Dunn's multiple comparisons (p = 0.0910).

2.5.2. The anatomical and biological measurement of selected *JL* rice leaves

2.5.2.1. The anatomical leaf structure of *JL4A* and *JL27B*

To confirm the internal leaf structures of the selected transgenic rice lines (*JL4A3,JL4A6 JL27B4* and control) from the previous experiment were grown in the same condition. Leaf 6 from 21 to 28 days old rice plants were sectioned by Technovit method. The 6 parameters of leaf structure; BSC area, MC area, MC lobiness, MC circularity, leaf thickness and IV distance were measured to observe the difference of cell size and shape between transgenic rice plants.

In the part of BSC area, the BS size of 3 *JL* lines showed no difference from a control plants as shown in Fig. 2.16A (Kruskal-Wallis test, p = 0.9925). Similar to MC area, The size of mesophyll cells in all 5 layers (Fig. 2.16B, Kruskal-Wallis, p = 0.1770) and individual layers (Fig. 2.17A-E) did not undergo any change when compared to a control line. With respect to MC shape, mesophyll lobiness in each layer was measured. Fig. 2.18A-E. displayed a significant decrease of MC lobing of 3 *JL* lines in in each layers (from 1 to 5) with p value less than 0.05. The degree of cell lobing of the *JL* lines in layer 3 was the lowest, which went down around 6.6% (Fig. 2.18C), whereas cell lobing in the other layers declined approximately 3-5% from controls. In addition, MC of lobiness of all mesophyll cells in 5 layers had less lobbed than a control plant (Fig. 2.18F, Kruskal-Wallis test, p = 0.0075). To validate cell lobing, the circularity value was calculated to investigate the degree of cell roundness. The higher values indicated a more circular shape. Figure 2.19F. illustrated a significant increase in circularity of the transgenic plants in all layers (Kruskal-Wallis, p = 0.0143) and in individual layers (Fig. 2.19A-E).

Leaf thickness and IV distance displayed a large variation between the different lines. Although, The size of MC and BS cells of *JL* lines were not different from a control plant and also leaf thickness (Fig. 2.20A, Kruskal-Wallis test, p = 0.1636) and IV distance values (Fig.2.20A, Kruskal-Wallis test, p = 0.2713) did not change. These results suggested that the inserted maize genes in the selected JL rice plants altered mesophyll cell shapes especially lobiness, but the genes did not alter MC size and other internal leaf structures. Due to the extreme range in MC lobing in all three

transgenic lines , these were taken forward to determine leaf gas exchange and the outcome on photosynthetic performance.
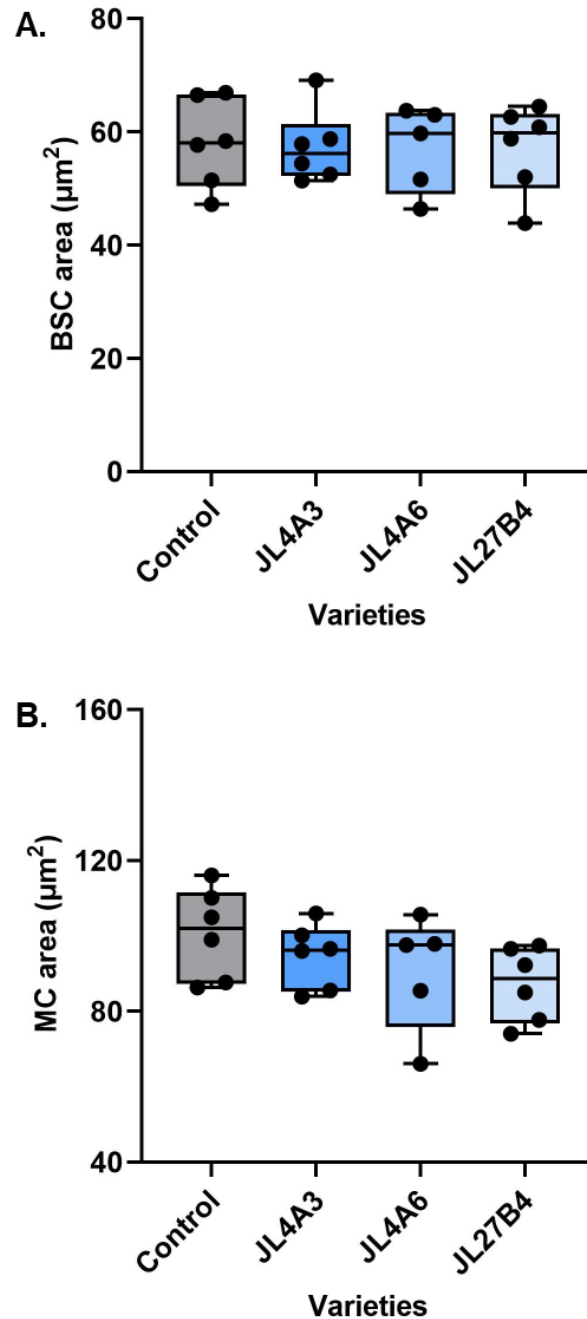
Figure 2.16. The graphs represented the measurement of bundle sheath (BS) and mesophyll cell (MC) area of *JL4A3, JLA6 and JL27B4*. The sections of rice leaf 6th of selected *JL* lines (28 days) were observed BS and MC under a light microscope before being captured and analysed by Fiji image J software. The image J script was applied to estimated cell size by calculating from the pixel of BS and MS cells as shown in A and B respectively. Box and Whiskers also represented min (minimal value), max (maximal value), and SD value (horizontal bar). small dots represented the replication number of each samples (n (Control) = 6, n (*JL4A3*) = 6 , n (*JL4A6*) = 5, and n (*JL27B4*) = 6). Kruskal-Wallis statistical was performed with p = 0.9925 (A) and p = 0.1770 (B).
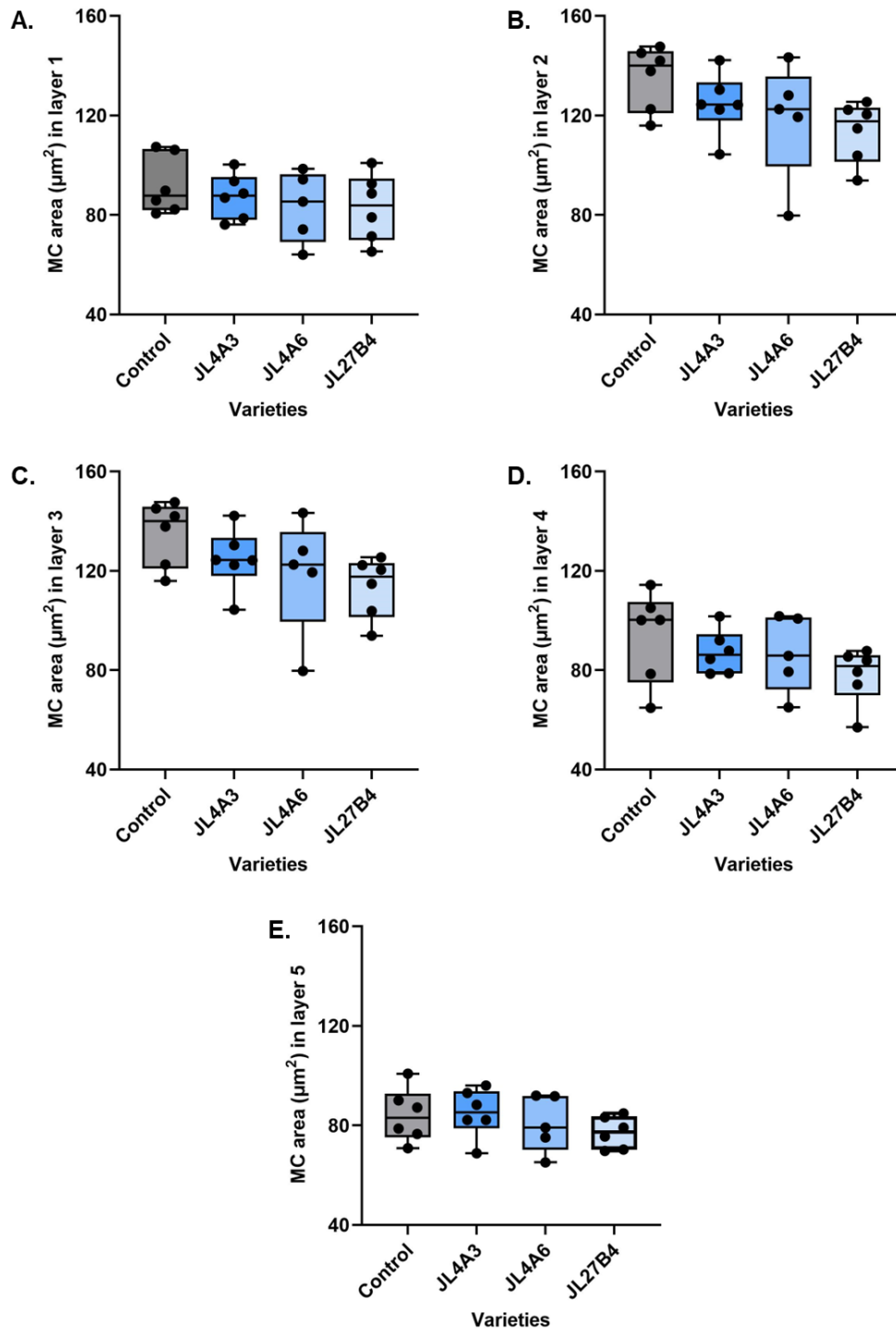
Figure 2.17. The data represented the measurement of mesophyll size in different layers of *JL4A3, 4A6 and 27B4*.The 28 day-old *JL* rice leaves were analysed MC area in 5 layers (A-E), which located between two minor veins from the middle of leaf 6th by calculated from the FIJI Image J script. The mean and SD values showed in the Box and Whiskers bar. This bar also showed the min and max values of MC size of each samples. The replication of each sample is n = 6 for Control, *JL4A3* and *JL27B4* and n = 5 for *JL4A6*. Kruskal-Wallis statistical test was performed with p = 0.6633 (A), 0.2929 (B), 0.05 (C), 0.4116 (D) and 0.5049 (E).
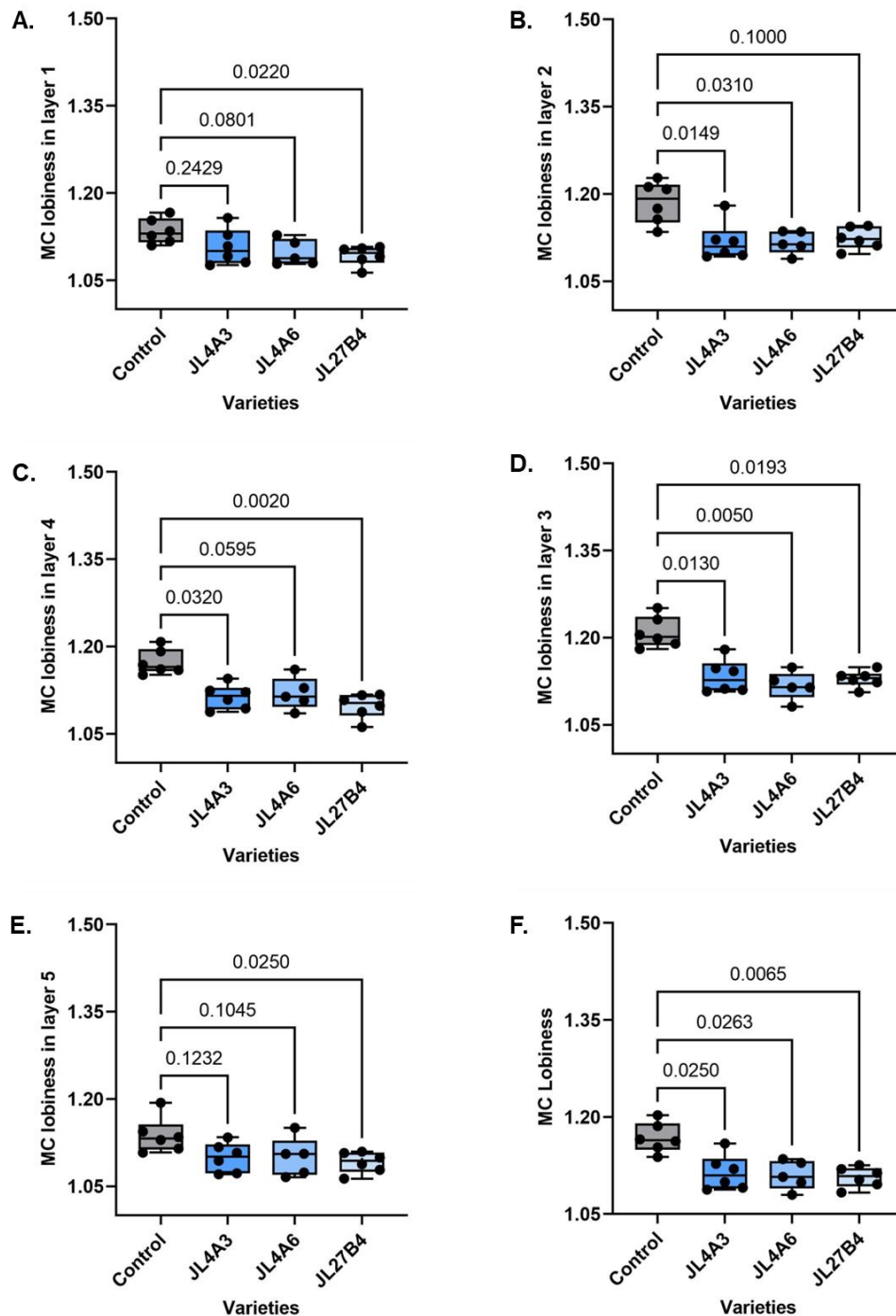
Figure 2.18. The graphs displayed the measurement of mesophyll lobiness in different layers of *JL4A3, 4A6* and *27B4.* The sections of rice leaf 6th of selected *JL* lines (28 days) were measured the degree of cell lobing in 5 layers (A-E). F, All MC of a leaf were also estimated by calculating from the ratio of MC pixel area to MC convex hull area. The less value of lobiness displayed the less lobed of mesophyll cell, The Box and Whiskers represented the min, max, mean and SD values with dots showed the replication number of individual samples. Statistical was analysed by Kruskal-Wallis statistical, Dunn's multiple comparisons with the presence of p values on the graphs.
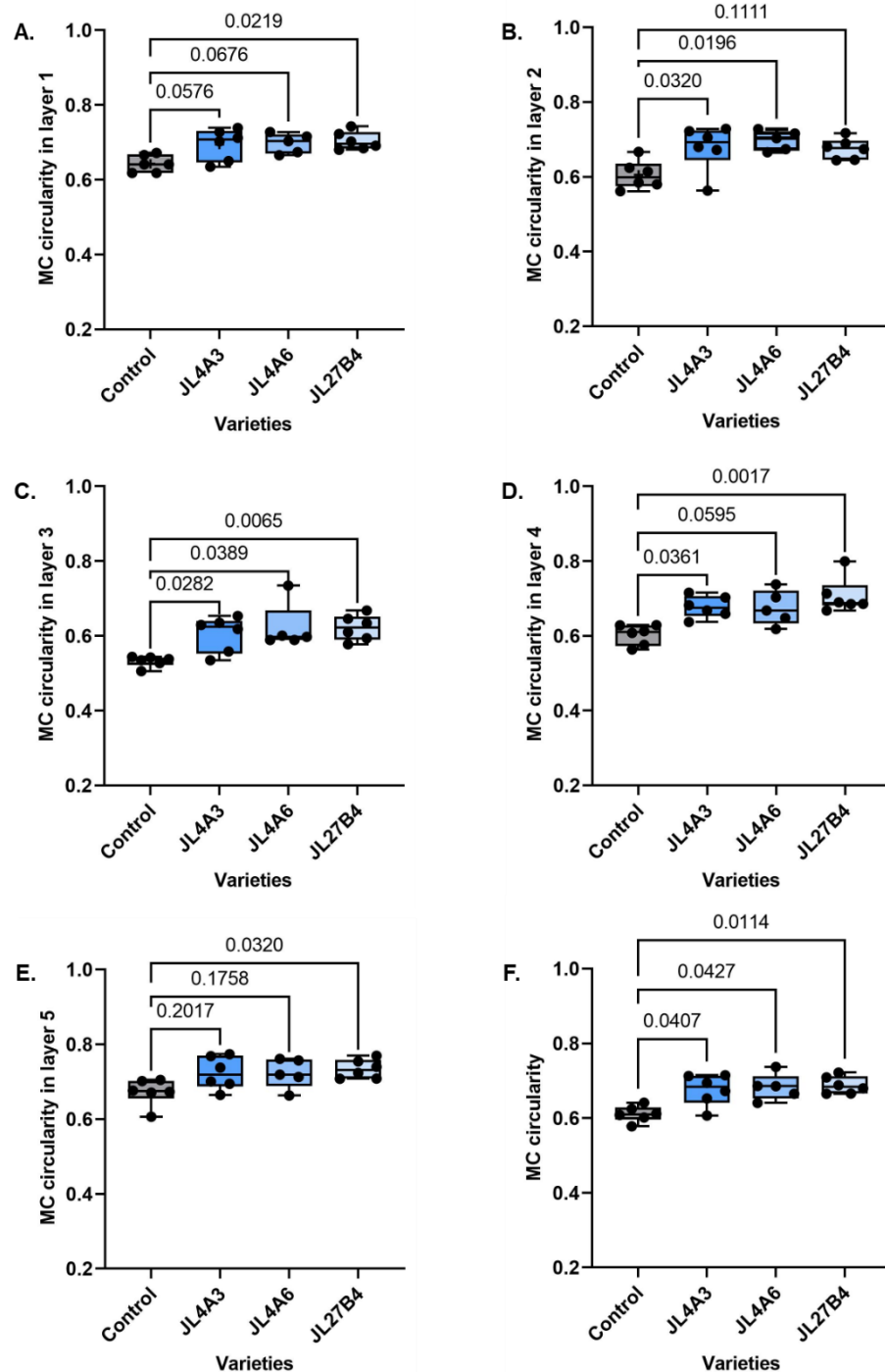
Figure 2.19. This figure showed the measurement of mesophyll circularity in different layers of *JL4A3, 4A6* and *27B4*. The sections of rice leaf 6 of selected *JL* lines (28 days) were measured the roundness of the cells located in five layers by calculating from the pixel of mesophyll circularity as showed in Box and Whiskers A-E. F, All MC circularity of a leaf were also analysed. The min, max, mean and SD values also showed on the graphs. The higher value represented the more circular of a cell. Statistical was calculated by Kruskal-Wallis statistical, Dunn's multiple comparisons. p values were shown on the graphs.
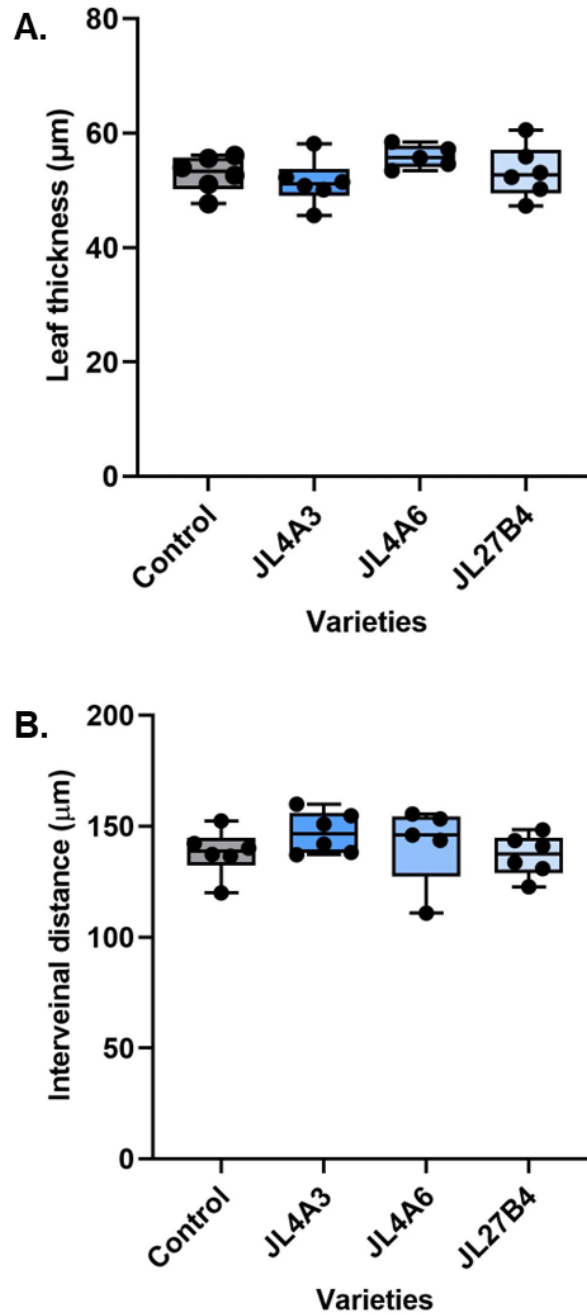
Figure 2.20. The leaf thickness and interveinal (IV) distance in different layers of *JL4A3, 4A6* and *27B4* was estimated from the sections of rice leaf 6 (28 days).To measure leaf thickness, the upper and lower epidermis were considered (A), and the distance between two minor veins was used to measure IV distance (B). Fiji Image J software was employed for these measurements. The Box and Whiskers plot displayed mean and SD values, while the highest and lowest values were also represented on the plot. The replication number for the control group, *JL4A3,* and *27B4* was 6, whereas 4A6 had 5 replicates. Kruskal-Wallis was used to calculated statistical data (p = 0.1636 (A) and 0.2713 (B)) with Dunn's multiple comparisons..

2.5.2.2. The photosynthetic performance of *JL4A* and *JL27B*

To investigate the potential link of altered cell lobing and size on photosynthesis in different CO_2 levels, the net CO_2 entering and H_2O (g) evaporating through stomata pores were measured by gas exchange (LI-COR). The parameters involved in photosynthesis such as CO_2 A rate, PhiPSII and stomatal conductance (g_s) from this analysis were plotted against the different C_i values, which showed how plant responded to different C_i levels started from 50, 100, 150, 200, 250, 300, 400, 500, 700, 800, 900, 1000, 1200, and 1500 ppm of CO_2, which illustrated in Fig.2.22, 2.24, 2.26 and 2.27.

The initial stage of A/C_i curve, CO_2 A of plants constantly increased as a linear response to an increased CO_2 level. At 400 ppm of CO_2 , the graph slowly increased and changed to a plateau of maximal A. The 3 transgenic lines and control plants showed the similar curve pattern, but the CO_2 A of *JL* lines tended to be lower compared to non-transgenic rice plants (Fig. 2.21). The CO_2 A of each *JL* lines was compared to the A rate of control plant in ambient CO_2 level (400 ppm) and high CO_2 level (1500 ppm) as shown in the scatter plot with mean and SD data (Fig. 2.22A and B). Both 400 and 1500 ppm were the estimated values of CO_2 conditions inside a leaf not being stable in the chamber. The results showed that A rate of *JL 4A3, 4A6* and *27B4* rice plants decreased significantly compared to the control plant at 400 ppm of CO_2 (Fig. 2.22A, Kruskal-Wallis test, $p = 0.0075$). On the other hand, the A rate of 3 *JL* lines at high CO_2 concentration showed no difference between lines (Fig. 2.22B, Kruskal-Wallis, $p = 0.0587$).

PhiPSII was also determined in both transgenic rice plants and non-transgenic rice plants (Fig. 2.23). The trend of the PhiPSII curves of rice plants is similar to AC_i curves, but PhiPSII of *JL* lines seemed lower than the control. After plotting the values of PhiPSII versus C_i at 400 and 1500 ppm of CO_2. the results (Fig. 2.24A) displayed a significant decline of PhiPSII value in *JL4A3* and *JL4A6* at ambient condition ($p = 0.0067$), but not in *JL27B4*, whereas PhiPSII of transgenic plants at high CO_2 did not change when compared to the control (Fig. 2.24B, Kruskal-Wallis, $p = 0.0667$).

With respect to the stomatal conductance (g_s), the data from Fig. 2.25 showed that the g_s of *JL* rice plants seemed lower than control. However, the statistical test presented no difference in g_s between transgenic rice and control at different CO_2 conditions, although the tendency for decreased stomata conductance of *JL* lines was interesting (Fig. 2.26A and B). In addition, the analysis of the AC_i curve was used to calculate more specific parameters, such as maximum carboxylation rate (V_{cmax}), maximum rate of electron transport for RuBP regeneration (J_{max}) and triose phosphate utilization (TPU) involved in CO_2 A. The results showed the variation of V_{cmax}, J_{max} and TPU values between *JL* lines and control. Interestingly, the J_{max} values of *JL4A3* and *JL4A6* were significantly decreased when compared to non-transgenic rice (Fig. 2.27B, (Fig. 2.24B, Kruskal-Wallis test, p = 0.0093) whereas the V_{cmax} and TPU of transgenic rice plants were not different from control (Fig. 2.27B-C).

These data suggested that the degree of MC lobing might be linked to the photosynthetic performance, especially at 400 ppm in term of enzyme kinetic processes or stomatal properties. The lower of C_i might affected to the ribulose 1-5-bisphosphate oxygenase/carboxylase (Rubisco) and other enzymes, which could activated the change of Rubisco activity (V_{cmax}) and the capacity of RuBP regeneration (J_{max}). Even though the g_s of transgenic plants represented no significant change, the result tended to be lower when compared to a control plant. So the stomatal properties such as stomatal anatomy and the maximum stomatal conductance (g_{smax}) were interesting to further investigate in the next step.
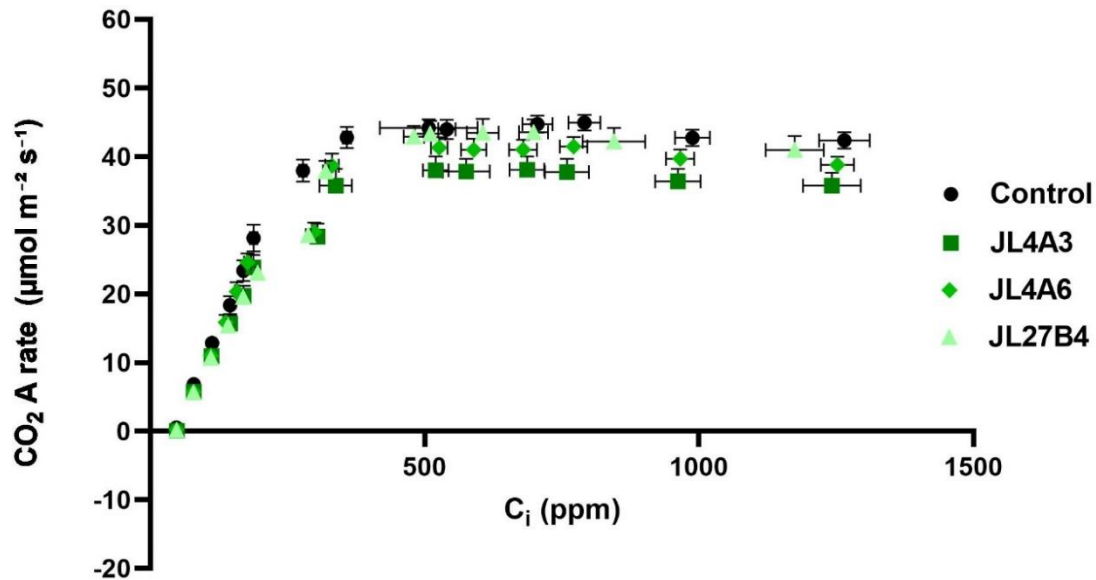
Figure 2.21. A 28-days old of *JL* rice leaf 6th was measured of CO_2 assimilation (A) rate of selected *JL* rice plants in different CO_2 conditions by LI-COR under several C_i conditions ranging from 50 ppm to 1500 ppm. All data were plotted in A/C_i curve with standard error of the mean (SEM) and mean Each plant varieties represented in the different symbols and colours.
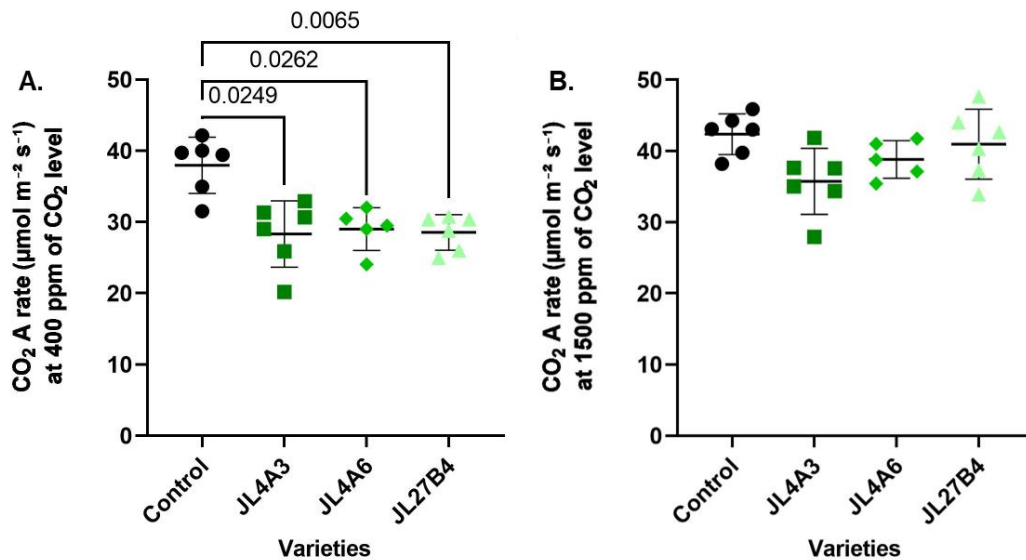
Figure 2.22. scatter plots showed mean and SD data of CO_2 A of 3 *JL* lines compared to a non-transgenic line at ambient (400 ppm) and high CO_2 (1500 ppm) conditions as shown in A and B. Each spot meaned the replication number (n) of control, *JL4A3, 4A6* and *27B4*, which were 6, 6, 5 and 6 respectively. The statistical analysis was performed using Kruskal-Wallis test (p = 0.0075 (A), 0.0587 (B)) with Dunn's multiple comparisons. The p-values from multiple comparisons were displayed on the graphs.
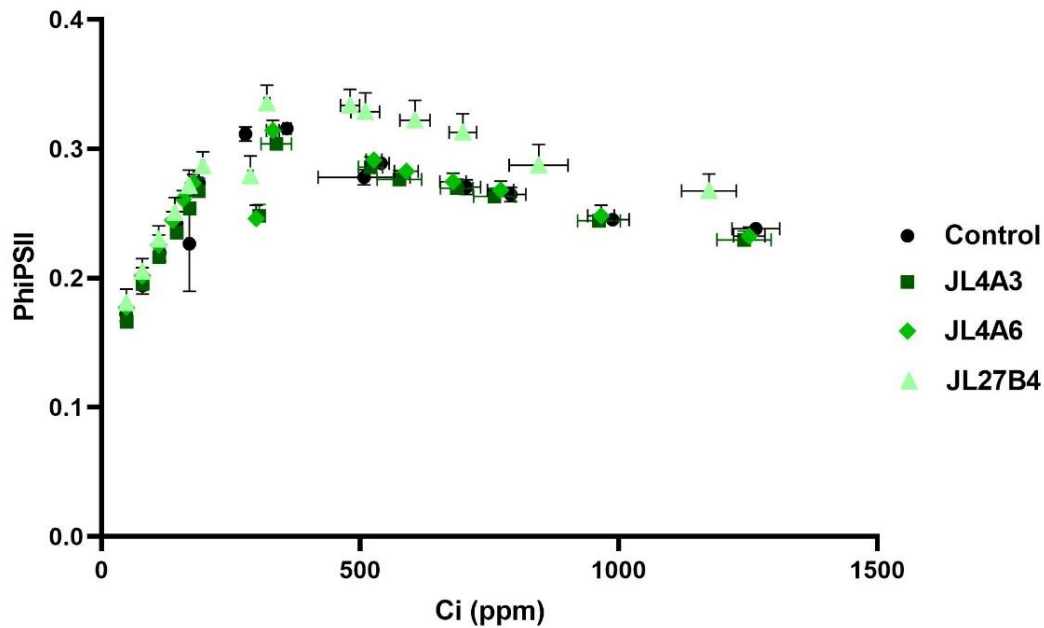
Figure 2.23. After gas exchange analysis of rice leaf 6th (28-days old) from 3 *JL* lines, All data of PhiPSII (Y-axis) were plotted against different CO_2 levels (50-1500 ppm) as displayed on X-axis. Mean and SEM values were calculated, which also represented in the curve.
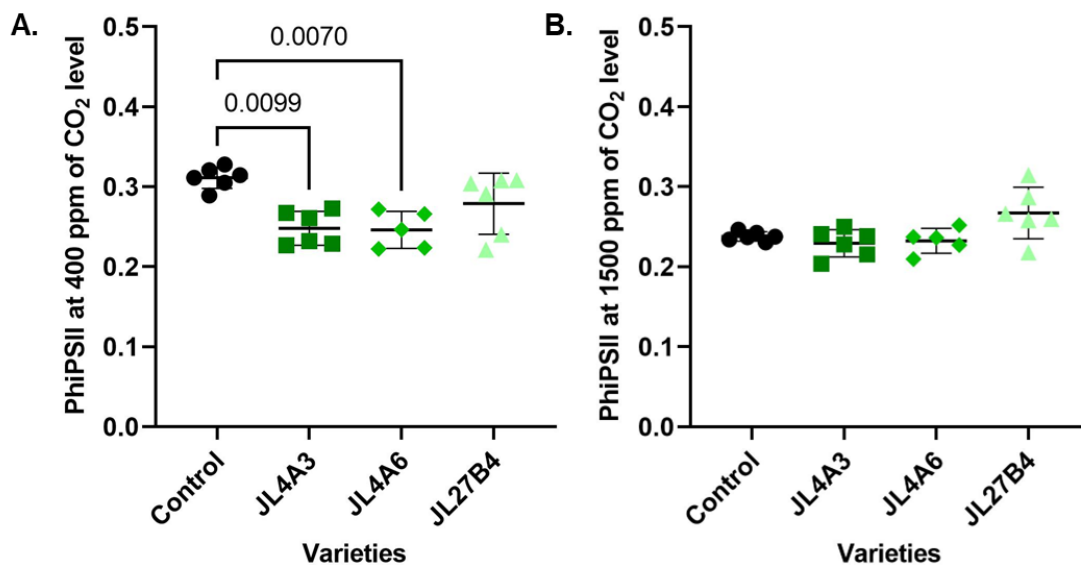
Figure 2.24. The figure represented mean and SD data of PhiPSII of *JL* transgenic lines compared to a control line at ambient CO_2 level, 400ppm (A) and high CO_2 level, 1500ppm (B), which represented in A and B. The replication number (n) displayed in small dots (n=6 for control, *JL4A3*, and *JL27B4* and n= 5 for *JL4A6*). The statistical analysis was performed using Kruskal-Wallis test (p = 0.0067 (A), 0.0667 (B)) with Dunn's multiple comparisons. The graphs included the presentation of the p-values of multiple comparisons.
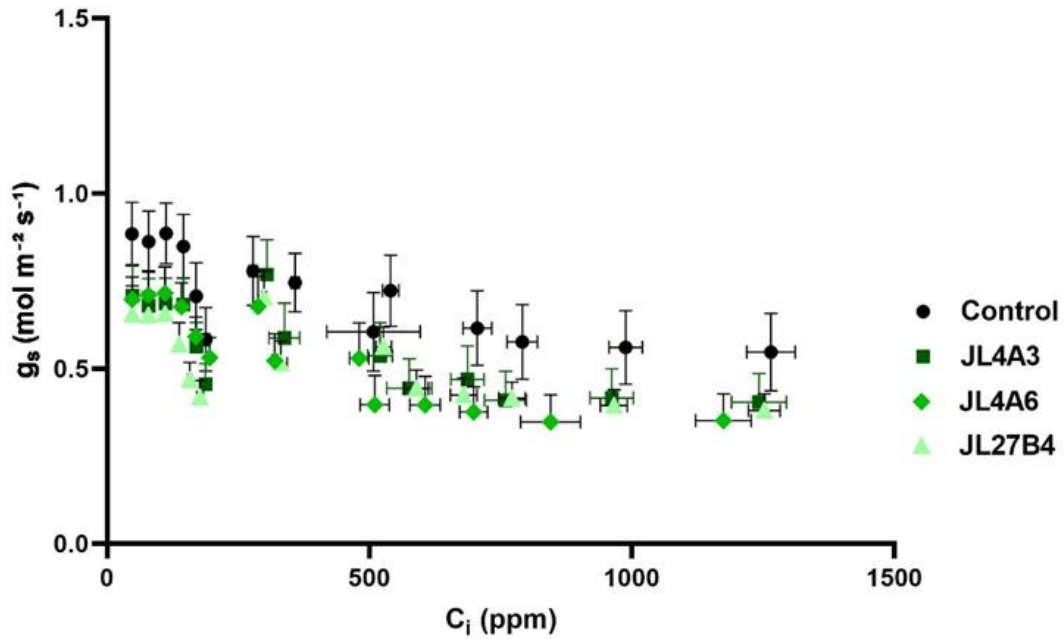
Figure 2.25. From LI-COR analysis, g_s values of 28-days old of 3 *JL* plants were plotted on the curve against the different C_i levels varied from 50 ppm to 1500 ppm. Each dots represented mean and SEM of each lines, which shown on horizontal and vertical lines respectively.
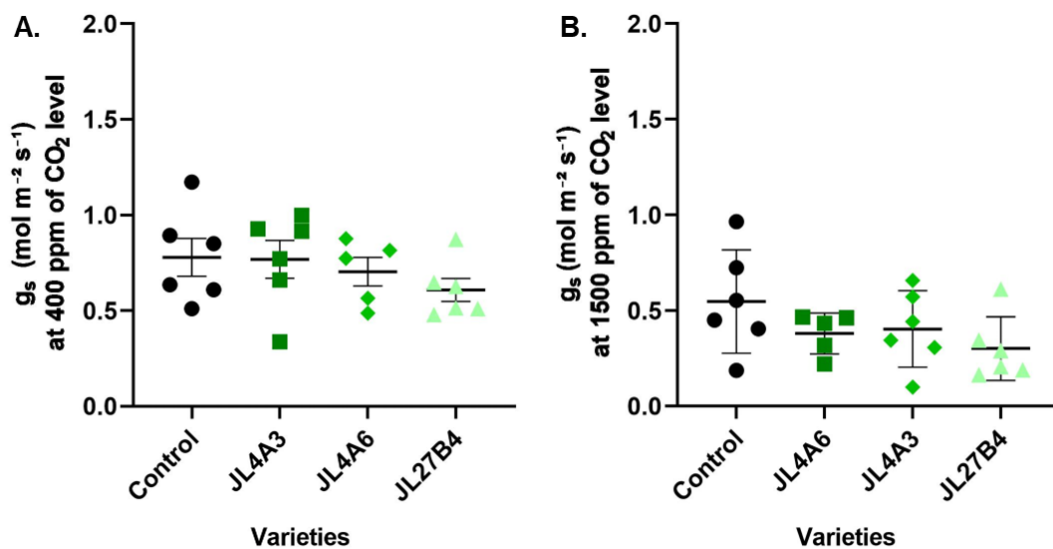
Figure 2.26. The g_s values of each transgenic rice lines (28-days old) from LI-COR measurement were plotted on the scatter plots at ambient (A) and high CO_2 (B) levels. The data also represented mean (horizontal line) and SD (vertical line) values. Each dots displayed the replication number, which were 5 for *JL4A6* and 6 for control, *JL4A3* and *JL27B4*. The statistical analysis was analysed by Kruskal-Wallis test (p = 0.3807 (A), 0.3179 (B)).
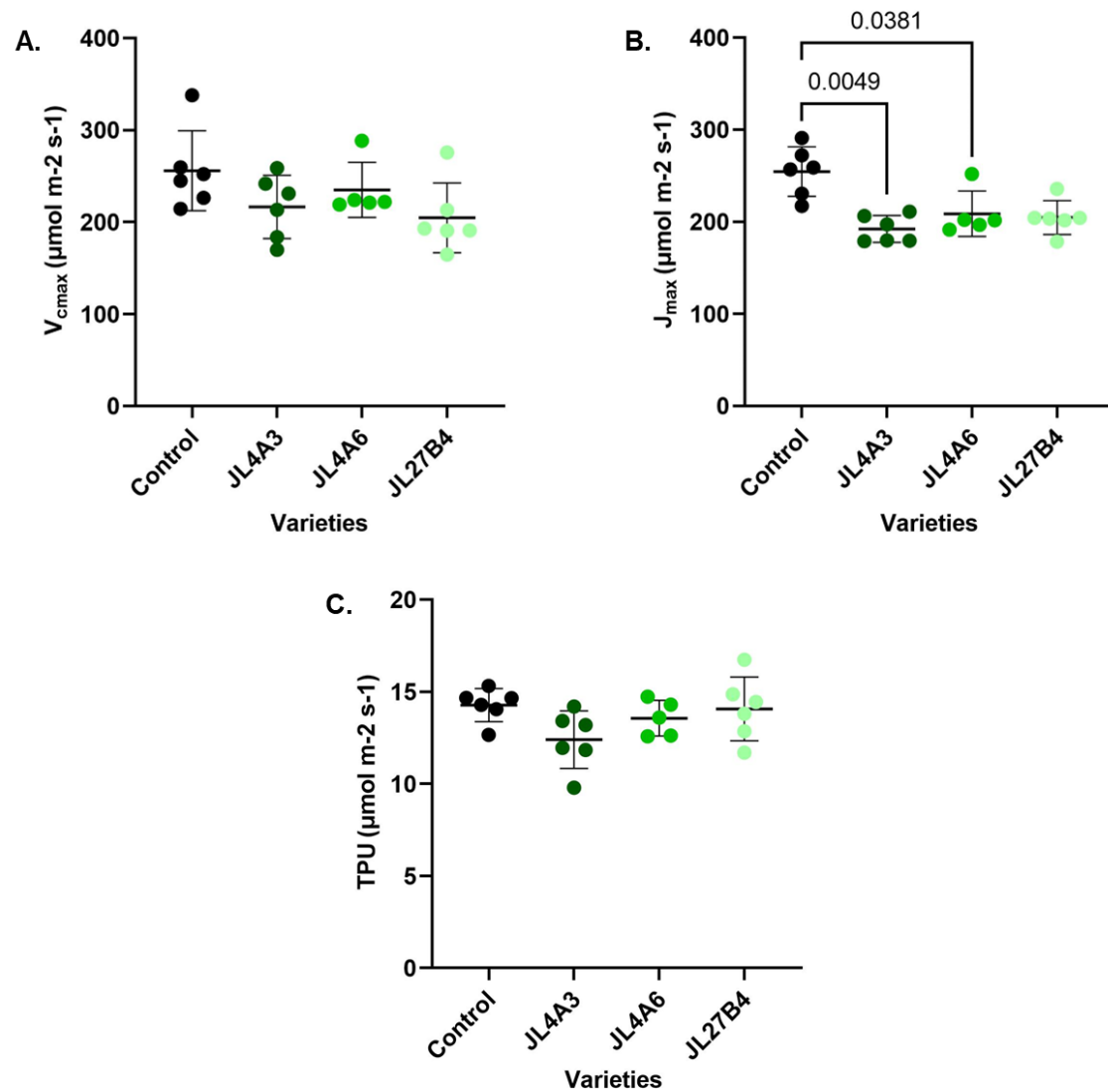
Figure 2.27. The data displayed the measurement of the maximum carboxylation rate (V_{cmax}), maximum rate of electron transport (J_{max}) and triose phosphate utilization (TPU) in the selected *JL* transgenic rice plant A/C_i curve was further analysed 3 more parameters; the J_{max}, V_{cmax} and TPU. All data were plotted in the individual data plots with mean and SD as shown from A-C. Each dots represented the replication number of each samples. The statistical analysis was analysed by Kruskal-Wallis test (p = 0.0913 (A), 0.0093 (B), 0.1276 (C)) with Dunn's multiple comparisons.

2.5.2.3. Stomatal measurement of *JL4A3, JL4A6 and JL27B4*

To investigate stomatal properties, the imprints of leaf 6th from 3 *JL* lines and control were observes and captured under the light microscope (LM) at the different magnifications; 20X for cell count and 40x for stomatal characteristics. 5 parameters were estimated, which were stomatal density, stomatal area, guard cell area (GC), pore length and g_{smax}. The g_{smax} value was used as an indicator of the gas exchange capacity of a leaf as represented in Fig. 2.28-2.29.

For the stomatal features, the stomatal area, GC area and stomatal pore area were estimated by the equation from Dow et. al, (2014; 2017). The result represented a variation of mean and SD between *JL* lines and control (Fig.2.28A-C). the estimated stomatal size of three *JL* lines seemed to be smaller than a control line, only *JL* 27B4 showed significantly decrease comparing to control plant (Fig. 2.28A, Kruskal-Wallis test with Dunn's multiple comparison, p = 0.0042). Similar to GC was decrease with statistical difference in *JL27B4* when compared to non-transgenic line (Fig. 2.28B, Kruskal-Wallis test with Dunn's multiple comparison, p = 0.0090). In Fig. 2.28C, JL4A6 (Kruskal-Wallis test with Dunn's multiple comparison, p = 0.0211) and JL27B4 (Kruskal-Wallis test with Dunn's multiple comparison, p = 0.0075) also displayed a decline of pore length between *JL* lines and control (Fig. 2.28C).

The numbers of stomata was also counted to calculate the stomatal density as showed in Fig. 2.29A. The individual plot showed the spreading mean values with SD of stomata density in *JL* lines ranging from around 100 to 200 stomates per mm^2, which significantly declined comparing with control (approximately 260 to 300 stomates per mm^2) (Kruskal-Wallis test, p = 0.0077). Then, the stomatal size and density were used to measure the maximum stomatal conductance (Anatomical g_{smax}) as showed in Fig. 2.29B. The graph displayed a significant almost twofold decline of g_{smax} values in *JL* lines (Kruskal-Wallis test, p = 0.0032). Together with the results from Fig. 2.28A and B suggested that the small size of stomata and the low numbers of stomata leaded to a decrease of g_{smax}.

Interestingly, the *JL* rice leaf contained less lobed of mesophyll cells affected to the changes of the stomatal properties especially stomatal density and the anatomical gs max. These results could lead to the questions that is altered mesophyll cell lobing in

rice *JL* lines linked to altered stomatal function? And what is the link between mesophyll cell lobing and stomatal function? For the next step, rice overexpressing *EPF1_oe* (with low stomata density) and overexpressing *EPFL9_oe* (with high stomatal density) were further investigated to validate the link between MC lobing and the stomata properties.
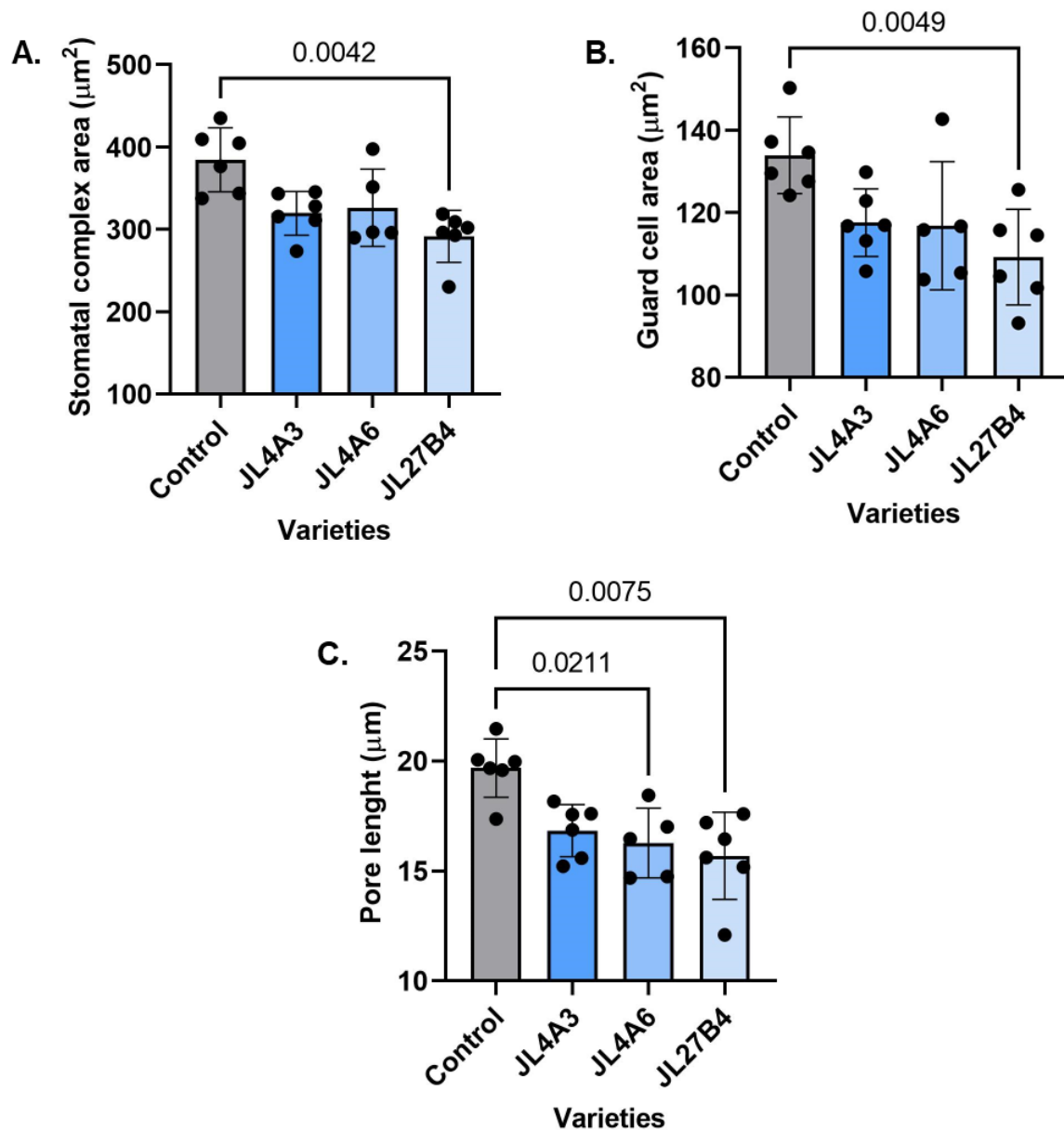
Figure 2.28. The picture represented the measurement of the stomatal characteristics of *JL4A3, JL 4A6* and *JL27B4* comparing to a control rice plant. The 28 day-old of *JL* leaf 6 was stomatal area, GC area, and pore area of 3 *JL* transgenic rice plants compared to IR64 as a control, which showed on the scatter plot and bar graph A - C. The data on bar graphs represented mean and SD values. The individual plots showed the replication number of each transgenic and non-transgenic plants. The graphs presented the p-values obtained from the analysis of the Kruskal-Wallis test with Dunn's multiple comparisons.
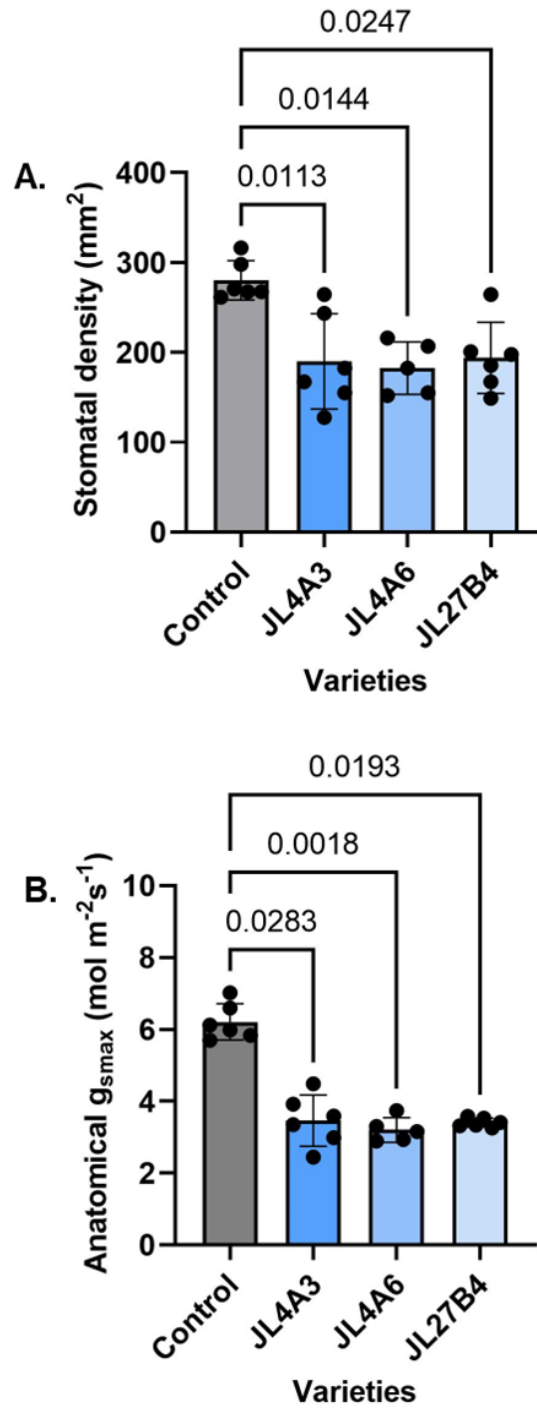
Figure 2.29. The stomata numbers of *JL4A3, JL4A6, JL27B4* and control were counted at 20X and calculated the density per mm^2 as showed in A, before being used to measure the anatomical g_{smax} (B). all information of these two values of JL lines were plotted on the scatter plots and bar graphs, which displayed mean, SD and replication numbers (n) of each rice plants (n=6 for control, *JL4A3* and *JL27B4*, n=5 for *JL4A6*). The p-values resulting from the Kruskal-Wallis test (p = 0.0077 (A), 0.0032 (B)) was performed and the p-values resulting from the Dunn's multiple comparisons were shown on the graphs in the analysis.

2.5.3. The leaf anatomical measurement of *osEPF1oe* and *osEPFL9oe* rice plants

2.5.3.1. The leaf structure of *osEPF1oe* and *osEPFL9oe* lines

Following the results of analysing the *JL* lines, *osEPF1_oeW and S*)with low stomatal density) and *osEPFL9_oeL2 and L3* (with high stomatal densities) were used to further analayse a potential link of mesophyll structure and stomatal gas exchange. Both *osEPF1_oe* and *osEPFL9_oe* lines were grown in the same condition as *JL* rice plants for 21 (*oeEPFL9_oe*) and 28 days (*osEPF1_oe*) before being sectioned to observe cell structure inside a leaf. 6 leaf anatomical features were analysed (cell lobiness and cell circularity, leaf thickness, the IV distance as shown in Fig. 2.30-2.37.

In Fig. 2.30A, The overexpressed *osEPF1_oe* lines had smaller BSC than non-transgenic IR64 rice plants with statistical significance (ANOVA, p = 0.0001). While, *osEPFL9_oe* lines had the larger bundle sheath size, especially *osEPFL9_oeL3* showed a significant increase almost 1.5 times when compared to IR64 control line (Fig. 2.30B, ANOVA, Dunnett's multiple comparisons, p = 0.0284). Similar to mesophyll size, the MC area showed a significant decrease in *osEPF1_oeW* and S as displayed in Fig. 2.31A (ANOVA, p = 0.0061), but MC size of *osEPFL9_oe* transgenic rice plants were not difference from a control line (Fig. 2.31B, ANOVA, p = 0.1961).

With respect to mesophyll shape, MC lobiness and MC circularity were calculated from MCs located in 5 different layers, which showed in Fig. 2.32A-F and 2.34A-F. Mesophyll lobiness of two *osEPF1_oe* lines had less lobed than control and showed significantly declined individual layers (Fig. 2.32F, ANOVA, p < 0.0001) with a higher cell circularity in all 5 layers (Fig. 2.33F, ANOVA, p < 0.0001). In contrast, the degree of cell lobing was significantly raised in *osEPFL9_oe* transgenic plants (Fig. 2.34F, ANOVA, p < 0.0001), which was opposite to the result of MC circularity from layer 1 to 5 as displayed in Fig. 2.35F (ANOVA, p < 0.0001).

Moreover, another 2 parameters of leaf structure namely leaf thickness and IV distance located between two minor veins were also assessed as shown from Fig.2. 36 to 2.37. The leaf thickness displayed in Fig. 2.36A significantly thinner in *osEPF1_oeW* and S (ANOVA, p = 0.0095) but were not different in *osEPFL9_oe* rice plants (Fig. 2.36B, ANOVA, p = 0.3449). In addition, in these transgenics, IV distance

showed significant difference between *osEPFL9_oe* was not difference in the both two transgenic leaves compared to a control plant (Fig. 2.37A and B).
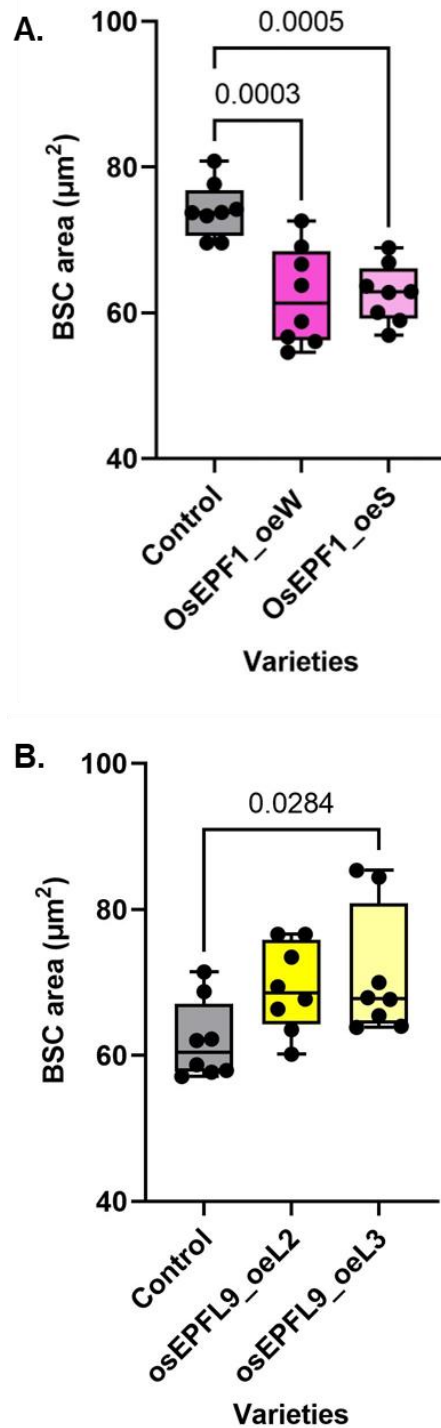
Figure 2.30. Rice leaf 6 of *osEPF1_oe lines* (28-day old), and *osEPFL9_oe* lines (21-day old) were measured BSC size by using FIJI ImageJ script. Box and Whisker showed a spread of min, max, mean and SD values of bundle sheath area. The analysis examined the BSC area of both *osEPF1_oeW* and *S*, as shown in (A), and the BSC area of both *osEPFL9_oeL2* and *L3*, as shown in (B). One-way ANOVA with Dunnett's multiple comparison (n = 8) was performed (p = 0.0001 (A) and 0.0365 (B)).
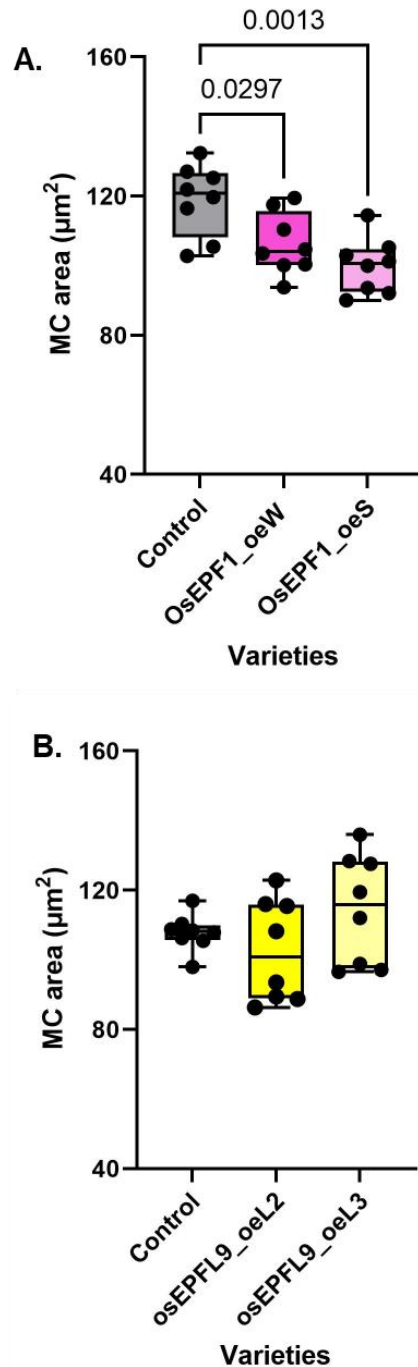
Figure 2.31. The size of the mesophyll cells in the leaf 6 of the *osEPF1_oe* lines (28-day old) and *osEPFL9_oe* lines (21-day old) in rice was measured using a FIJI ImageJ script. The Box and Whisker plots were used to display the minimum, maximum, mean, and standard deviation values of the mesophyll area. The analysis focused on the mesophyll cell area of both *osEPF1_oeW* and *S*, shown in (A), and *osEPFL9_oeL2* and *L3*, shown in (B). Statistical analysis including one-way ANOVA (n = 8) was performed with p = 0.0016 (A) and p = 0.1961 (B).
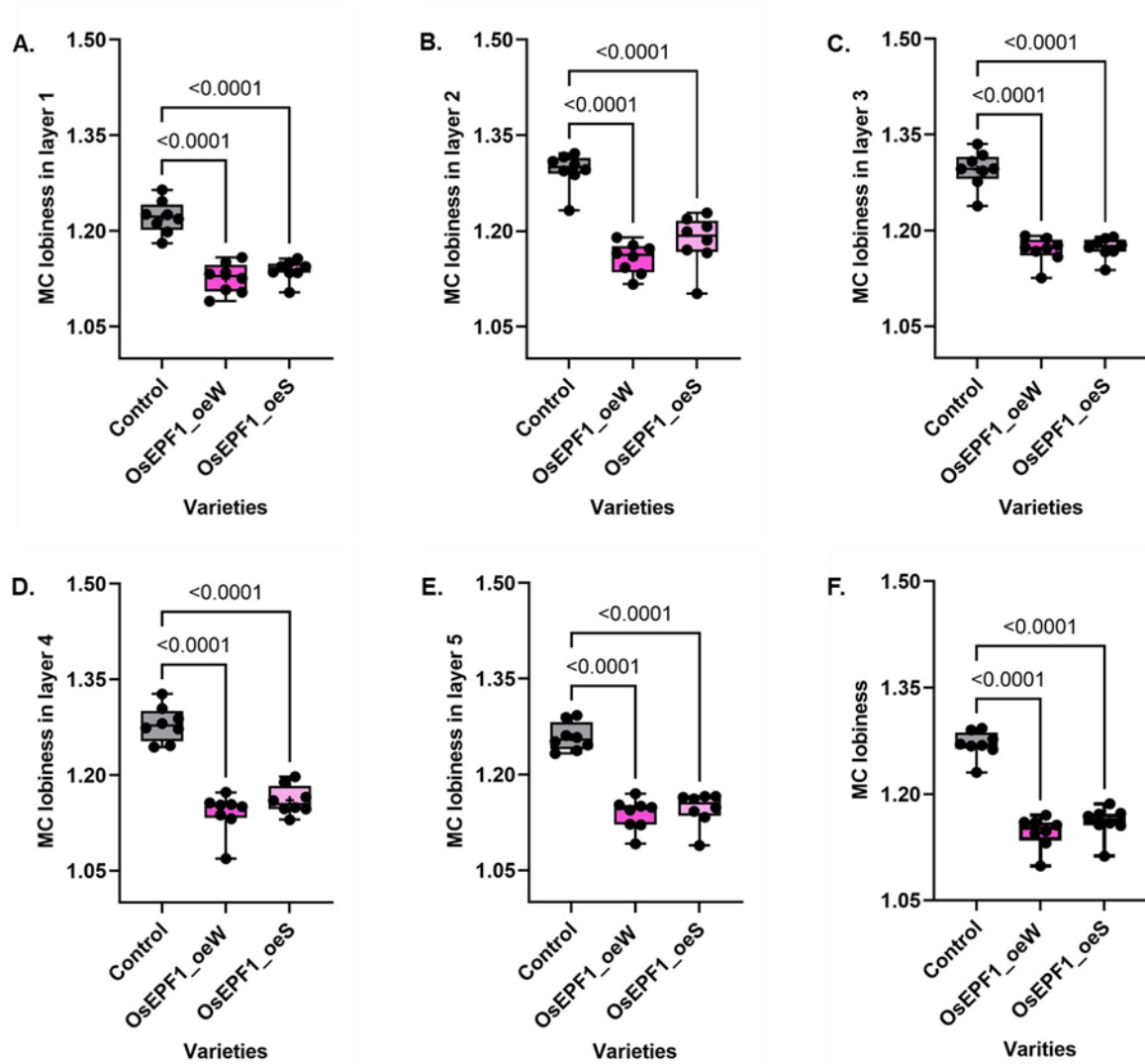
Figure 2.32. Each rice leaf 6 of *osEPF1_oeW* and *osEPF1_oeS* lines (28-day old) was analysed the degree of cell lobing of MCs which located in 5 different layers as displayed in Box and Whisker plots with mean and SD values from (A) to (E) Also, cell lobiness of each transgenic rice plants was measured comparing to a control line in (F). Box and Whisker displayed a spread of min, max, mean and SD values of cell lobiness. One-way ANOVA, p value is less than 0.0001 (n = 8) with Dunnett's multiple comparison test was applied for statistical analysis.
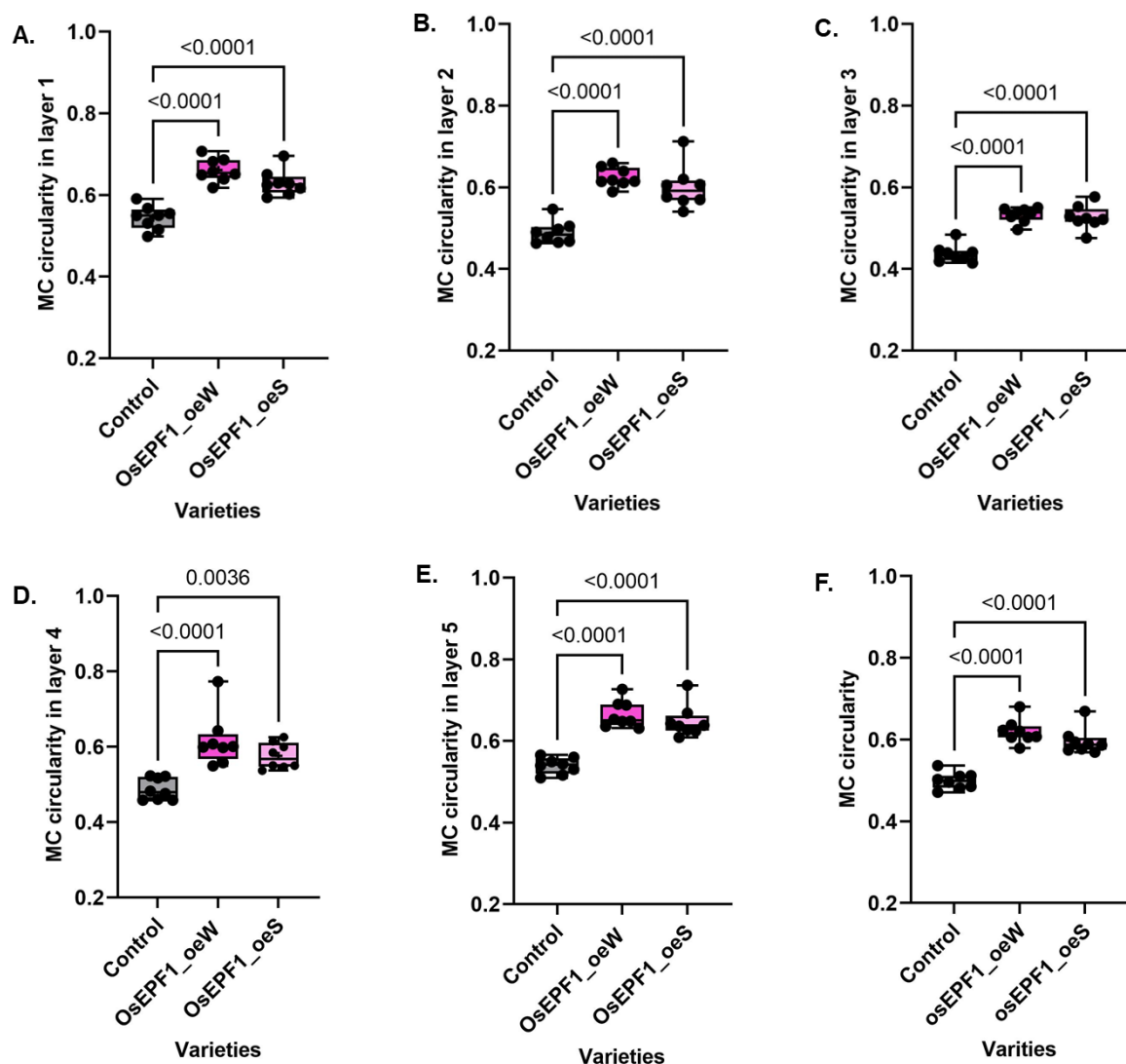
Figure 2.33. Rice leaf 6 of both *osEPF1_oeW* and *osEPF1_oeS* lines (28-day old) was analysed the cell roundness of MCs which located in 5 different layers as displayed in Box and Whisker plots with mean and SD values in (A-E). Also, cell circularity of each transgenic rice plants was measured comparing to a control line in F. Box and Whisker displayed a spread of min, max, mean and SD values of cell lobiness. One-way ANOVA, The p-values (n = 8) were displayed on the graphs to show the statistical significance of the results.
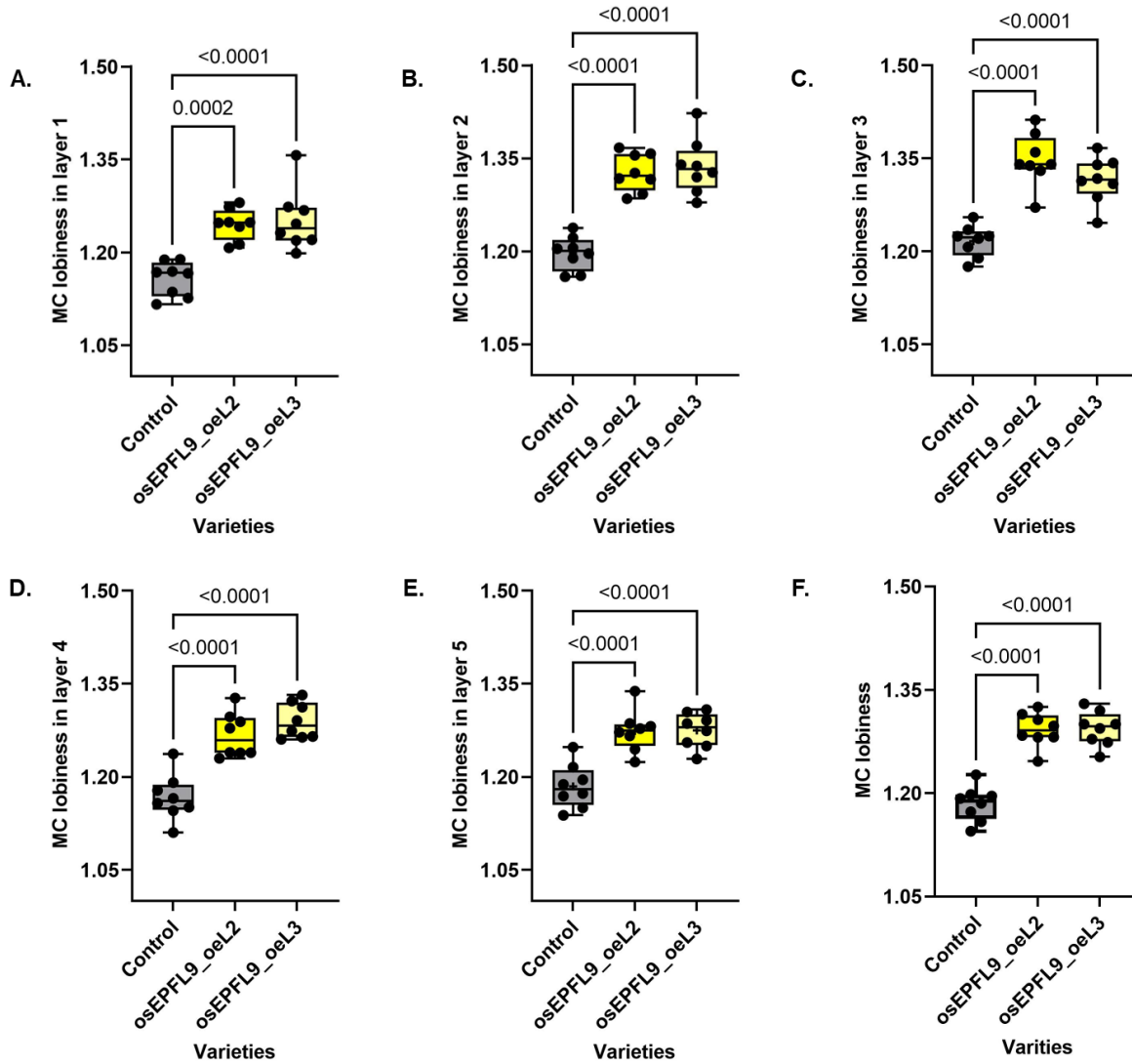
Figure 2.34. The study assessed the degree of cell lobing in MCs located in 5 different layers of each 21-day-old rice leaf 6 for *osEPFL9_oeL2* and *osEPFL9_oeL3* lines. Box and Whisker plots were used to display the mean and standard deviation (SD) values from (A) to (E). Additionally, the degree of cell lobiness of each transgenic rice plant was measured by comparing it to a control line, and Box and Whisker plots were used to show the range of minimum, maximum, mean, and SD values of cell lobiness. Statistical analysis was conducted using one-way ANOVA with Dunnett's multiple comparison test (n = 8), p-value is less than 0.0001.
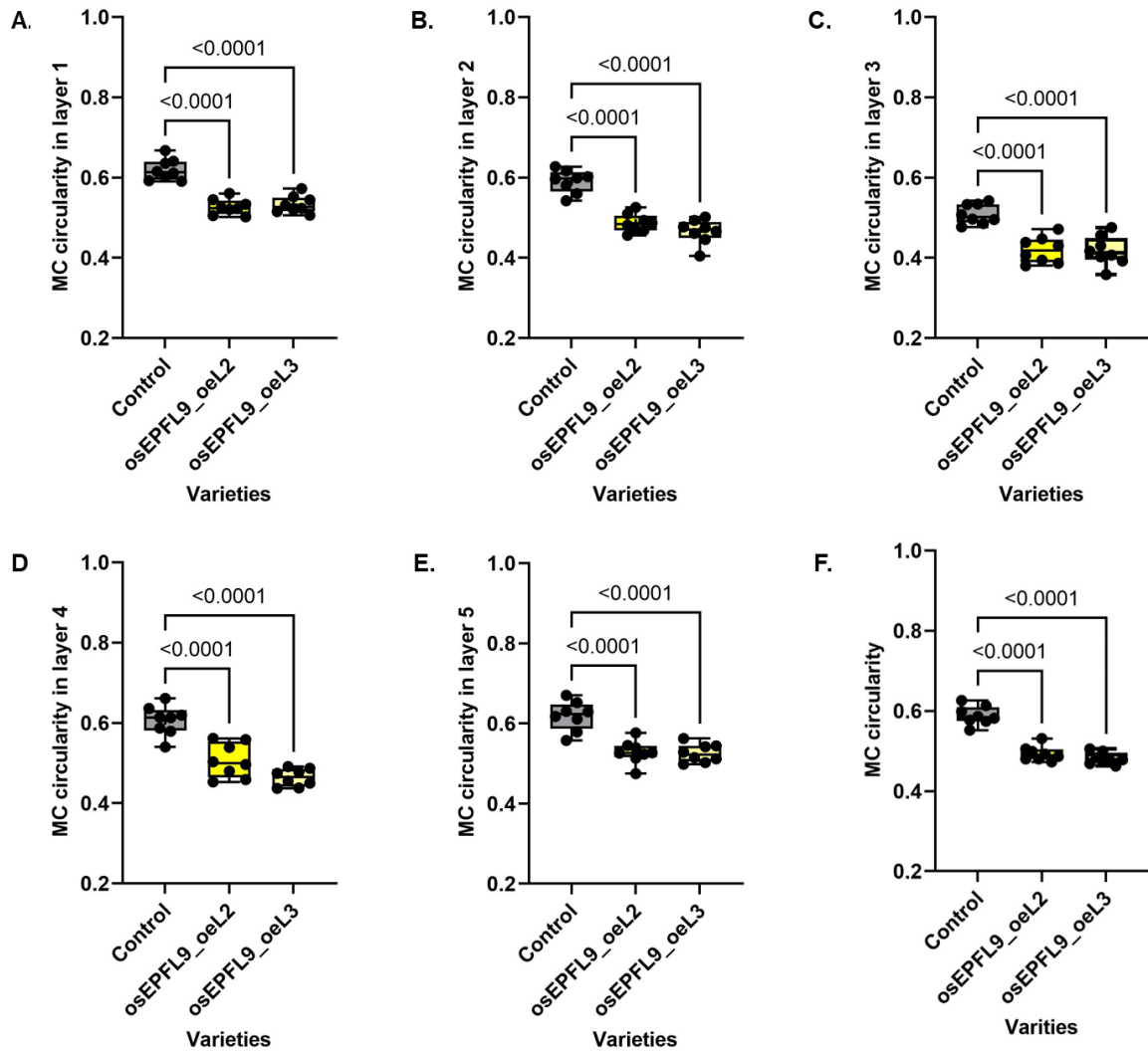
Figure 2.35. The analysis focused on the cell roundness of MCs in rice leaf 6 of *osEPFL9_oeL2* and *osEPFL9_oeL3* lines, which were 21-day old. The cell roundness in these lines was examined in 5 different layers and presented in Box and Whisker plots that displayed mean and standard deviation (SD) values for each layer (A-E). In addition, the cell circularity of each transgenic rice plant was compared to a control line and shown in plots, F. To analyse the data statistically, a one-way ANOVA was performed with Dunnett's multiple comparison test (n = 8), resulting in a p-value of less than 0.0001
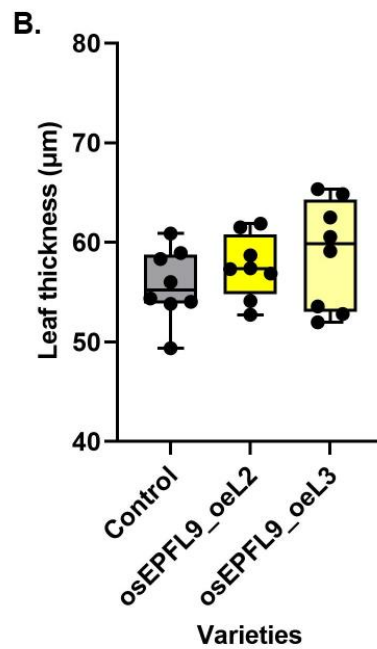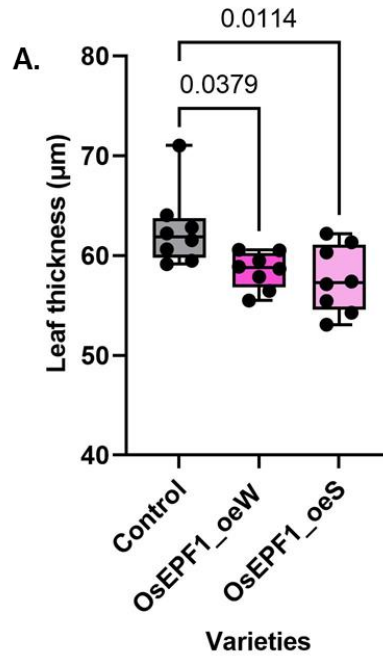
Figure 2.36. The leaf thickness of the leaf 6 in *osEPF1_oe* lines (28-day old) and *osEPFL9_oe* lines (21-day old) in rice was measured using a FIJI ImageJ script. The measured data was presented in the Box and Whisker plots which showed the minimum, maximum, mean, and standard deviation values of the leaf thickness. The analysis compared the leaf thickness of both *osEPF1_oeW* and *S*, shown in (A), and *osEPFL9_oeL2* and *L3*, shown in (B). A statistical analysis was performed by using one-way ANOVA with Dunnett's multiple comparison (n = 8) to assess the data. The p-values, which indicated the level of statistical significance, were displayed on the graphs.
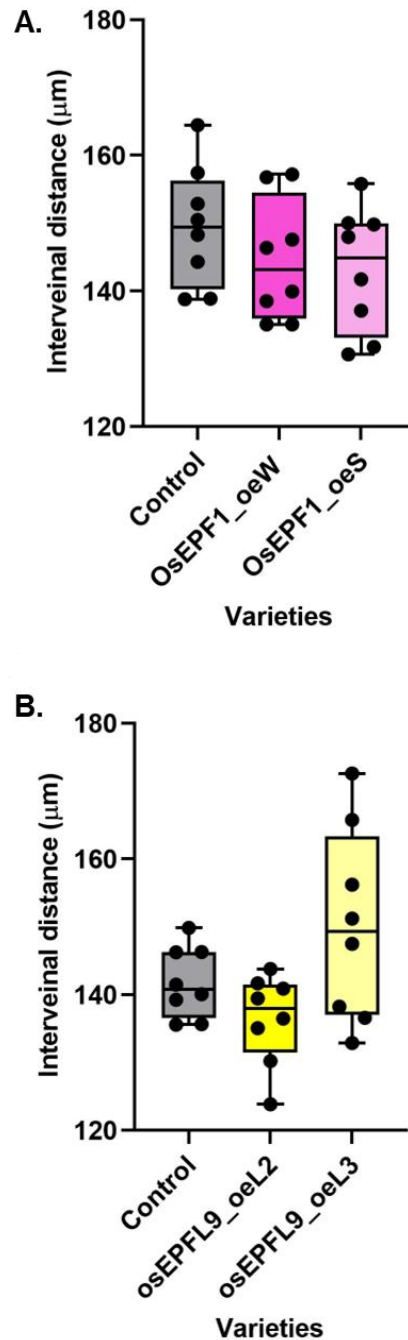
Figure 2.37. The interveinal distance (IV) between two minor veins of the leaf 6 in *osEPF1_oe* lines (28-day old) and *osEPFL9_oe* lines (21-day old) in rice was measured using a FIJI ImageJ script. The data was presented using Box and Whisker plots, which showed the minimum, maximum, mean, and standard deviation values of the IV distance. The analysis compared the IV distance of both *osEPF1_oeW* and *S*, shown in (A), and *osEPFL9_oeL2* and *L3*, shown in (B). A statistical analysis was performed by using one-way ANOVA to analyse the data with p = 0.3573 (A) and p = 0.0298 (B).

2.5.4. The stomatal characteristics of *osEPF1oe* and *osEPFL9oe* lines

To investigate stomatal features, The imprint of abaxial leaf surface from 28-day-old of *osEPF1_oe* and 21-day-old *osEPFL9_oe* lines were taken to observe stomatal area, guard cell (GC) area, pore length (L_p), stomatal density (SD) and anatomical g_{smax} under the light microscope at 20X for stomatal count and 40X for stomatal characteristics. The control line used for comparison was *IR64* rice plants. One-way ANOVA with Dunnett's multiple comparison (n = 8) was used to analyse statistical data and the results were presented in Fig. 2.38 - 2.39.

The stomatal size of *osEPF1_oeW and S* rice leaves were not different from the control (Fig. 2.38A) as well as GC area and pore length (Fig. 2.38B and C), while the stomatal size of *osEPFL9_oeL3* leaves showed a significant decrease (Fig. 2.38D, p = 0.0022). Similar to GC area and pore length are smaller and shorter with the statistical difference when compared to control as displayed in Fig. 2.38E (p = 0.0399) and F (p = 0.0084).

After counting stomatal numbers, the density of stomata was calculated in the curved area of the adaxial epidermis of rice leaf. All transgenic lines displayed altered numbers of stomata on leaf surface in comparison to control plants. The genotypes overexpressing *EPF1* gene had a significant decrease in stomatal density (Fig. 2.39A, p < 0.0001), whereas *osEPFL9_oe* lines had a significant increase of SD (Fig. 2.39B, p < 0.0006 for osEPFL9_oeL2 and p = 0.0002 for osEPFL9_oeL3). In addition, g_{smax} was assessed in these transgenic lines to estimate gas exchange capacity, *osEPF1_oeW and S* rice leaves displayed a significant decline of g_{smax} in *osEPF1_oe* rice plants (Fig.2.39C, p < 0.0001), but a significant increase in *osEPFL9_oe* lines (Fig.2.39D, p = 0.0077 (osEPFL9_oeL2) and p = 0.0113 (osEPFL9_oeL3)) indicated that changing stomatal numbers led to alter stomatal conductance and affected leaf cell structure especially and MC size and shape in the rice leaf.
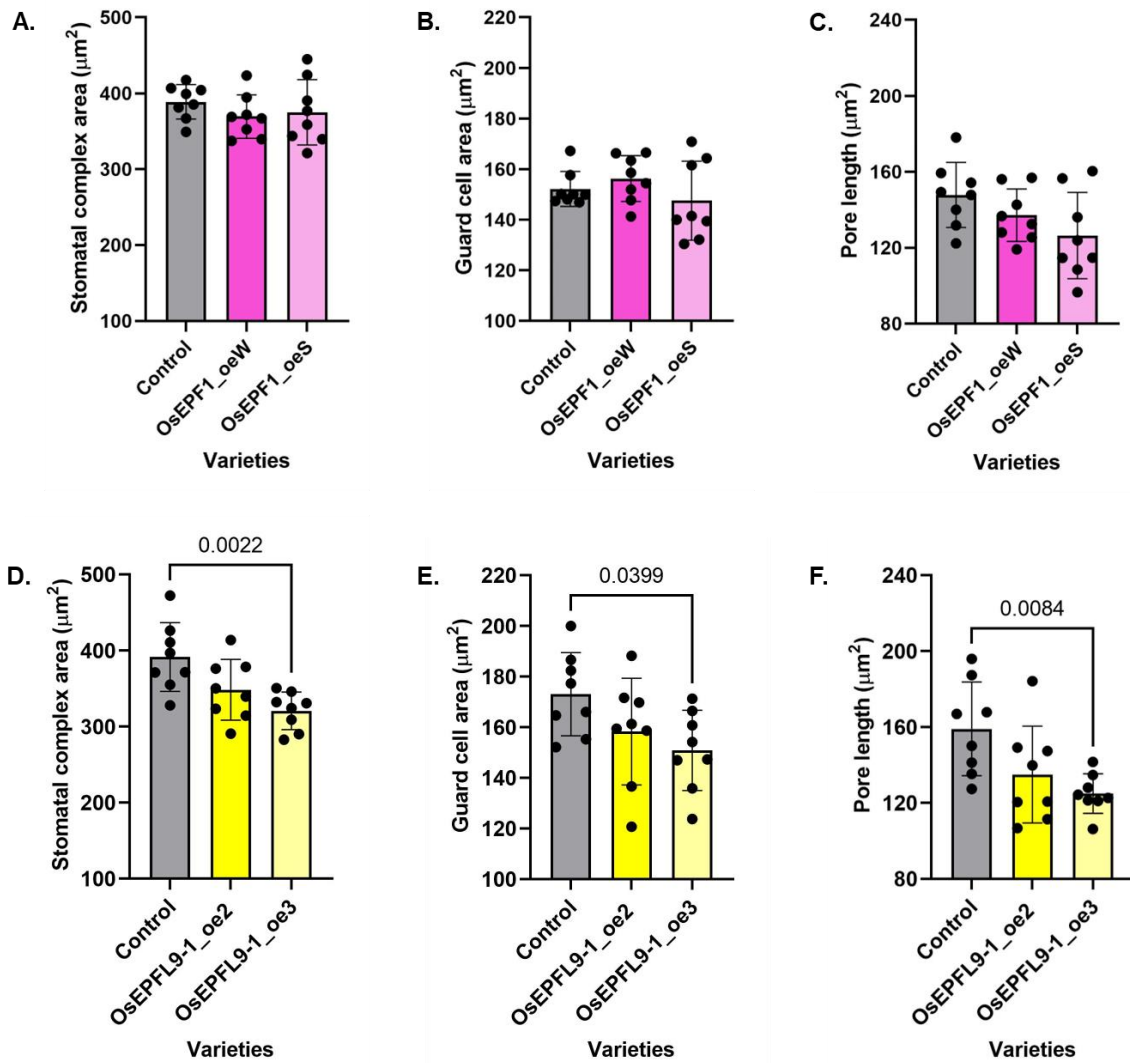
Figure 2.38. The leaf 6 imprints of 28-day old of *osEPF1_oe* rice (L2 and L3) and 21-day old of *osEPFL9_oe* leaves (W and S) were used to investigate the stomatal complex area (A, D), Guard cell area (B, E) and pore length (C, F). All data were plotted in the column charts with mean and SD. Each small dots represented the plant replicates (n = 8). A statistical analysis was performed by using one-way ANOVA with Dunnett's multiple comparison. The graphs illustrated the p-values, which indicated the level of statistical significance.
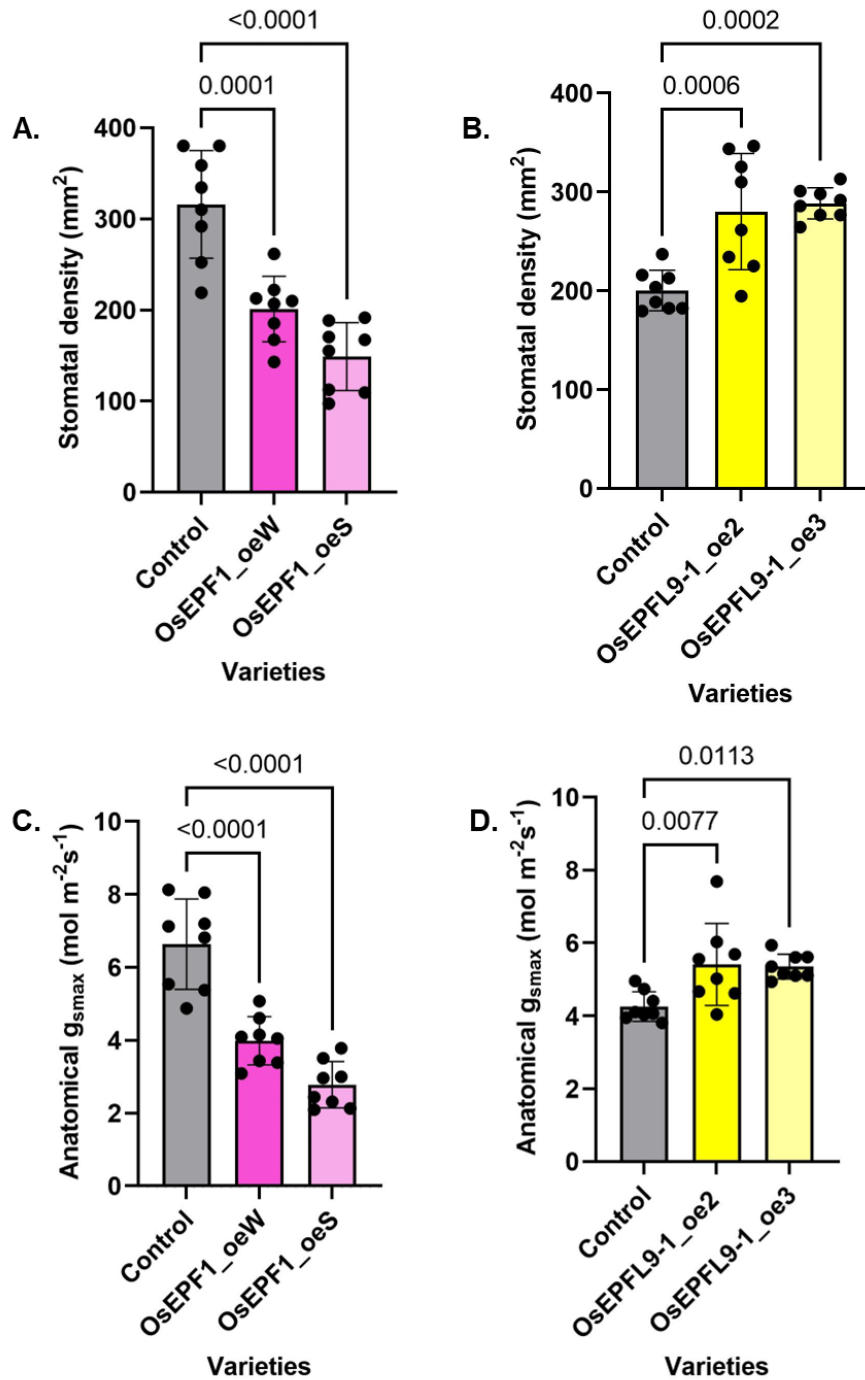
Figure 2.39. The leaf imprints of 28-days old of *osEPF1_oe* rice leaves 6 (L2 and L3) and 21-day old of *osEPFL9_oe* leaves (W and S) were calculated stomatal density and g_{smax}, which plotted in the column graphs as shown in (A-D) with mean and SD values. One-way ANOVA with Dunnett's multiple comparison was applied to analyse the statistics. The graphs displayed the p-values, which indicated the degree of statistical significance.

2.5.5. The relationship between the stomatal density, g_{smax} and mesophyll shape (lobiness) of JL, *osEPF1oe* and *osEPFL9oe* rice plants

According to the previous results, the altered stomatal density (SD) and g_{smax} could influence leaf structure, especially MC shape and lobiness of transgenic of rice plants; *JL4A3, JL4A6, 27B4, osEPF1_oeW, osEPF1_oeS, osEPFL9_oeL2* and *osEPFL9_oeL3*. All the data of SD, g_{smax}, MC area and MC lobiness from each transgenic rice leaf and control were plotted on a graph to investigate the relationship between these two variables, as shown in Fig. 2.40 and 2.41.

In Fig.2.40A, the stomatal density of three transgenic lines were plotted against the average MC area, as represented in the scatterplots. The plot pattern of *osEPF1_oe* and control lines displayed a positive linear association with SD (P(two-tale), p = 0.0003, R squared = 45.85%). MC areas of the other two lines were not associated with SD, which showed the strong outliers in the graph. When SD data were plotted against cell lobiness (Fig. 2.40B), the trending of the scatterplots illustrated a moderately strong, positive, linear association with significant correlation between the two variables in *JL* (p < 0.0001, R^2 = 52.51%), *osEPF1_oe* (p < 0.0001, R^2 = 53.75%) and *osEPFL9_oe* lines (p = 0.0001, R^2=49.53%) with a few outliers.

Moreover, the relationship between g_{smax} and MC size and shape was also investigated. For g_{smax} and MC size (Fig. 2.41A), the graph pattern *osEPF1_oe* line displayed an association which is positive linear with a few outliers (p = 0.0005, R^2 = 42.77%). Similar to g_{smax} and MC lobiness, a positive linear association between the two variables was observed, with outliers. A two-tail test was applied with p < 0.0001, R^2 = 62.27% (*JL* lines), p < 0.0001, R^2 = 58.39% (*osEPF1_oe* lines) and p = 0.0299, R^2 = 19.68% (*osEPFL9_oe* lines) as shown in Fig. 2.41B.

The results in this chapter indicated that altered SD and anatomical g_{smax} had a positive correlation with MC shape (degree of cell lobing). This leads to the next question: when does mesophyll cell lobing occur in rice leaf development? Leaf samples were sectioned and analysed for structure at early stages of development, as represented in Chapter 3. In addition, stomatal function was further investigated to see how it could modulate mesophyll cell shape, addressing questions such as: Are cells

measuring CO_2? Are cell measuring the output of photosynthesis? These analyses are reported in Chapter 4.
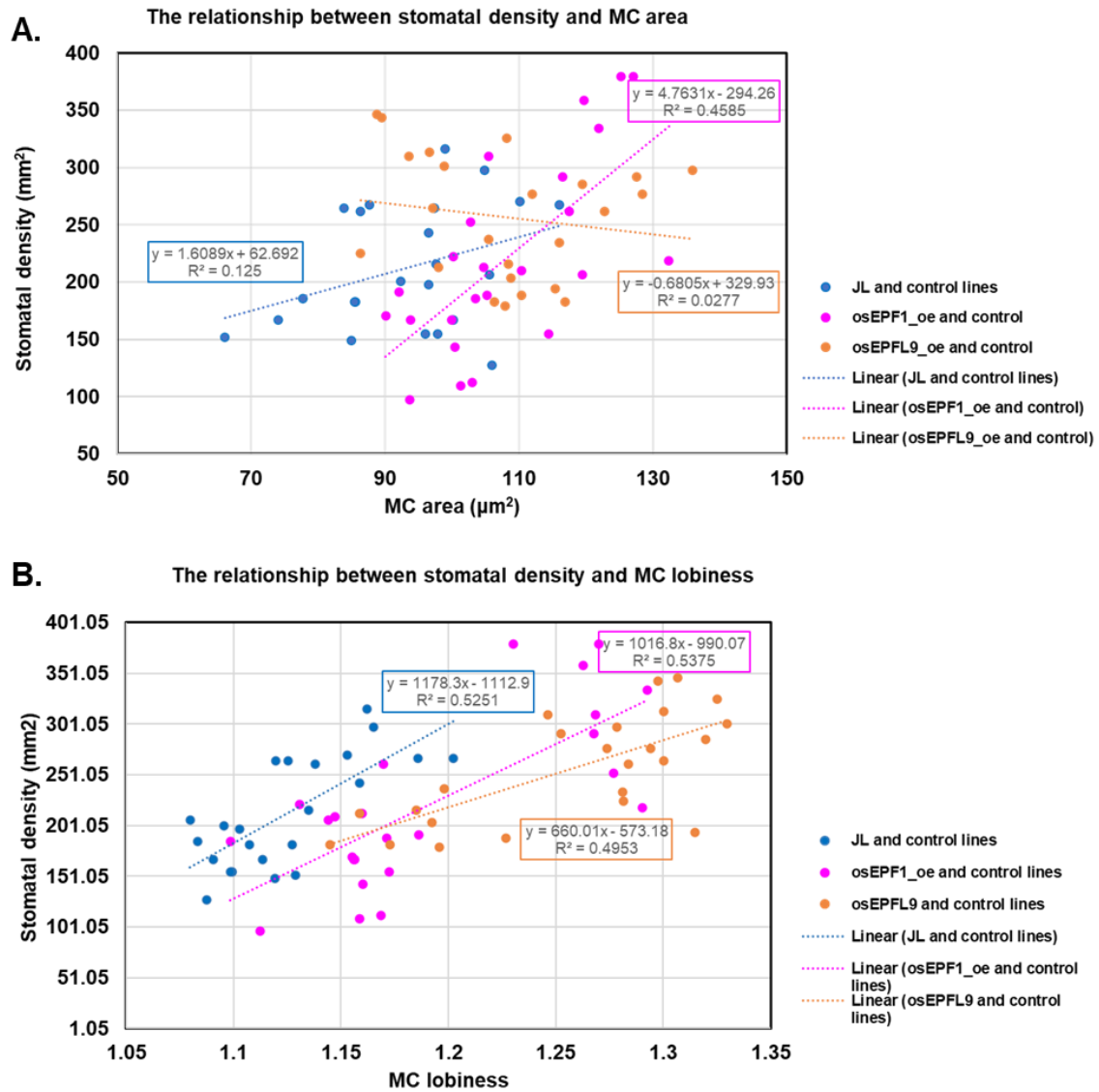
Figure 2.40. A). MC area of *JL*, *osEPFL1_oe* and *osEPFL9_oe* lines were plotted against stomatal density (SD). *osEPF1_oe* lines showed a positive linear association between MC area and SD (pink) with p (two-tale) = 0.0003, R^2 = 45.85%. B). The diagram showed positive relationship between two varieties (stomata density and MC lobiness). The various variables on the X-axis and Y-axis went up with few outliers, which indicated the moderate positive relationship of *JL* (blue, $p < 0.0001$), *osEPFL1_oe* (pink, $p < 0.0001$) and *osEPFL9_oe* lines (orange, p = 0.0001). R^2 also displayed on the graph. Two-tale statistics was used to analysed the data. The control of each transgenic lines were included in the scatter plots.

The relationship between Anatomical g$_{smax}$ and MC area

$y = 0.1023x - 6.6158$
$R^2 = 0.4277$

$y = -0.0143x + 6.555$
$R^2 = 0.0462$

$y = 0.0385x + 0.5095$
$R^2 = 0.115$

- JL and control lines
- osEPF1_oe and control lines
- osEPFL9_oe and control lines
- Linear (JL and control lines)
- Linear (osEPF1_oe and control lines)
- Linear (osEPFL9_oe and control lines)

The relationship between Anatomical g$_{smax}$ and MC lobiness

$y = 32.017x - 31.922$
$R^2 = 0.6227$

$y = 23.555x - 23.612$
$R^2 = 0.5839$

$y = 6.7544x - 3.4796$
$R^2 = 0.1968$

- JL and control lines
- osEPF1_oe and control lines
- osEPFL9_oe and control lines
- Linear (JL and control lines)
- Linear (osEPF1_oe and control lines)
- Linear (osEPFL9_oe and control lines)

Figure 2.41. A). MC area of *JL*, *osEPFL1_oe* and *osEPFL9_oe* lines were plotted against g$_{smax}$. Only *osEPF1_oe* line showed a positive linear association between MC area and g$_{smax}$ (pink) with p (two-tale) = 0.0005, R^2 = 42.77%. B). The diagram showed positive relationship between two varieties (g$_{smax}$ and MC lobiness). The two data sets on the -axis and Y-axis increased with few outliers, which suggested the moderate positive relationship between *JL* (blue, p < 0.0001), *osEPFL1_oe* (pink, p < 0.0001) and *osEPFL9_oe* lines (orange, p = 0.0299) and g$_{smax}$. R^2 also displayed on the graph. Two-tale statistics was applied to analysed the data. The scatterplots included the control for each transgenic line.

2.6. Discussion

2.6.1. MC size and shape affect to photosynthetic performance

As part of a global effort to modify C3 leaf anatomy in rice towards a more C4-like structure to improve photosynthesis, Peng Wang and colleagues from the Department of Plant Sciences, The University of Oxford inserted more than 50 candidate genes involved in Kranz anatomy development in maize (Zea mays into Kitaake or IR64 rice varieties (Wang et al. 2016). The study did not report on any major change in leaf structure consistent with a more C4-like anatomy, there did appear to be changes in both mesophyll and bundle sheath cell size in some of the lines.

Base on Fig. 2.57, 2.8 and data from Wang study (Wang et. al.,2016), *JL4, 13, 15, 27, and 34* lines were then selected to screen the leaf anatomy. These 5 *JL* lines showed a spread mean value in 6 parameters (BS area, MC area, the ratio of MC/BSC, MC lobiness, cell circularity, and IV distance). Notably, the number of MC lobes of *JL4* and *27* were slightly increased from other *JL* lines (Fig. 2.13). Although these results were preliminary due to the limited numbers of replication. *JL4* and *27* lines were selected to re-examine internal cell structures; BSC size, MC size, MC shape (lobiness and circularity), leaf thickness and IV distance between two minor veins. Interestingly, the mesophyll cells of these two lines had less lobing and high cell circularity in all 5 layers compared to control (Fig. 2.18 and 2.19), while, there was no difference in cell size compared to *IR64* control plants (Fig. 2.16 and 2.17).

In addition, The *JL* transgenic rice plants with less lobiness showed the reduction in A (Fig. 2.22) and PhiPSII (Fig. 2.24) under ambient CO_2 condition at light intensities around 1000 µmol m^{-2}s^{-1}. Moreover, the data of A rate and internal CO_2 (C_i) were plotted in A/Ci curve, a tool to analyse V_{cmax}, J_{max} and TPU values as parameters involved in photosynthesis. 3 *JL* lines represented a decrease of J_{max} comparing to *IR64* control (Fig. 2.27B), whereas V_{cmax} and TPU showed no reduction in transgenic lines.

In theory, chlorophyll pigments inside chloroplasts capture light energy and turn it to chemical energy as the main source energy for photosynthetic process. A small number of lobes decrease cell surface area, thus declining the area for CO_2 diffusion, which affect to photosynthetic performance of a leaf (Roddy et al., 2020; Rancourt et al.,2021). However, it is possible that the decreased distribution of chloroplasts via cell lobes might influence light capture. If this is true, then a decrease in cell lobes might decrease light capture, decreasing the rate of Rubisco carboxylase activity, V_{max} and/or electron flow, J_{max} and thus decrease carbon assimilation and PhiPSII. The decrease in stomatal conductance might be a consequence of this decrease in A, which support the hypothesis that the MC shape inside leaves influence photosynthetic performance in rice.

2.6.2. Stomatal function affect to mesophyll cell structure

According to the result of *JL* lines, *osEPF1_oe* lines with low stomatal density and *osEPFL9_oe* lines with high stomatal density obtained from the Gray lab (Caine et al. 2019) were used to observe the corelation of mesophyll cell size/ shape and the stomatal properties. *osEPF1_oe* lines overexpress an Epidermal-patterning factor (*EPF1*) which functions as a negative regulator gene of stomatal density. Two lines were used, *EPF1oeW and S*, which show a weak and strong phenotype. In contrast *osEPFL9_oe* lines (*L2 and L3*) over-express the *EPFL9* gene which promotes stomatal development.

Theoretically, stomatal pores on the leaf surface and mesophyll cell porosity are the important keys to enhance plant gas exchange for photosynthesis and transpiration (Baillie and Fleming 2019). A previous study in *Arabidopsis* and wheat has shown that the development of mesophyll cell structure is regulated by the stomatal properties to improve the ability of gas flux through the cell (Lundgren et al., 2019; Wilson et al., 2021). This data supports my hypothesis that the altered MC size/shape link to the altered stomatal function. In the leaf with less mesophyll lobing displayed a decrease of stomatal density and g_{smax} as shown in *JL4A3, JL4A6, JL27B4* (Fig. 2.29B) and *osEPF1oe* lines (Fig. 2.39C). While, MCs with an increase cell lobing (Fig. 2.34) affect to high stomal density Fig. 2.39B with increased g_{smax} 2.39D. In term of MC size, only

osEPF1_oe lines shows a smaller MCs while other transgenic lines do not display any statistical significant difference of mesophyll cell area.

The exposition of MC surface area to airspaces influences the diffusion of CO_2 from outside atmosphere through the stomata on leaf surface. CO_2 moves from internal airspace to chloroplasts inside MCs, which contain the Rubisco enzyme to trap CO_2 for photosynthetic (Evans and Caemmerer, 1996; Kaldenhoff, 2012).

However, the mechanism of the regulation of MC size and shape is still unclear. Increasing MC surface area might affect to both MC size and lobing. To test this hypothesis further, rice plants with different MC size should be studied to see how this influences photosynthetic performance.

Chapter 3

The development of lobing in rice mesophyll cells

3.1. Introduction

The apical meristem is an area where a group of undifferentiated cells is capable of renewing themselves through cell division and expansion (Veit, 2003; Kwiatkowska, 2008). This region is essential to form the primary plant body. There are two types of apical meristems; shoot apical meristem (SAM), which produces meristematic cells to differentiate to be the aerial parts of a plant such as stems, leaves and flowers, and root apical meristem (RAM), which generates cells for root growth and development (Miwa, et al., 2009; Drisch and Stahl, 2015).

Each rice leaf primordia is formed from the cells at the SAM. Each leaf originates from a small nodule located on the flank of the shoot apical meristem (Ha, 2010). The young primordium then grows and develops under the control of a complex genetic program in which a number of key gene have been identified (e.g., Knotted-type homeobox (OSH1), OsPNH1, SCARECROW (OSsCR) and DROOPINGLEAF (DL). These genes function to regulate cell division and differentiation over time and space, leading to the mature leaf structure, and maintaining the SAM for further leaf initiation (Nishimura et al., 2002; Kamiya et al., 2003 and Yamaguchi et al., 2004; Lui et al., 2019). These genes can also be used as molecular markers expressed in different developmental stages. In general, the morphology of the primordium is classified by a measure of developmental the time, the plastochron number (Pi) ranging from P0 to P6, as shown in Fig.3.1 (Itoh et al., 2005).

Stage: P0

The leaf founder cells are firstly established at this stage, forming a half-ring domain in the periphery of SAM opposite the youngest leaf primordium. Although, the morphology in P0 stage is difficult to characterize from other cells presented in SAM,

the expression of OSH1 and OsPNH1 genes can be detected with a decrease and increase gene expression level respectively (Nishimura et al., 2002).

Stage: P1

The young leaf forms into a crescent-shaped (Fig. 3.1A) small protrusion on the flank of the SAM. Cells in P1 divide more rapidly than the SAM, indicated by the expression of histone H4, a histone protein highly expressed during the cell cycle process (Itoh et al. 2000a). There are two gene markers that can be used to distinguish between P0 to P1 stage. The first gene is *OsSCR* that is preferentially expressed in epidermal layer. The *DL* gene is first present in the central region of primordium, and later which modulates midrib formation and carpel development (Yamaguchi et al. 2004 and Kamiya et al. 2003)

Stage: P2

After cell elongation and division, a hood-shaped primordium is constructed (Fig. 3.1B) and a procambial strand is initially formed in the centre of leaf. The evidence of molecular markers has not been reported for the P2 stage (Itoh et al. 2005).

Stage: P3

During the P3 stage of rice leaf development, the two margins of the primordium overlap and completely encircle the shoot apical meristem (SAM). The primordium then undergoes elongation and takes on a cone-like shape (Fig. 3.1C). At this stage, the periclinal division of epidermal cells generates the organization of the ligule, which becomes visible at the boundary region between the blade and sheath of the adaxial (upper) side of the leaf. Along with this, other internal tissues are also formed (Itoh et al. 2005).

Moreover, various vascular bundles are established during the P3 stage, with the formation of xylem and phloem specifically occurring at the midvein (Fig.3.1E). The OsSCR gene marker is reported to be expressed in the epidermis layer of the leaf during this stage (Kamiya et al. 2003 and Itoh et al. 2005).

Stage: P4

During the P4 stage of rice leaf development, there is rapid elongation of the leaf. This elongation is primarily driven by the intercalary meristem located at the base of the leaf blade (Fig.3.1D). In this stage, certain genes involved in cell and tissue differentiation, such as OsSCR, OsPNH1, and DL, are down-regulated suggesting that the activity or expression of these genes is reduced in P4 stage (Itoh et al. 2005)..

Stage: P5

Once the elongation of the leaf blade is complete, the leaf sheath undergoes a period of rapid elongation. Consequently, the tip of the leaf blade becomes visible as it emerges from the sheath of the sixth leaf. During this process, lacuna, which are small cavities, form in both the midrib of the leaf and the sheath. These lacuna develop in a basipetal direction, meaning they appear closer to the lower end or base of the leaf. (Itoh et al. 2005; Miya et al.,2021).

Stage: P6

Growth and differentiation terminates to form the mature leaf. Leaf blade bending takes place at the lamina joint (Itoh et al., 2005).
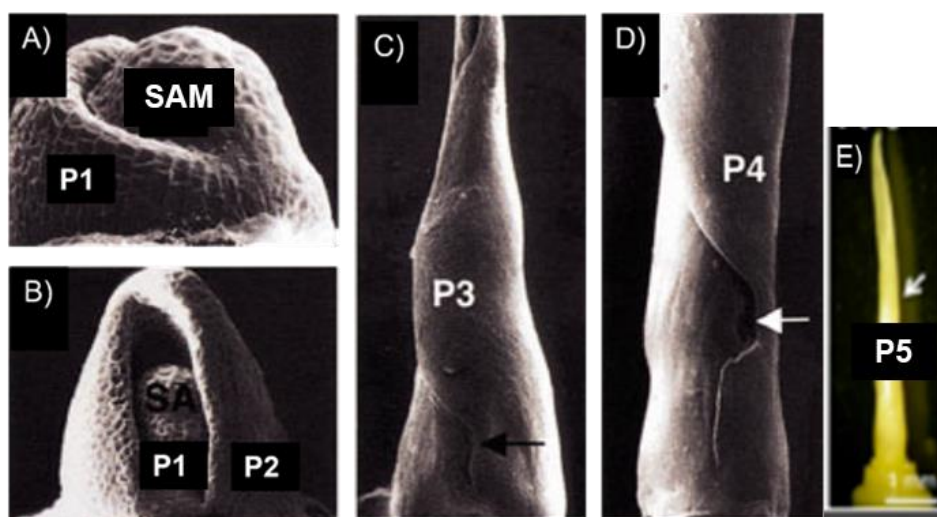
Figure 3.1. The figure represents the five stages of leaf development categorized by Pi (i = plastochron number) and observed under scanning electron microscope or SEM. (A) SEM image displaying the shoot apical meristem (SAM) and a mature P1 (late-stage) primordium.

in crescent shape. (B) P1 and P2 stage, the primordium forms the hood-like shape and develop to P3 stage (C) until establishes conical shape and the blade sheath boundary is visible as shown in black arrow in stage P4 stage. But the sheath hasn't elongated yet (D). In stage P5, the elongation of the leaf blade is complete. The picture from this figure is modified by Itoh et al. (2005) and .Wang et al. (2013)

3.2. The development mesophyll lobing and stomata of a leaf

In monocot leaves, the shoot apical meristem consists of two layers of cells; L1 and L2 (Brutnell and Langdale, 1998). The epidermis and stomata are developed from the outer layer (L1) (Filippis et al., 2013), while the inner parts of a plant are developed from subepidermal L2 and L3 layers such as mesophyll cells, MCs (Pyke, 2012). The SAM is also divided into 3 main regions; a central zone, CZ (slow cell division), a peripheral zone, PZ (rapid cell division) and a lower rib zone, RZ (acting as a boundary to separate from non-meristematic tissues) (Shah and Fahim, 2020).

For mesophyll cells, the protodermal cells from L2 are expanded asymmetrically in size and shape (Menke and Scheres, 2009) to form the primitive tissue known as Chlorenchyma. This tissue can develop to be palisade MCs (cylindrical shape) or spongy MCs (irregular shape) (Yahia et al.,2019). In C3 plants, the protodermal cells form uniformly layers in a leaf, such as rice and wheat, then become lobed from the long axis which aligns perpendicular to the plant veins (Chatterjee et al., 2016). The co-ordination of cortical microtubules (MTs) and actin filaments (AFs) play a major role in cell morphogenesis to provide the intercellular space for gas exchange inside a leaf (Panteris and Galatis,2005). This mechanism is also found in both monocot leaves such as grasses (Wernicke & Jung, 1992; Apostolakos et al., 1991) and dicot leaves (Wernicke et al., 1993; Panteris et al., 1993a,c). The arrangement of mesophyll cells creates the airspaces between the cell, which is essential gas exchange. The mesophyll airspaces are developed at the early stage of leaf development at three-cell junctions to generate small intercellular gaps throughout a leaf (Baillie and Fleming, 2019).

Although some understanding of the process of cell lobing exists, it is still uncertain whether a similar process occurs in rice mesophyll cells. Additionally, it remains unclear during which stage of rice leaf development mesophyll cell lobing first occurs.

The findings from the previous chapter are consistent with the hypothesis that mesophyll cell lobing is linked to stomatal function. This raises question of when do mesophyll cells in rice first display lobing during the normal process of leaf development? The research conducted in this chapter aims to address these fundamental questions.
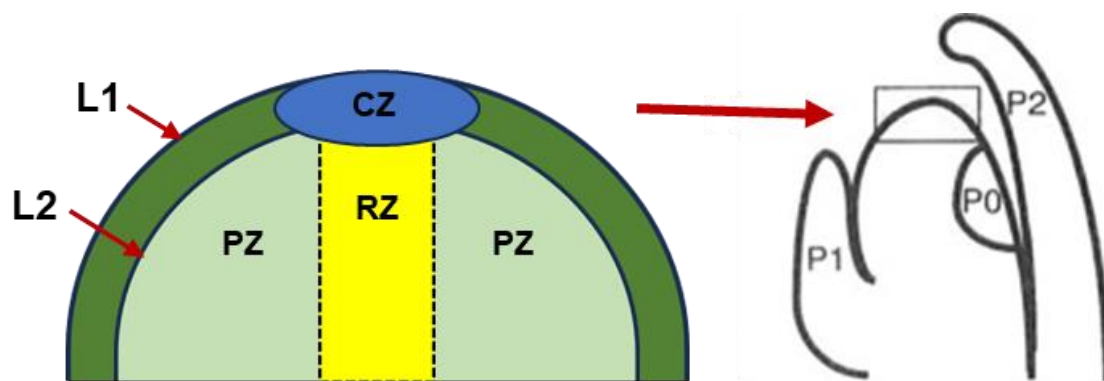
Figure 3.2. The picture displays the shoot apex of a monocot leaf. On the left, The area of SAM composes of 3 main regions; the slow cell division (CZ), rapid cell division (PZ) and lower rib zone (RZ). CZ area is flanked by peripheral area. On the right, the picture shows the region that these cell area located on primordium. The plastochron number is designated to display the area of the next leaf will grow. This picture is adjusted from Brutnell and Langdale (1998).
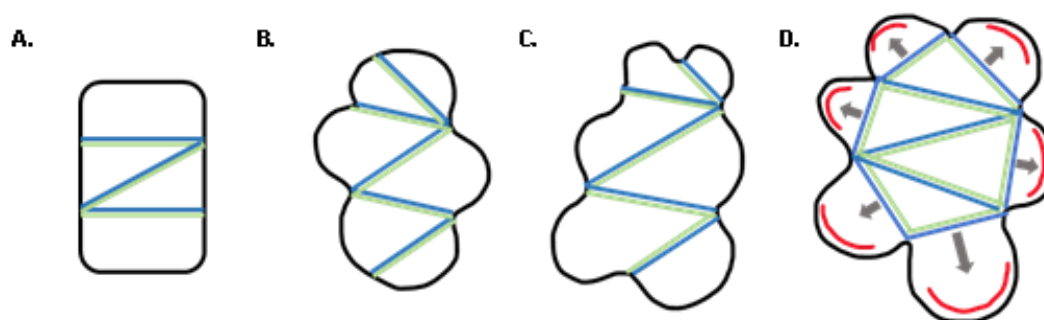
Figure 3.3. The microtubules (blue) and cellulose microfilaments (green) plays a major role in the formation of plant mesophyll cells, which anchor parallel inside the young MCs (A), mesophyll shape start having lobbing (B), and having more lobes during developmental stage (C). The actin microfilaments, Afs (red) appear in the mature MCs to support cell structure (D). This picture was edited from Panteris and Galatis. (2005).

3.3. Hypothesis: The development of mesophyll cells occur at the early stage of leaf development.

3.4. Aim: To analyse mesophyll cell differentiation in rice and to characterise when lobing starts during leaf development

3.5. Materials and Methods

3.5.1. Germination

Oryza sativa ssp. Indica var. *IR64* rice plants (T3 generation) propagated by Dr. Naomi Cox from Flemming's laboratory were used in this experiment. All seeds were germinated on the filter papers in the petri dishes before adding water almost the half of a plate. Then the dishes were incubated in growth environmental control chamber cabinet (Conviron, Winnipeg, MB,Canada), on a 12 hours at 28°C/ 12 hours at 24°C light/ dark for 7 days.

3.5.2. Hydroponic plant growth

In this research, all IR64 non-transgenic rice plants were grown by hydroponic technique because of a high numbers of plants (around 40) with the limit of space in a chamber. This line was used as a model of study. Before growing plants, the growth media; 40% Long Ashton (LA) solution with 2mM ammonium nitrate was prepared in 5L container as showed in Table. 3.1. The media was adjusted from (Murchies et al. 2005) by the previous lab members (Van Campen, Thesis, 2016). Each seeds was put in a 1.5 ml centrifuge tube which was cut at the bottom to create a small hold prior to place into polystyrene racks. The racks was then transferred to the 5L of hydroponic growth media in the 5L container. After that, plants were moved to grow in the environmental chamber under the condition as follow; the level of CO_2 = 420 ppm, 12 hours light (28°C), 12 hours dark (24°C), PAR = 1000 µmol-2s-1, and 60% relatively humidity. The media level was maintained by adding water every 1-2 weeks. A rice leaf 6 was collected at day 9, 10, 11 and 12.

Table 3.1. 40% Long Ashton (LA) solution with 2mM ammonium nitrate for hydroponic growth

Compound	40% LA molarity (mM)
Macronutrients	
K_2SO_4	0.8
$CaCl_2.H_2O$	1.6
$MgSO_4.7H_2O$	0.6
Na_2HPO_4	0.56
NH_4NO_3	2
Micronutrients	
Fe (III) EDTA	0.04
$ZnSO_4.7H_2O$	0.004
$MnSO_4.4H_2O$	0.04
$CuSO_4.5H_2O$	0.004
H_3BO_3	0.002
$Na_2MoO_4.2H_2O$	0.0002
NaCl	0.04

3.5.3. Rice leaf section and the analysis of MC size and shape

Each rice leaves was peeled the outer leaves such as leaf 1 , 2, 3, 4, and 5 off the stem gently. Then the length of leaf 6 was measured from the root to the tip, and separated into 3 parts equally; tip, middle and base as shown in Fig.3.4. Around 1 cm of leaf portion was cut at the middle of each parts, then sectioned in transverse direction as thin as possible by a sharp blade.

All cross sections from Part 1 to 3 were observed under the light microscope at 40x magnification and took pictures by using an Olympus microscope (BX51) with an Olympus camera (DP71) as shown in Fig.3.5. Two pictures from each parts were selected to analyse mesophyll cell size and shape by using FIJI image J script. mesophyll cell size and shape (the degree of cell lobing and cell circularity) were measured by using the same formula as *JL* and *osEPF_oe* lines as represented in Chapter 2. The hand section method was quicker than Technovit section method, but the quality of the pictures, especially with regards to cell boundaries, may not be very clear to observe due to the chlorophyll pigment background. Additionally, the hand section method relies on the operator's manual skill for sectioning and might require the amount of time to develop proficiency.
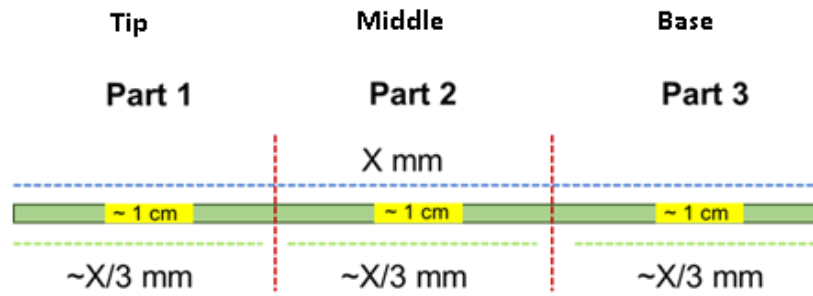
Figure.3.4. The IR64 rice plants with different ages (from 9 to 12 days) was removed the outer leaves (leaf 1 to 5) until a young leaf 6 was visible. Root was removed. The whole of rice leaf 6 as shown in this picture was divided into 3 parts equally; tip (part 1), middle (part 2) and base (part 3). Root was removed. Then around 1 cm of leaf portion at the middle area from each part was taken to do hand cross sections and analysed rice leaf structures.
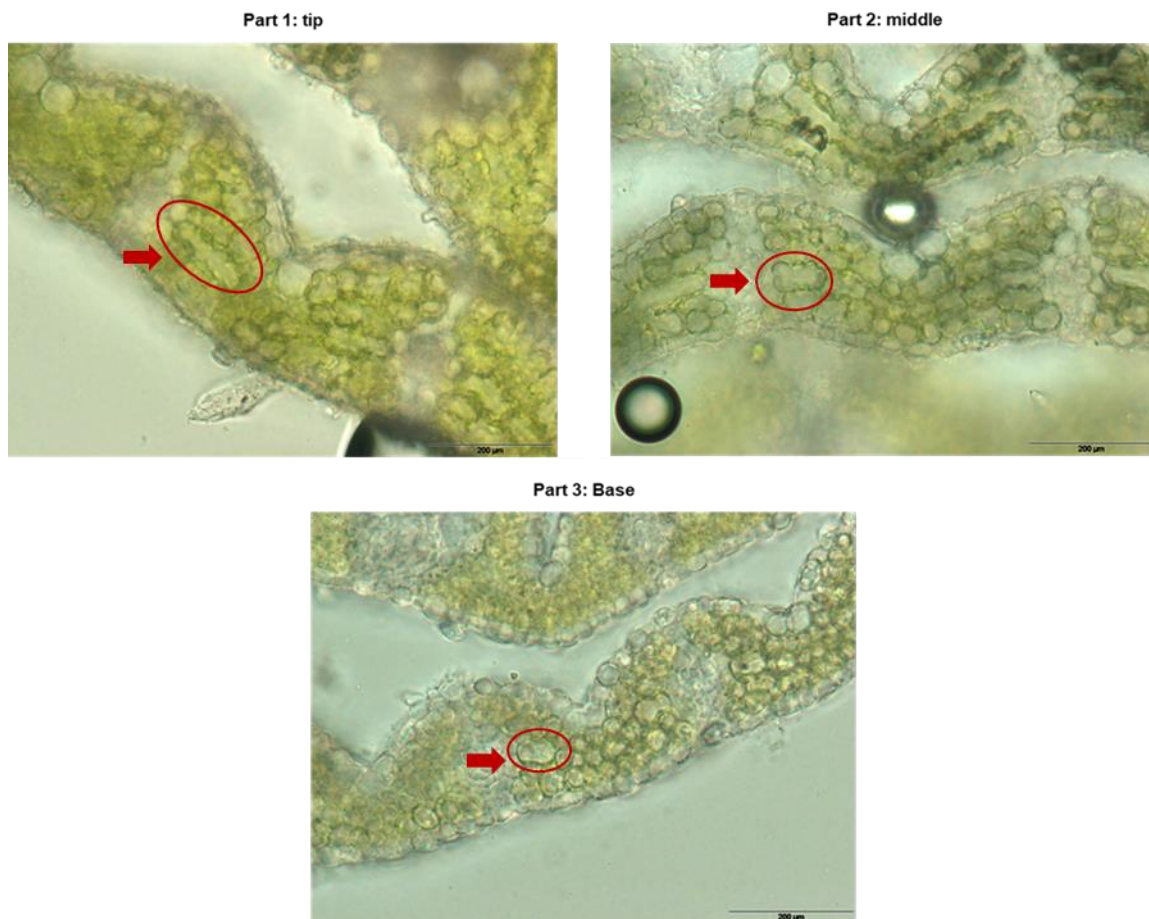
Figure. 3.5. The picture showed internal leaf structure of IR64 rice plant. 101 mm length of Rice leaf 6 was sectioned by hands and separated to three parts from tip to base. Each parts was observe leaf anatomical features under light microscope with 40x modification. MC shape especially cell lobing presented in all 3 parts of a plant, which shown in red circles.

3.6. Results

To investigate the development of lobing in rice mesophyll cells (MCs) I performed an analysis of the leaf 6 of IR64 plants. Plants were collected at different days of growth in a hydroponic system. The various leaf lengths, ranging from around 2 mm to 125 mm, were measured, then hand-sections taken from regions at the tip, middle and base of the leaf (as shown in Fig. 3.4). Direct visualisation of mesophyll cells by light microscopy allowed measurement of cell area and shape from images of the sections. Kruskal-Wallis test with Dunn's multiple comparisons was performed and displayed in the bar graphs (Fig. .3.6 - 3.11).

As shown in Fig. 3.6A, for MCs towards the tip of the leaf there was an increase in cell size as leaf length increased, with tip mesophyll cells being significantly smaller in leaves less than 20 mm long compared with leaves longer than 100 mm (p = 0.0280). Similar observations were made for sections taken from the middle (Fig. 3.6B, p = 0.0280) and base of the leaf (Fig. 3.6C, p < 0.05). MCs were significantly smaller in shorter (younger) leaves than in longer (older) leaves. To observe the relationship between MC area and different leaf lengths, the data of these two values taken from the tip of the leaf showed no obvious correlation of cell area and leaf age (Fig. 3.6D). In contrast, for sections taken from the middle (Fig. 3.6E, p = 0.0003, R^2 = 53.12%) and base parts of the leaf (part 3), there were a positive correlation of cell size and leaf lengths with few outliers (Fig. 3.6F, p = 0.0007, R^2 = 47.98%). The correlations observed in Fig. 3.6D and Fig. 3.6E were to a large part driven by the presence of relatively small cells (<100 μm^2) in the shorter leaves which were absent in the longer leaves.

These data fitted to a picture of cell division occurring towards the base of grass leaves, leading to a predominance of smaller cells in this region. As cells derived from the basal meristem mature and differentiate, they tended to become larger, leading to a preponderance of larger cells towards the leaf tip (part 1), as observed in these data and supported by statistical analysis (cells in the basal region of the leaf (part 3) were the smallest cells compared to the cells from other two areas, irrespective of the length (age) of leaf observed.

Having characterised the change in MC size in different regions of rice leaves during development, I analysed MC shape using two measures of the degree of cell curvature (1) "lobiness" in which the actual cell perimeter was divided by the perimeter of the minimal energy curve that could encompass the cell (see Methods) and (2) circularity, which expresses the similarity of the cell shape to a circle. In both measures, cells that were perfect circles would score 1, with increased lobing leading to lobiness values above 1, and distance from circularity leading to score below 1.

As shown in Fig 3.7A, at the tip of the leaf (part 1) cells in shorter, younger leaves were significantly less lobed than equivalent cells in longer, older leaves (p = 0.0436). A similar pattern was observed in MCs in the middle region (Fig. 3.7B, p < 0.05) and basal regions of leaves (Fig. 3.7C, < 0.05). In the basal region of the leaf (part 3) MCs tended to be less lobed than cells observed in middle and tip regions, irrespective of the length (age) of the leaf analysed. Thus, a gradient of leaf lobing was observed both within a leaf of any particular developmental age and between leaves of a particular developmental age when focussing on a specific region of the leaf. A positive correlation was observed between cell lobiness and leaf lengths in every parts of the leaves (Fig. 3.7D-F, $R^2 = 38.63\%$, p = 0.0045 (part 1), $R^2 = 53.37\%$, p = 0.0003 (part 2), and $R^2 = 41.39\%$, p = 0.0022 (part 3)). In all regions and leaf ages, even the basal region of the shortest (youngest) leaves, some degree of mesophyll lobing was measured (lobiness >1), suggesting that the initiation of lobing occurred before this stage.

When cell shape was calculated based on circularity, a similar picture emerged. Thus, at the tip, middle and base of the leaf, the highest degree of circularity was observed in short (young leaves), and this relatively high degree of circularity was observed in shorter leas irrespective of the region of the leaf where mesophyll cells were observed (Fig. 3.8A-C, p < 0.05) against leaf ages, an inverse correlation with cell circularity was observed in all regions of the leaf (from base to tip), with the steepest gradient observed in the middle region of the leaf when comparing leaves of different sizes (ages) (Fig. 3.8D-F, $R^2 = 57.99\%$, p = 0.0002 (part 1), $R^2 = 64.56\%$, p < 0.0001 (part 2), and $R^2 = 55.52\%$, p = 0.0002 (part 3)). Even in the basal region of the youngest leaves, MC circularity was approximately 0.9, indicating that for these cells cross-sectional area was not circular. When MC circularity was plotted against leaf length there was

a gradient of circularity, with cells in shorter, younger leaves being more circular in all regions. The patterns of cell lobiness, circularity and cell size across all the leaves examined in this study are examined in Fig. 3.9. These data show that cells towards the base of the leaf (part 3) are the least lobed (Fig. 3.9B, $p < 0.05$), most circular (Fig. 3.9C, $p < 0.05$) and smallest (Fig. 3.9A, $p = 0.0191$). With respect to size (Fig. 3.9A and B), MCs in the tip and middle of the leaf (parts 1 and 2) cannot be distinguished from each other.

These data fit to a scenario where MCs were differentiating at the base of the leaf from cells derived from the meristematic region. In the smallest leaves analysed here (< 20 mm in length) there was a slight gradient in lobing comparing the base, middle and tip of the leaf (compare 3.7A-C) but this gradient was already much more marked in slightly longer, older leaves (leaf length 21-60mm). Thus a major increase in MC lobing occurred during this developmental stage. Although some degree of mesophyll lobing was presented even at the youngest leaf stages analysed here, there was a window of development following this stage when increased lobing was happening. I speculated that during this stage the MCs might be sensitive to environmental factors which modulated the final degree of MC lobing.
.
In addition, I also analysed parameters of leaf features during development since this would set the boundaries within which the MCs were packed, thus the number of MCs within different regions of the leaf as it grew. As shown in Fig. 3.10, leaf thickness increased in all regions of the leaf, especially middle (Fig. 3.10B, $p = 0.0495$,) and base (Fig. 3.10C, $p = 0.0362$) as leaves got longer, with maximal thickness being achieved when leaves were 60 mm in length or longer. On average, over the lifetime of a leaf there was no major difference in thickness across the different parts of the leaf. Within the leaf, the distance between veins (which sets the lateral boundaries for MC packing within the leaf) increased as leaf length increased (Fig. 3.11). This occurred in an approximately similar pattern in the three regions of the leaf analysed (tip, middle, base) (Fig. 3.11A-C, $p < 0.05$). When interveinal distance was compared between the different leaf regions for all stages of leaf development, there was a similar pattern, though the interveinal distance at the base of the leaf was generally smaller than in other regions (Fig. 3.11D, $p = 0.0109$).
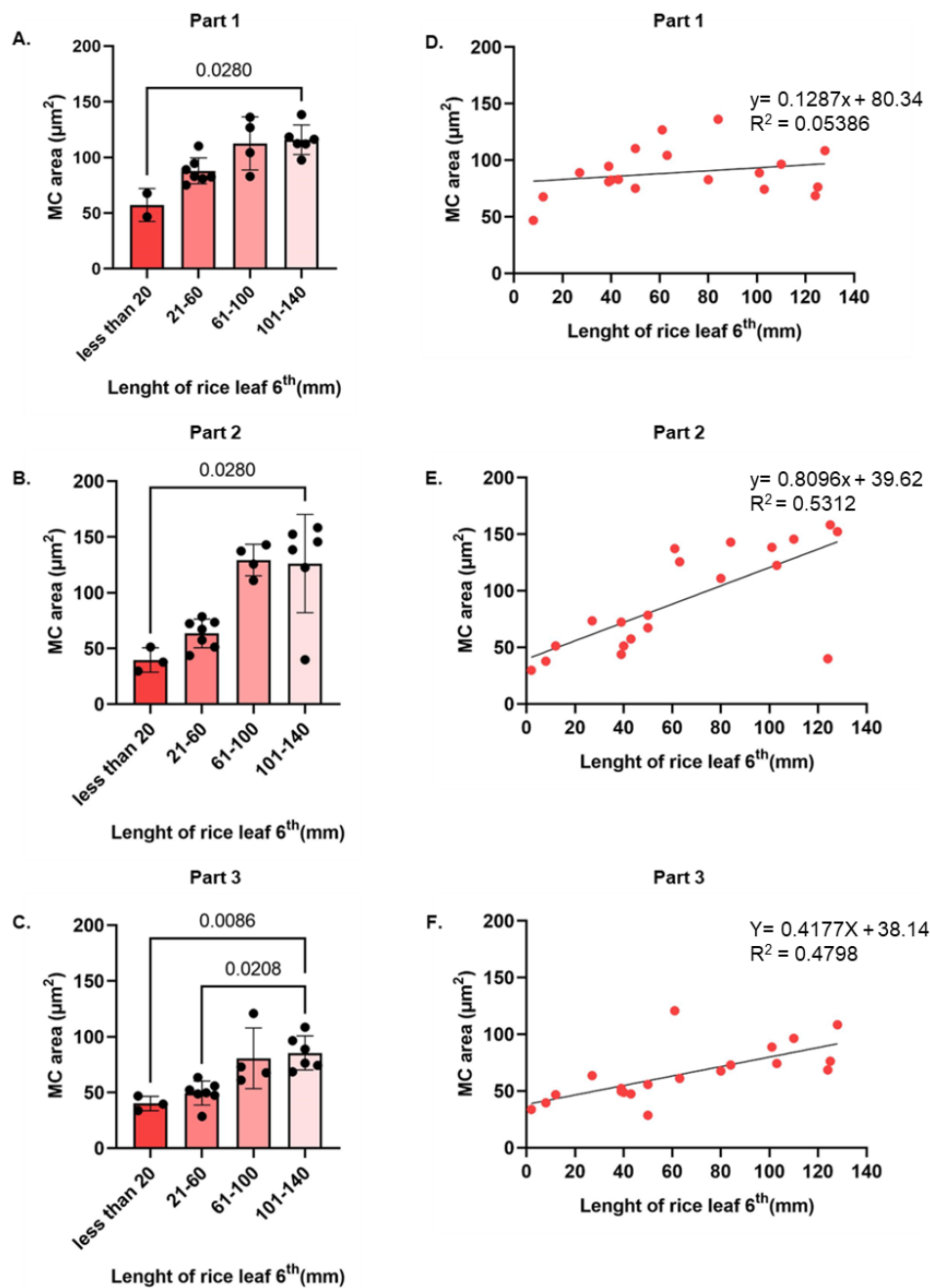
Figure 3.6. Mesophyll cell area in *IR64* leaves of various ages (9 to 12-day-old leaf 6) was estimated. The bar graphs (A to C) showed the mean and standard deviation of MC area in different leaf regions. The statistical analysis was performed using the Kruskal-Wallis test with Dunn's multiple comparison, and the resulting p-values were displayed in the graphs. The values of MC area were plotted against the length of rice leaf 6 aged from 9 to 12 days to investigate the relationship between these two values. The samples obtained from the tip (D, p = 0.3390), middle (E, p = 0.0003), and base (F, p = 0.0007) regions as displayed in simple linear regression. Two-tale statistics was used to analysed the data with the presence of R^2 on the graphs.
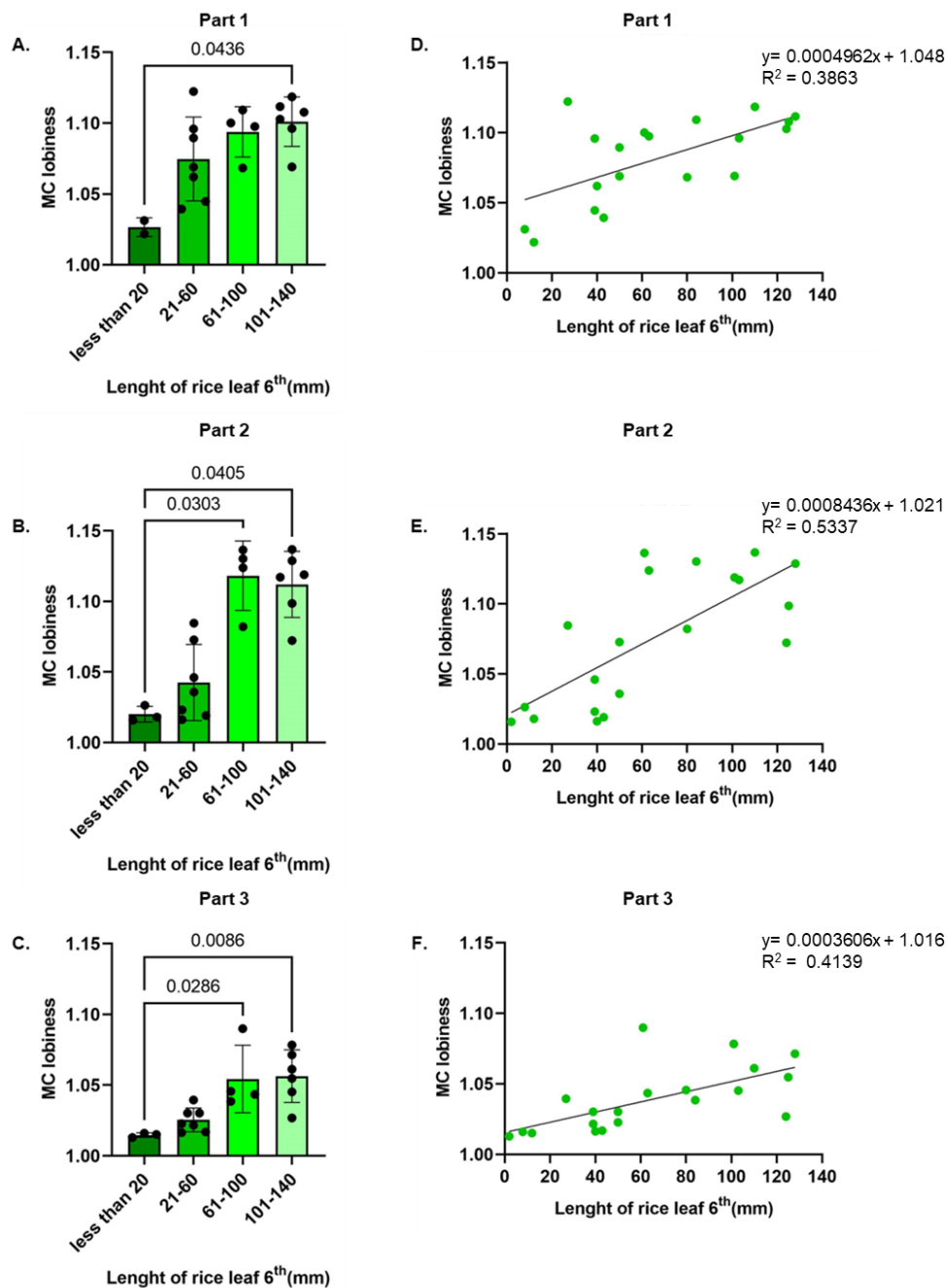
Figure 3.7. The mesophyll cell lobiness of I*R64* leaves, which had different ages (between 9 to 12 days), was determined. The mean and standard deviation of cell lobiness from different areas of the leaf are displayed in bar graphs (A to C). The Kruskal-Wallis test with Dunn's multiple comparison was used for the statistical analysis, and the graphs display the presented p-values. To explore the correlation between MC lobiness and the length of rice leaf 6 (9-12 days old), the data of MC lobiness from samples collected from the tip (D, p = 0.0045), middle (E, p = 0.0003) and base (F, p = 0.0022) were plotted against the difference of leaf lengths. The data was analyzed using two-tailed statistics, and the graphs included values for R^2.
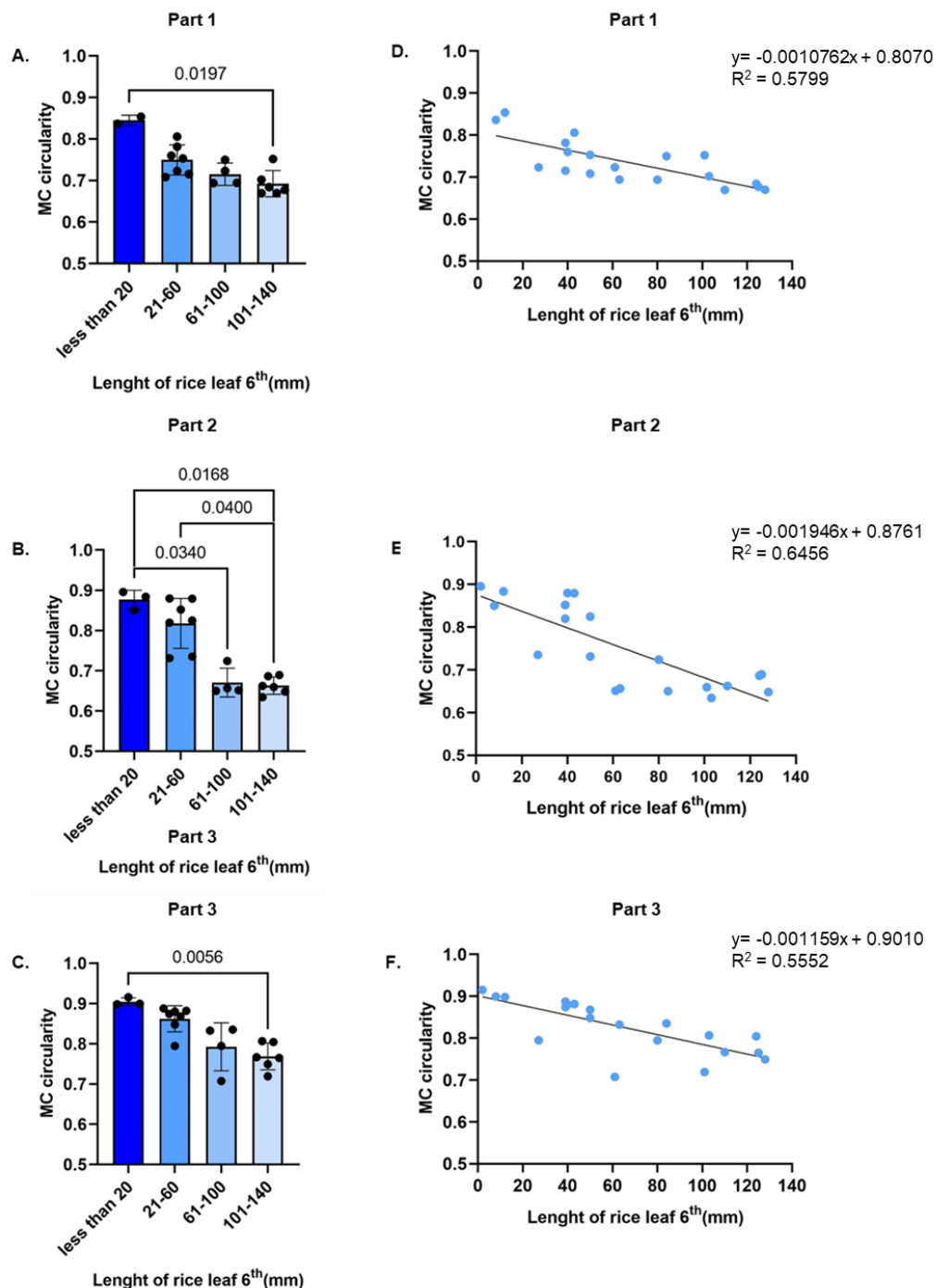
Figure 3.8. Mesophyll cell circularity of *IR64* leaves with different ages (9 to12 days) was calculated. Mean and SD of cell circularity from different leaf area showed in bar graph from A to C. The statistical analysis was conducted using the Kruskal-Wallis test with Dunn's multiple comparison, and the p-values were presented in the graphs. To investigate the correlation between MC circularity and the length of rice leaf 6 (9-12 days old), the data of MC circularity obtained from samples taken from the tip (D, p = 0.0002), middle (E, p < 0.0001), and base (F, p = 0.0002) regions were plotted against the difference in leaf lengths. Two-tailed statistic was used to analyse the data, and the graphs displayed R² values.
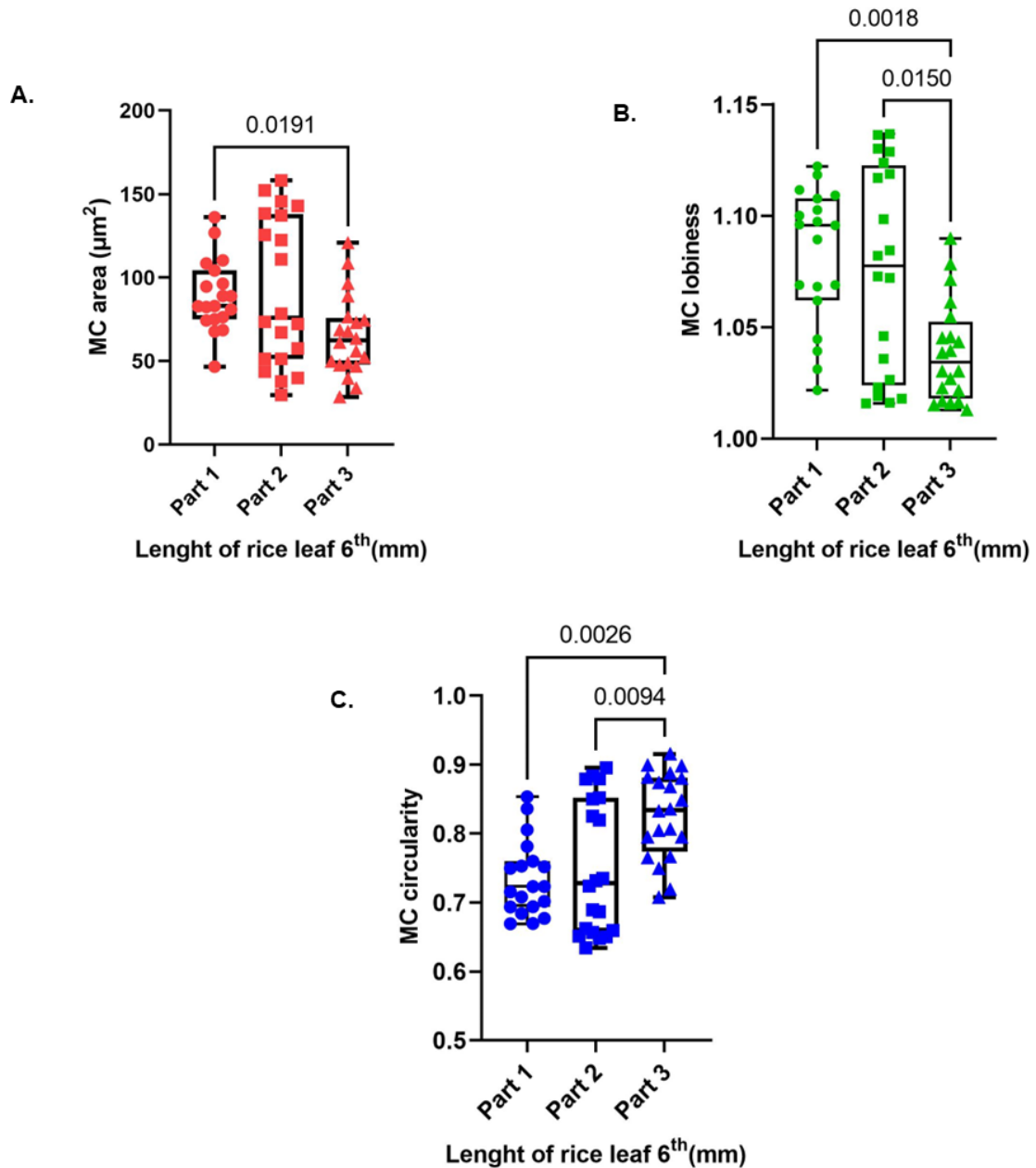
Figure 3.9. All data of MC area and shape, including cell lobiness and circularity, from three parts of *IR64* leaves (9 to 12 day-old leaf 6) were analysed and plotted in a Box and Whisker plot. The plot included the mean, standard deviation, minimum, and maximum values as shown in A-C. The statistical analysis was performed using the Kruskal-Wallis test with Dunn's multiple comparison, and the p-values were presented on the plots.
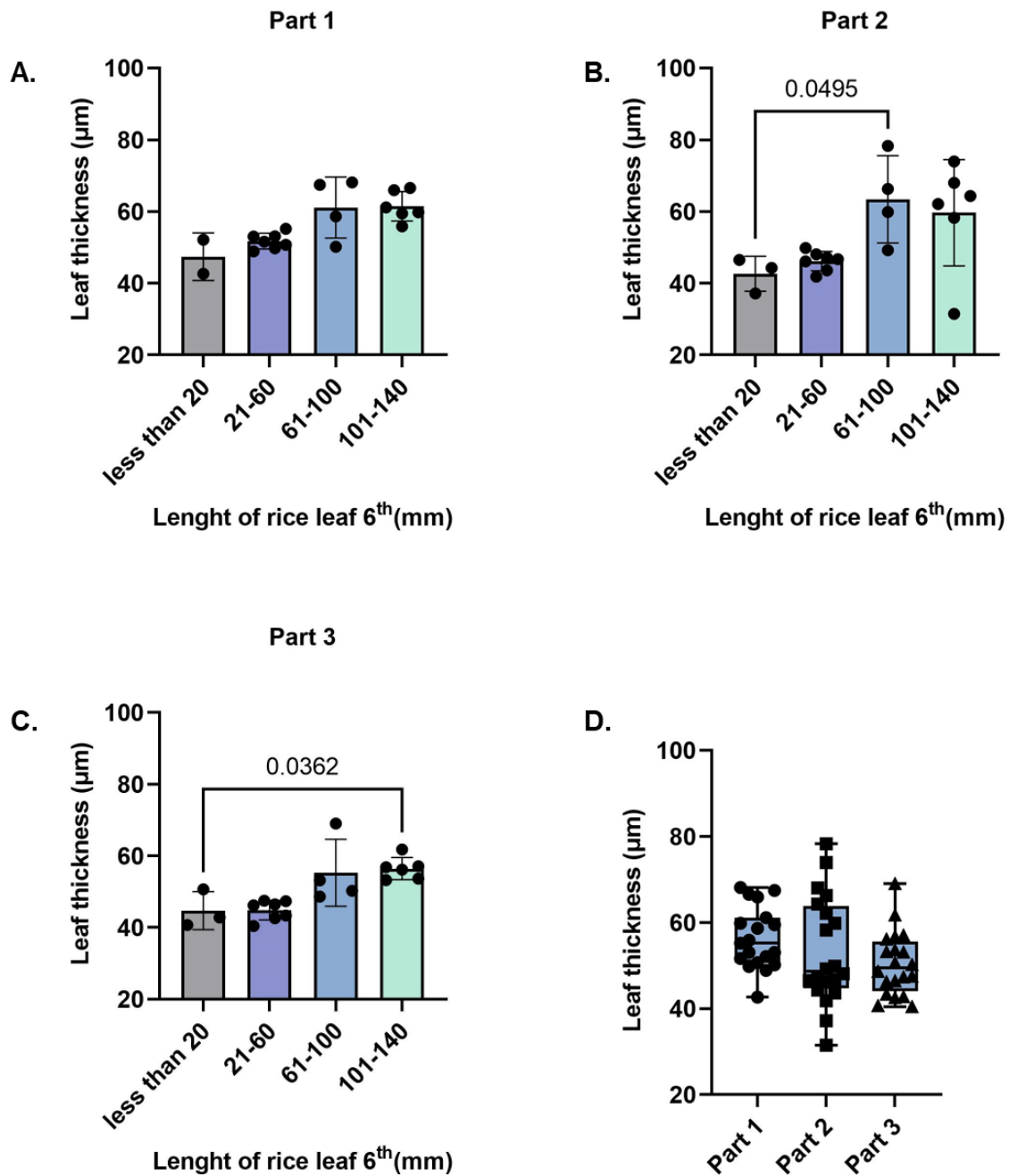
Figure 3.10. The picture displayed the measurement of leaf thickness of *IR64* (9 to 12-day-old leaf 6). Three main regions were calculated and represented in column graphs as shown in A, tip (part 1); B, middle region (part 2) and C, base (part 3) of each leaves. D, the data of leaf thickness in all regions was plotted in Box and Whisker with mean, SD, min and max values. Statistical analysis was performed by Kruskal Wallis, p = 0.0042 (A), p = 0.0246 (B), p = 0.0032 (C) and p = 0.0830 (D) with Dunn's multiple comparison. Each dot corresponded to the number of replications for the rice plants.
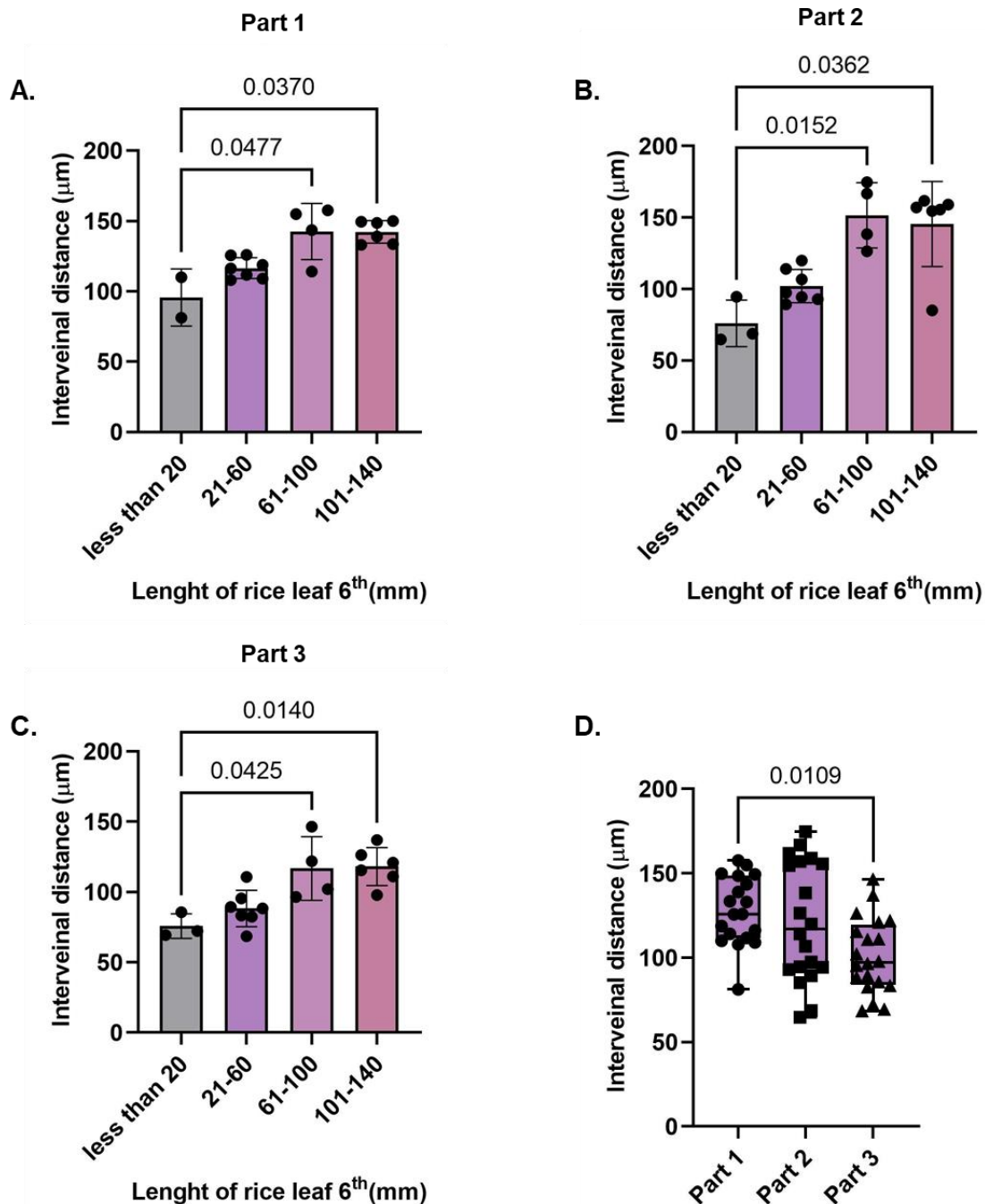
Figure 3.11. The picture illustrated the measurements of interveinal distance between two minor veins in different regions of *IR64* leaves. The three main regions, namely the tip (A), middle region (B), and base (C) of each leaf, were represented in column graphs with mean and SD. Additionally, the data for leaf thickness in all regions is displayed in a Box and Whisker plot (D), showing the mean, standard deviation, minimum, and maximum values. The statistical analysis was analysed by the Kruskal-Wallis test, with p-values showed in the graphs. Each dot in the picture represented the number of replications for the rice plants.

3.7. Discussion

Rice mesophyll cells are distinguished by their high degree of lobing, a feature that has been linked to providing a higher surface area for gas exchange for photosynthesis and transpiration. My results from Chapter 2 showed that the degree of lobing in rice mesophyll cells was responsive to the environment, supporting a link between gas flux via stomata and the degree of MC lobing. This raised the questions such as: when did MC lobing first become apparent during leaf development? Did this co-inside with, e.g., stomatal differentiation and/or active photosynthesis? To address these questions, I undertook a series of experiments to characterise when MC lobing occurred during rice leaf development.

In this chapter, I examined MCs in three different regions of the leaf (tip, middle, base) at different stages of growth of leaf 6 of IR64 plants. The results indicated that mesophyll cells in the basal (part 3) of the leaves analysed here were generally smaller than cells in the more apical regions (parts 1 and 2) (Fig. 3.6). Although MC lobing increased during growth in all regions of the leaf, some degree of lobing was already detectable in the youngest leaves analysed (< 20mm length) in all regions (Fig. 3.7). MCs in the most basal region (part 3) of the youngest leaves (< 20mm) showed some lobing, indicating that altered perimeter shape is a very early event in rice leaf development (Fig. 3.7C). The earliest stage in which mesophyll lobing was obviously seen under the light microscope is in part 1 of young leaf with length 2 mm, while in other parts lobing was not seen clearly.

In theory, the shoot apical meristem (SAM) of monocot leaves such as rice forms laterally around the base of a single cotyledon. The initiated group of the cells is recruited to this area and divide unidirectionally before being differentiated to a leaf primordia at the flank of SAM (Miwa, et al., 2009; Drisch and Stahl, 2015). Leaves have a region of cell division towards the base of the leaf. Cells towards the more distal part of this region gradually terminate division and enter a phase of differentiation and expansion. Consistent with this, cell size in the basal area is smaller than the apical regions. At the tip, the leaves contain the older cells which will be differentiate to generate the specific cells such as mesophyll and other cell components. The

degree of lobing obviously seen in part1 (tip) and/or part 2 (middle) support the hypothesis that the development of mesophyll cells occurs at an early stage of leaf development.

However, there is no clear evidence to show the stage of mesophyll and stomatal development of rice leaf 6. The previous data from Dr. Naomi Cox (Cox, 2020) suggested that rice leaf 5 in P3/P4 stage (less than 1 cm) was capable of performing photosynthesis. The stage of leaf development was estimated from the length of rice leaf 3. More details are shown in her research (Cox, 2020). The initiation of small vascular bundle and epidermal cell development was established in stage P3. The blade–sheath boundary ligule primordium was also present in this stage. During P4 leaf development, the epidermal cells were differentiated to specific cells such as bulliform cells, silica cells, cork cells and stomata. Moreover, around 4 to 6 mesophyll cells were generate between individual veins, indicating that the photosynthetic process first occurred at the P3 and P4 stage. These data suggest that the structure of mesophyll cell could be regulated by the alteration of stomata pattern on the leaf surface before or after the P3/P4 stage, however more experimental data are needed to test my hypothesis.

Chapter 4

How do stomata influence mesophyll cell lobing?

4.1. Introduction

The data from Chapter 2 suggested that there was a causal relationship between the anatomical g_{smax} and mesophyll cell lobing. The *osEPF1_oe* lines with low stomata density (SD) and a decrease in maximum stomata conductance (g_{smax}) had less lobed mesophyll cells, whereas the MCs of *osEPFL9_oe* lines with an increased stomata density and higher g_{smax} showed increased cell lobing. These data suggested that the alteration of SD and/or g_{smax} might induce a change of MC cell shape.

In general, plants response to a range of the external environmental signal, including CO_2 (Ainsworth and Rogers 2017, Taub 2010). For example, plants regulate CO_2 uptake for photosynthetic and transpiration processes through stomatal pores on the leaf surface (Misra et al. 2015; Cominelli et al.2010). Each pore is sensitive to the external and internal environment, and CO_2 functions as a signal to regulate stomatal movement. At ambient CO_2 conditions in the presence of light, the stomata open to let the CO_2 from the air flow into the leaf. On the other hand, under high CO_2 level, the pore closes, consequently reducing the stomata conductance (g_s) to prevent the water loss by transpiration process while maintaining photosynthesis due to the higher values of C_i (Horak et al. 2016; Sujimoto et al. 2016).

Opening and closing of stomata is set by the turgor pressure in the guard cells (Misra et al. 2015) with the pore opened by an increase of turgor pressure. H^+-ATPases on the plasma membrane are activated via phosphorylation of the penultimate threonine which leads to membrane hypo-polarization, allowing K^+ influx through ion channels (Assmann et al.1985; Schroeder et al. 1984). The guard cells then swell as they uptake water inside the cells (Shimazaki et al. 2007). High CO_2 has been reported to restrain proton pumping (Edwards and Bowling, 1985) and stimulate anion channel activity to discharge K^+ through ion channels (Raschke et al. 2003). Chlorine then effluxes from the guard cells, resulting in membrane depolarization and a decrease in the turgor

pressure to close the stomatal pore. Stomatal movement requires the primary sensor to detect the CO_2 levels allowing stomata to respond to different environments, but the nature of this sensor remains controversial.

4.2. The regulation of stomatal movement and *HT1* rice plants

The response of stomata to CO_2 is crucial for plant growth and helps regulate their water efficiency. This response requires the activity of carbonic anhydrases, which facilitate the conversion of CO_2 to bicarbonate ions and protons. These bicarbonate ions play an important role in triggering the closure of stomata, thus regulating the plant's gas exchange. However, the exact mechanism by which plants sense CO_2 and bicarbonate ions remains unknown (Takahashi et al.,2022; Xue et al.2011). It is known that this sensor requires protein phosphorylation to drive CO_2 for stomatal regulation.

Three main types of protein kinases (MPK4/MPK12, HT1, and CBC (CONVERGENCE OF BLUE LIGHT AND CO_2 1 and 2) have been reported to function as protein regulators to modulate stomatal movement (Takahashi et al.,2022; Tõldsepp et al. 2018; Hiyama et al. 2017). A high CO_2 level in plants triggers the interaction between two MAP kinases; MPK4 and MPK12, with HT1 protein kinase. The reversible interaction between MPK4/12 and HT1 protein kinase serves as a CO_2/bicarbonate sensor mechanism in plants. When CO_2 level is elevated, this sensor is triggered, leading to the closure of stomata. Under low CO_2 condition, HT1 phosphorylates and activates another kinase called CBC1, which negatively regulates the CO_2 response in stomatal function. When activated, the phosphorylation and activation of CBC1 by HT1 creates a signaling cascade that inhibits the opening of stomata, keeping them closed (Takahashi et al.,2022).

Ht1 mutants were originally identified from a screen of Arabidopsis thaliana plants showing higher temperature. Seven HT1 alleles (HT1-1, HT1-2, HT1-3, HT1-4, HT1-5, HT1-6, and HT1-7) were identified (Sugimoto et al 2016). The HT1 gene encoded a protein kinase and two alleles (HT 1-1 and HT1-2) was mainly expressed in guard cells, functioning in protein phosphorylation in CO_2-induced stomatal movement (Hashimoto et al. 2006). The recessive HT1-2 mutant of *Arabidopsis thaliana* exhibited a closed stomatal phenotype similar to what was typically observed in the presence of

high CO_2 levels. Unlike normal stomata, these mutant stomata maintained a closed state regardless of the actual CO_2 concentration in the environment. This meant that even under conditions of low CO_2 levels, the mutant stomata remain closed as if there is an abundance of CO_2 (Hashimoto et al. 2006; (Takahashi et al.,2022). However, the details of exactly how the HT1 gene mediates stomatal opening/closure to CO_2 in rice plants remains unclear. Nevertheless, the mutants provide a tool to manipulate stomatal conductance. Importantly, for this project the HT1 mutants in Arabidopsis showed normal stomatal size and density, thus the changes in g_s were not due to changes in physical properties of the stomata.

During this project, another student in the group (Shanshan Wang with Emily Harrison, working with partners at Durham University) created and characterised mutants of HT1 in rice to investigate whether the gene played a similar role in modulating stomatal response to different CO_2 levels as described for Arabidopsis. Since the initial results of this investigation were promising (the plants showed altered growth from control lines under different CO_2 levels), I decided to use these novel rice mutants as a tool to investigate whether altered stomatal function in different CO2 conditions (ambient and CO_2 level) led to a change in mesophyll cell lobing. This would allow me to see whether the altered lobing observed in the *osEPF_oe* mutants (described in the previous chapter) reflected a general link of abnormal g_s and altered mesophyll cell shape.

4.3. Hypothesis: Altered stomatal density and/or g_{smax} in *HT1* mutant lines in rice influences mesophyll cell shape (lobing) with varying CO_2 conditions.

4.4. Aim: To investigate the link between stomatal properties and the leaf structure of *HT1* mutant rice plants under ambient (400 ppm) and high CO_2 (800 ppm) levels.

4.5. Materials and methods

4.5.1. Seed germination and growing

HT1 mutant rice seeds were germinated in two different growth chamber (Conviron, Winnipeg, MB,Canada) with two different CO_2 conditions; at ambient (420 ppm) and high CO_2 (800 ppm) levels. Both chambers were adjust the internal environments as follow; light = 28˚C (12 hours) , dark = 24˚C (12 hours), light = 1000 μmol^{-2s-1}, humidity = 60% for 7 days. Then germinated seeds were transferred to the mixed soil with fertilizer. The recipe to prepare the soil for 15 pots is 2:1 Kettering Loam: John Innes no. 3, mixing with 30 ml Osmocote® fertiliser (Ipswich, UK) and 120 ml of silica sand by volume in pots. The plants were grown in the same chamber with the same condition for 21 days until leaf 6 was fully mature. Plants were watered every 2 or 3 days a week and add around 1 or 2 inches of water level in the tray to keep the moisture of the roots. After 28 days, the fertilizer was added to the plants once a week until seedling stage.

4.5.2. The analysis of stomatal properties and leaf structures

On day 21, rice leaf 6 was imprinted by applying the 1 cm of vinyl polysiloxane, VPS (ImpressPLUS Wash, Perfection Plus Ltd, Hants, UK) on the adaxial leaf surface and peel the imprints off to measure the stomata characteristics. The portion of leaf 6 (around 1 cm) was then collected to observe the anatomical leaf structures. The parameters and methods were mentioned in Chapter 2.

4.6. Results

To further investigate the relationship between stomatal function and mesophyll cell lobing, I examined two gene-edited lines of rice (cv *Nipponbare*) in which the *HT1* gene had been mutated, leading to stomata which no longer responded normally to altered CO_2 level by pore closure. This should lead to alter gas exchange via the stomata, thus a tool to examine whether there was link between gas exchange and cell lobing. Two lines (*HT1 15-1; HT1 15-2*) were used. These lines were generated by gene editing, with *HT1 15-1* having a 2 bp deletion and *HT1 15-2* having a 36bp deletion, with both expected to lead to a loss of *HT1* gene function.

To check whether the mutations in the *HT1* gene led to any indirect outcome on physical stomatal characteristics (which might influence gas exchange), I first analysed the two *HT1* mutants made available to me (*HT1 15-1, HT1 15-2*) for stomatal complex area, guard cell area and pore area (Fig. 4.1A-C). These measurements were made in plants grown under ambient and elevated CO_2 since the experimental design and nature of the mutants should lead to altered stomatal function at different CO_2 levels. Stomata were measured in the mid-region of the mature 6 leaf in both treatments and for all genotypes. Under both ambient and elevated CO_2 there was no difference in stomatal size between the control and *HT1* mutants, with the exception of pore area for the *HT1 5-2* mutant at ambient CO_2 where there was a significant increase relative to the control (Fig. 4.1C, Kruskal-Wallis test, Dunn's multiple comparisons, p = 0.0402).

In addition to pore size, the number of pores per area (stomatal density, SD) influenced gas exchange across the epidermis. I therefore investigated whether there was any difference in this parameter in the *HT1* mutants and the control line. The results showed that the SD of the *HT1 15-1* and *15-2* mutant rice plants were not different from the control plants in both ambient (Fig. 4.2A, Kruskal -Wallis test, p = 0.0836) and high CO_2 levels (Fig. 4.2B, ANOVA, p = 0.0886). However, even though, SD showed no difference, the numbers of stomata per area of these two mutant lines was slightly higher under both two CO_2 regimes. This was potentially important since the calculation of theoretical maximum value of stomatal conductance, g_{smax}, depended upon the squared value of SD. Indeed, when the anatomical g_{smax} was calculated, a

significant increase in value compared to control was observed, both for the *HT1* mutant lines grown under ambient CO_2 (Fig. 4.3A, Kruskal -Wallis test, p = 0.0161) and at elevated CO_2 (Fig. 4.3B, ANOVA, p = 0.0141). Thus although the *HT1* mutants theoretically only impact the sensitivity of stomata to CO_2, there was the potential that the relatively small changes in stomatal density accompanying these mutants does influence g_s.

Having characterised the physical parameters of stomatal size and density, I proceeded to examine whether there was any change in mesophyll cell shape in the *HT1* mutants compared with the control line under ambient CO_2 conditions. The results indicated that in both *HT1* mutants there was a significant increase in cell lobiness (Fig. 4.4A, Kruskal -Wallis test, p < 0.0001). This increase in mesophyll cell lobiness was also observed when the plants were grown at elevated CO_2 (Fig. 4.5A, ANOVA, p < 0.0001) of CO_2 levels.

To investigate whether the increase in cell lobing reported in Fig 4.4A reflected altered cell shape throughout the mesophyll of the leaves or whether increased lobing was occurring in specific regions of the leaf, I calculated the cell lobing values based on layer location (layers 1-5 of the mesophyll). These results indicated that the increased lobing in the *HT-1* mutants occurred in all layers at both ambient (Fig. 4.4B-F, Kruskal Wallis, p = 0.0008 (B), p = 0.0007 (C), 0.0009 (D), p = 0.0002 (E), p = 0.0007 (F)) and elevated CO_2 level (Fig. 4.5 B-F, one-way ANOVA, p = 0.0005 (B) , p < 0.0001 (C-E), and p = 0.0004 (F)), with the difference relative to control being statistically significant for almost all comparisons. Analysis of mesophyll cell circularity agreed with the analysis of cell lobing. Thus cell circularity of the *HT1* mutants was lower at both ambient CO_2 (Fig. 4.6A, Kruskal Wallis, p = 0.0006) and elevated CO_2 (Fig. 4.7A, one-way ANOVA, p < 0.0001, n = 8). This decrease in cell circularity was measured within each of the 5 cell layers analysed within the rice leaves for both ambient CO_2 (Fig 4.6 A-E, Kruskal Wallis, p = 0.0009 (B), p = 0.0007 (C), 0.0009 (D), p = 0.0002 (E), p = 0.0006 (F)) and elevated CO_2 (Fig. 4.7A-E, one-way ANOVA, p = 0.0004 (B), p < 0.0001 (C - E), p = 0.0002 (F), n = 8), with virtually all comparisons supporting a significant difference in circularity value between the mutant and the control. This decrease in cell circularity fits to the calculated increase in cell lobiness.

When mesophyll cell size was measured, a significant decrease was calculated in the *HT1* mutants compared with the control at ambient CO_2 (Fig. 4.8A, Kruskal-Wallis test, p = 0.0005). This was observed in all layers of the mesophyll for both mutant lines (Fig. 4.8B-F, Kruskal Wallis, p = 0.0070 (layer 1), p = 0.0005 (layer 2), p = 0.0009 (layer 3), p = 0.0006 (layer 4), p = 0.0056 (layer 5)). Thus under ambient CO_2, mesophyll cells are generally smaller in the *HT1* mutants.

To investigate whether the changes in mesophyll cell size in the *HT1* mutants were reflected in alterations in other aspects of leaf structure, I measured a range of other parameters. Bundle sheath cell size was significantly smaller in both *HT1* mutant lines compared to control and this was the case for plants grown under both ambient CO_2 (Fig. 4.10A, Kruskal-Wallis test, p = 0.0009) and elevated CO_2 (Fig. 4.10B, one-way ANOVA, p = 0.0099). At the larger scale of leaf anatomy, the interveinal distance was decreased in the *HT1* mutants compared to control leaves, both under ambient CO_2 (Fig. 4.11A, Kruskal Wallis, p = 0.0009) and elevated CO_2 (Fig. 4.11B, ANOVA, p = 0.0007). Similarly, leaf thickness was less in the *HT1* mutant lines compared with the controls, again under both ambient and elevated CO_2 levels (Fig. 4.11, Kruskal-Wallis test, p = 0.0009 (C), ANOVA, p = 0.0110 (D)).
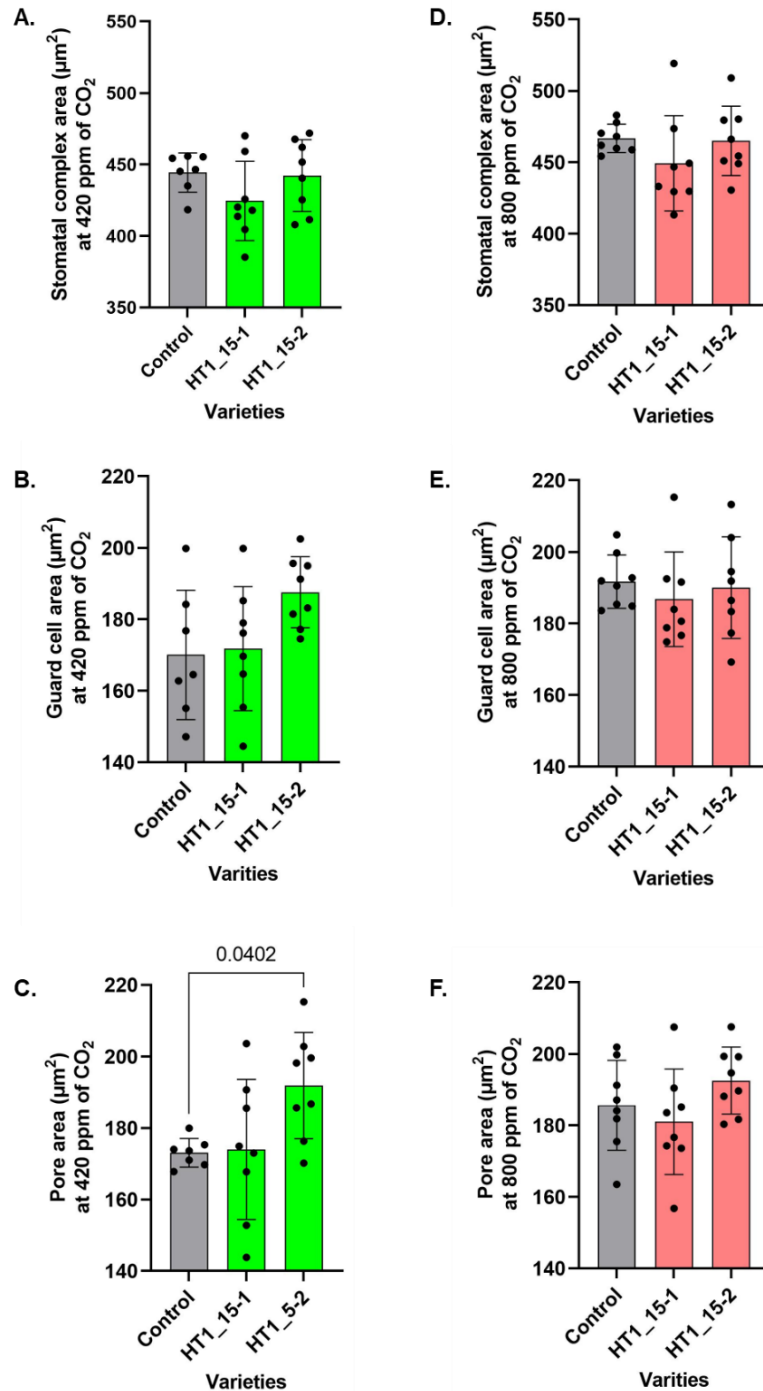
Figure 4.1. The HIGH TEMPERATURE 1 (*HT1*) negatively regulates stomatal function in *Arabidopsis thaliana. The mutant HT1 genes (HT1_15-1 and HT1_15-2) were introduced in* rice plants (*Oryza sativa* ssp. *japonica* cv. *Nipponbare*).The measurement of stomata characteristics of 21-day old rice leaf 6 at ambient and high CO_2 levels was estimated. Bar graphs represented the stomatal complex area (A, D) , guard cell area (B, E) and pore area (C,F) of *HT1 15-1* and 15-2 mutants and a control plant at 420 ppm (green) and 800 ppm (red). The spots on each column showed the numbers of individual plants (n). The error bar showed mean value with standard deviation (SD) of each parameters of stomatal features.
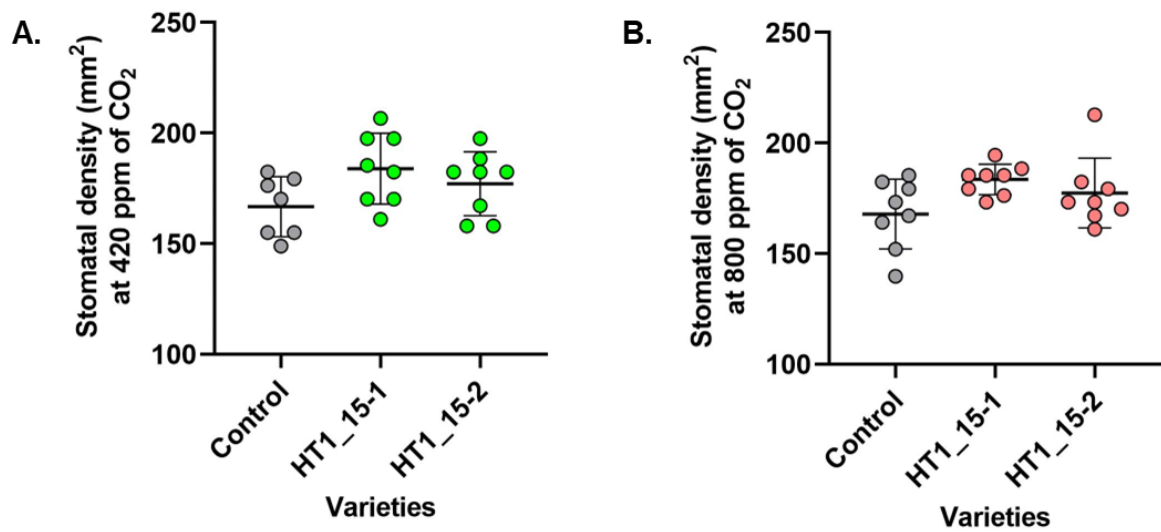
Figure 4.2. The scattering individual plots of showed the stomatal density of *HT1* mutants and wild type (21 day) with mean (horizontal line) and SD (vertical line) in 1 square metres area under 420 ppm (A, Kruskal -Wallis test, p = 0.0836) and 800 ppm (B, one-way ANOVA, p = 0.0886, n = 8) of external CO_2 level. Each spots represented the replication numbers of individual plant varieties.
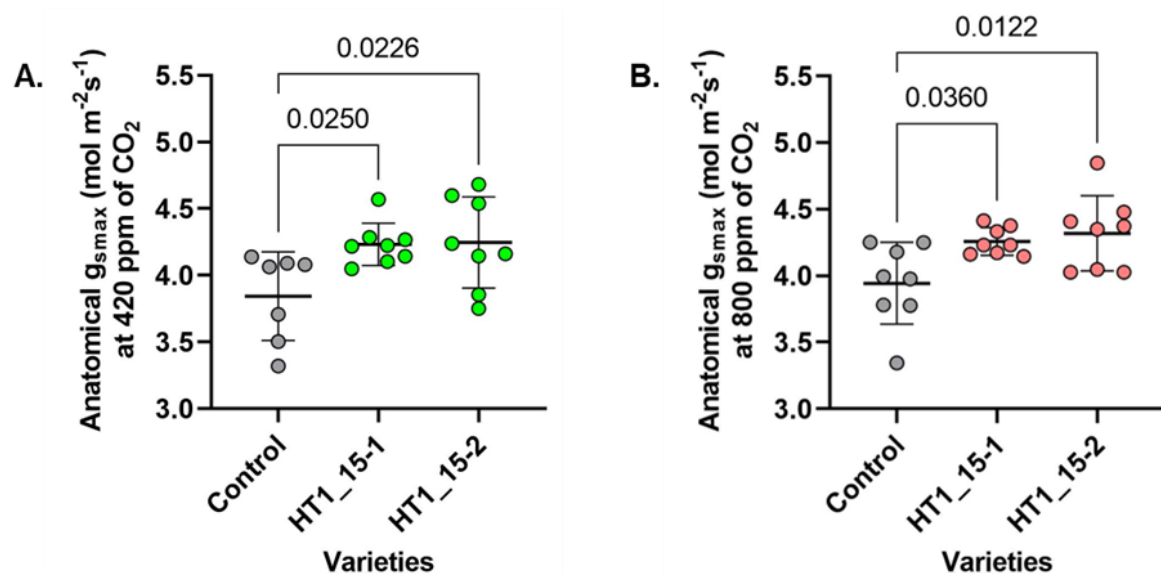
Figure 4.3. An increase of the maximum stomata conductance g_{smax} of *HT1* and control lines (21-day old) was presented in scattering individual plots in both ambient (A, Kruskal -Wallis test, p = 0.0161) and high CO_2 conditions (B, one-way ANOWA, p = 0.0141, n = 8). The plots displayed both the p-values from multiple comparisons and the numbers of plant replications. Each spots showed the replication numbers of each plants with in different colour.
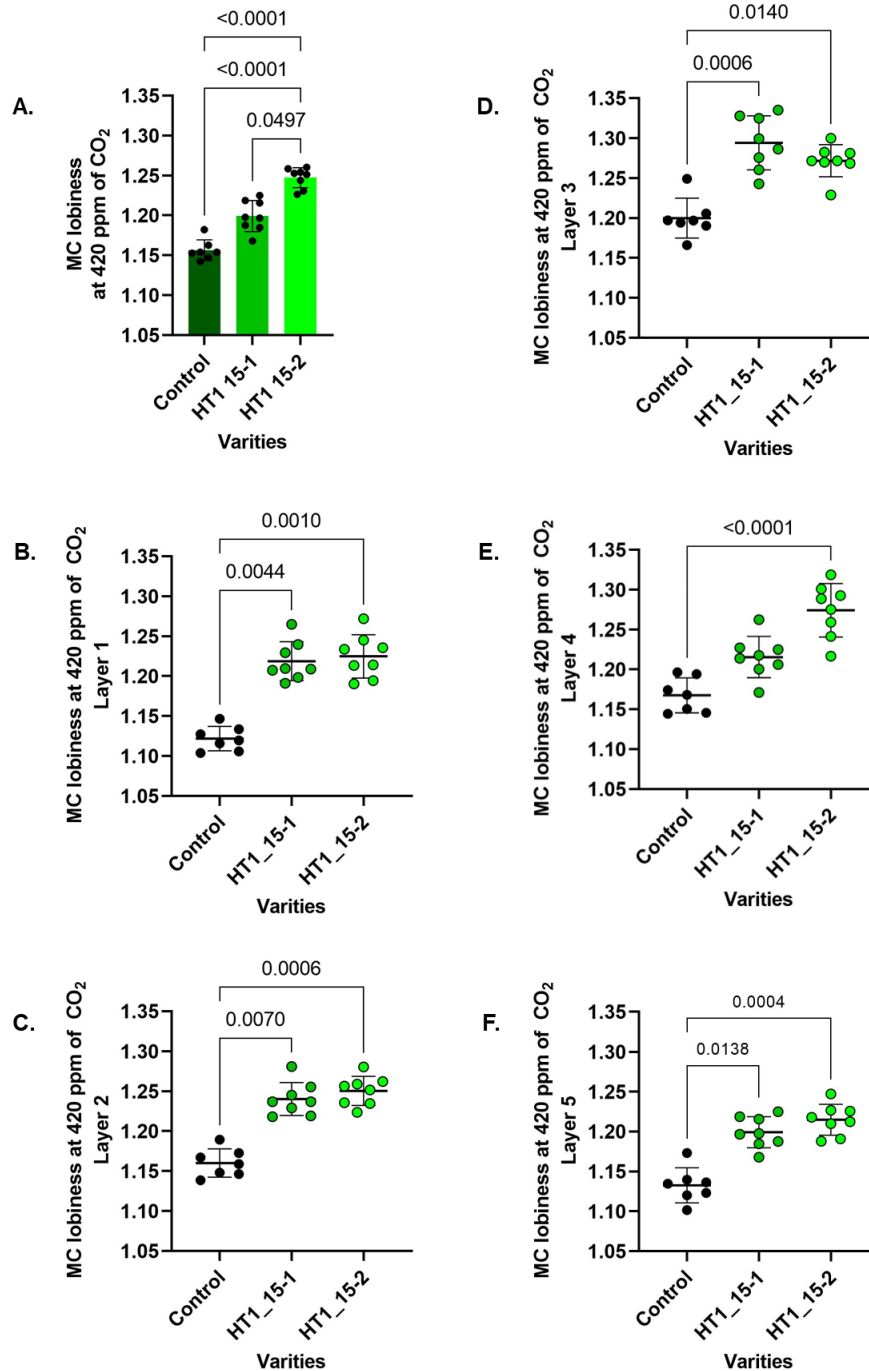
Figure 4.4. At 420 ppm of CO_2 level, the degree of cell lobing in rice leaves (*HT1* mutants and wild type) was analysed. The analysis was represented using scatter plots with mean and standard deviation. The *HT1* mutant leaves (*HT1_15-1* and *HT1_15-2*) exhibited significantly higher cell lobiness compared to the control group (A, Kruskal Wallis, p < 0.0001). Furthermore, B-F, the cell lobiness of each cell layer from 1 to 5 was also measured (Kruskal Wallis, p = 0.0008 (B), p = 0.0007 (C), 0.0009 (D), p = 0.0002 (E), p = 0.0007 (F). The plots included the presentation of p-values from multiple comparisons and the numbers of plant replications.
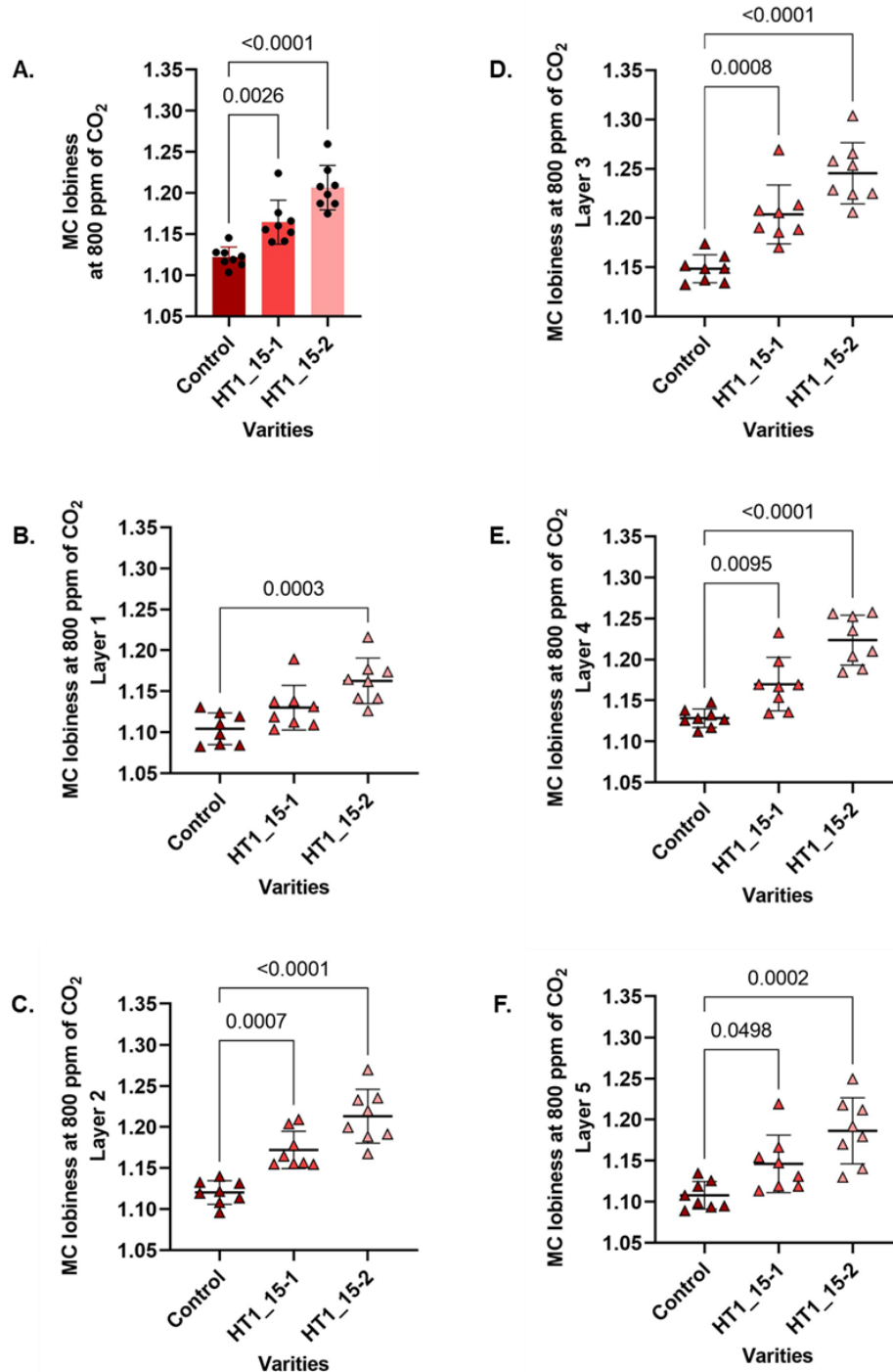
Figure 4.5. At 800 ppm, each portions of rice leaf (*HT1* mutants and wild type) were analysed the degree of cell lobing as shown in scatter plots with mean and SD. The MC lobiness of *HT1* mutant leaves (*HT1_15-1 and HT1_15-2*) is significantly higher than a control (A, one-way ANOVA, p = 0.0066). MC lobiness of each cell layer from 1 to 5 was also measured as displayed a significant increase in *HT1* mutants (one-way ANOVA, p = 0.0005 (B, layer 1), p < 0.0001 (C-E, layer 2 to 4), and p = 0.0004 (F, layer 5)). The plots displayed the inclusion of p-values derived from multiple comparisons and the corresponding numbers of plant replications (n = 8).
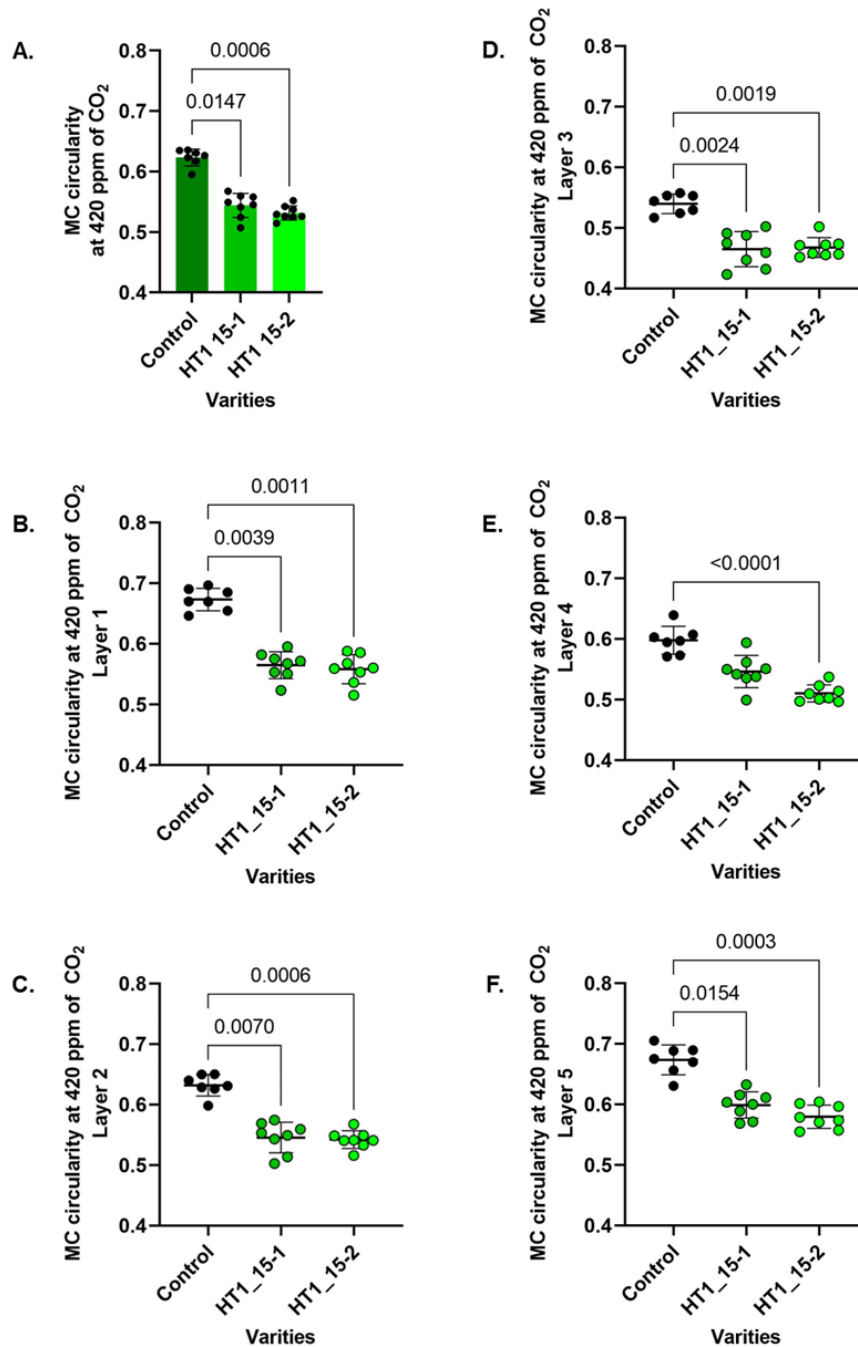
Figure 4.6. At 420 ppm of CO_2 concentration, the roundness of mesophyll cells was calculated. The circularity of cells in rice leaves (*HT1* mutants and wild type) was analysed. The analysis was represented using scatter plots with mean and standard deviation. A, The *HT1* mutant leaves (*HT1_15-1 and HT1_15-2*) exhibited significantly lower cell circularity compared to the control group (Kruskal Wallis, p = 0.0006). Additionally, the cell circularity of each cell layer from 1 to 5 was measured, and it showed a significant decrease in *HT1* mutants (Kruskal Wallis, p = 0.0009 (B), p = 0.0007 (C), 0.0009 (D), p = 0.0002 (E), p = 0.0006 (F)). The p-values obtained from multiple comparisons and the corresponding numbers of plant replications (n=8) were both shown in the plots.
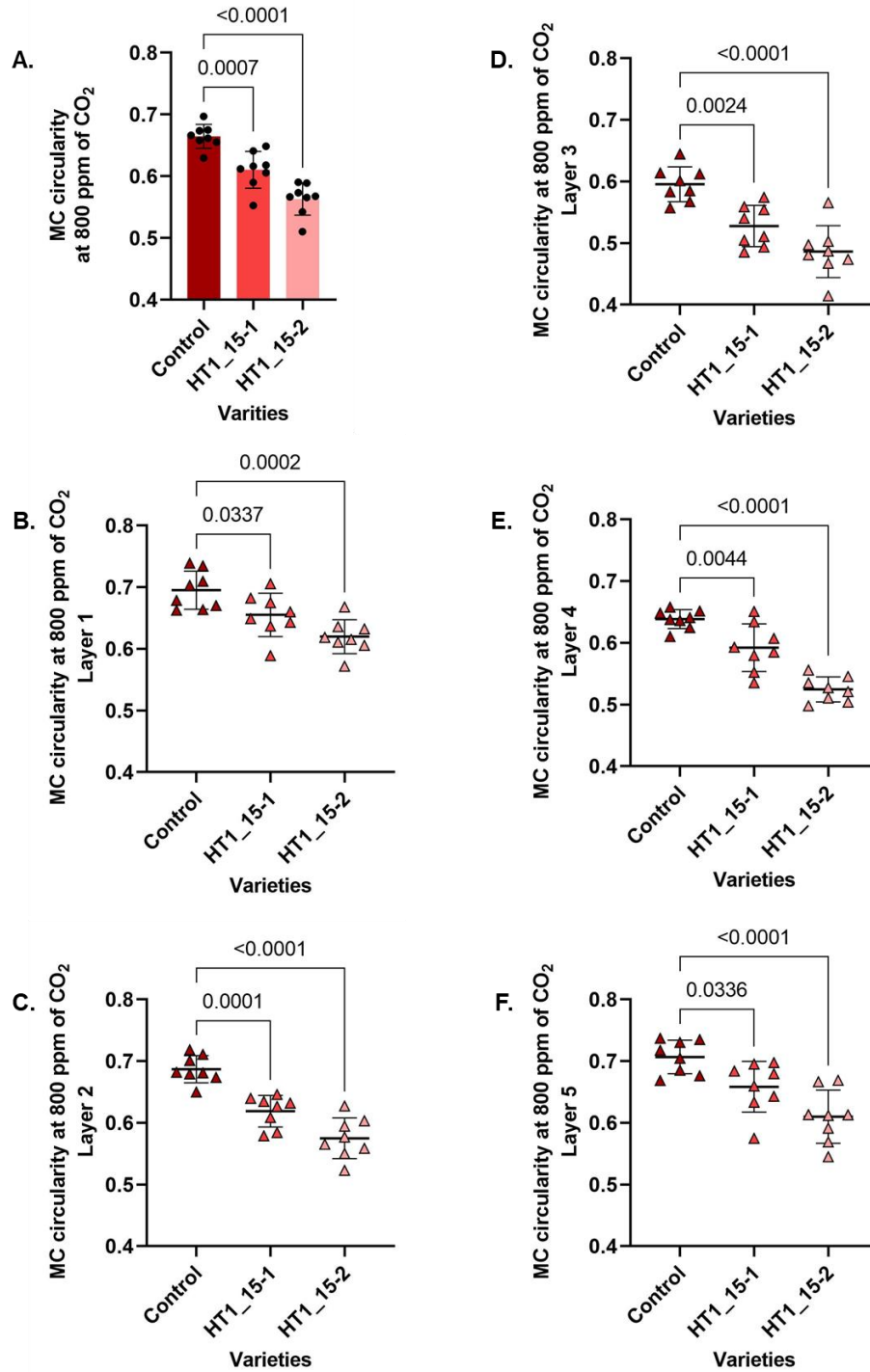
Figure 4.7. The roundness of mesophyll cells in rice leaves was analysed at a carbon dioxide concentration of 800 ppm. The comparison of cell circularity between *HT1* mutants and a wild type was presented in scatter plots displaying the mean and standard deviation. Cell circularity of the *HT1* mutant leaves (*HT1_15-1* and *HT1_15-2*) had significantly lower compared to control (A, one-way ANOVA, $p < 0.0001$, n = 8). In addition, B-F, the analysis revealed a significant decrease in cell circularity across all cell layers (1 to 5) in the *HT1* mutants (one-way ANOVA, $p = 0.0004$ (B), $p < 0.0001$ (C - E), $p = 0.0002$ (F), n = 8). The plots demonstrated the p-values that were obtained from multiple comparisons.
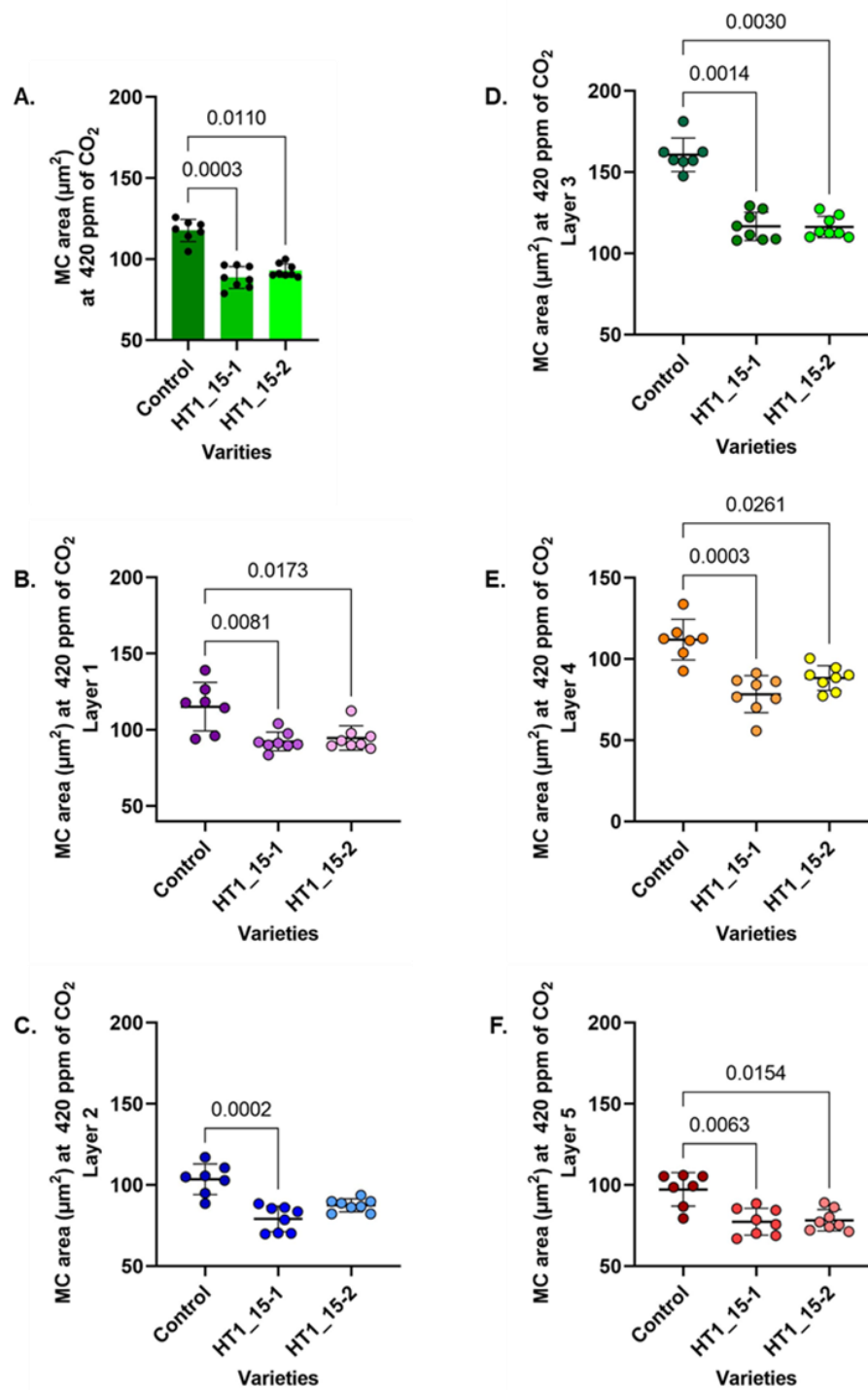
Figure 4.8. At 420 ppm, the mesophyll cell size of *HT1* mutant and non-mutant plants were measured by the calculation of Fiji image J script, which displayed a significant smaller in *HT1_15-1* and *HT1_15-1* (A, p = 0.0005, Kruskal Wallis). Similar to mesophyll cell area of mutant lines from layer 1-5 was also presented a significant decrease in *HT1* mutants (B-F, Kruskal Wallis, p = 0.0070 (layer 1), p = 0.0005 (layer 2), p = 0.0009 (layer 3), p = 0.0006 (layer 4), p = 0.0056 (layer 5)). The data of MC area was showed in scatter plots with mean and SD values. P-values from multiple comparisons and plant replication numbers were shown in the plots.
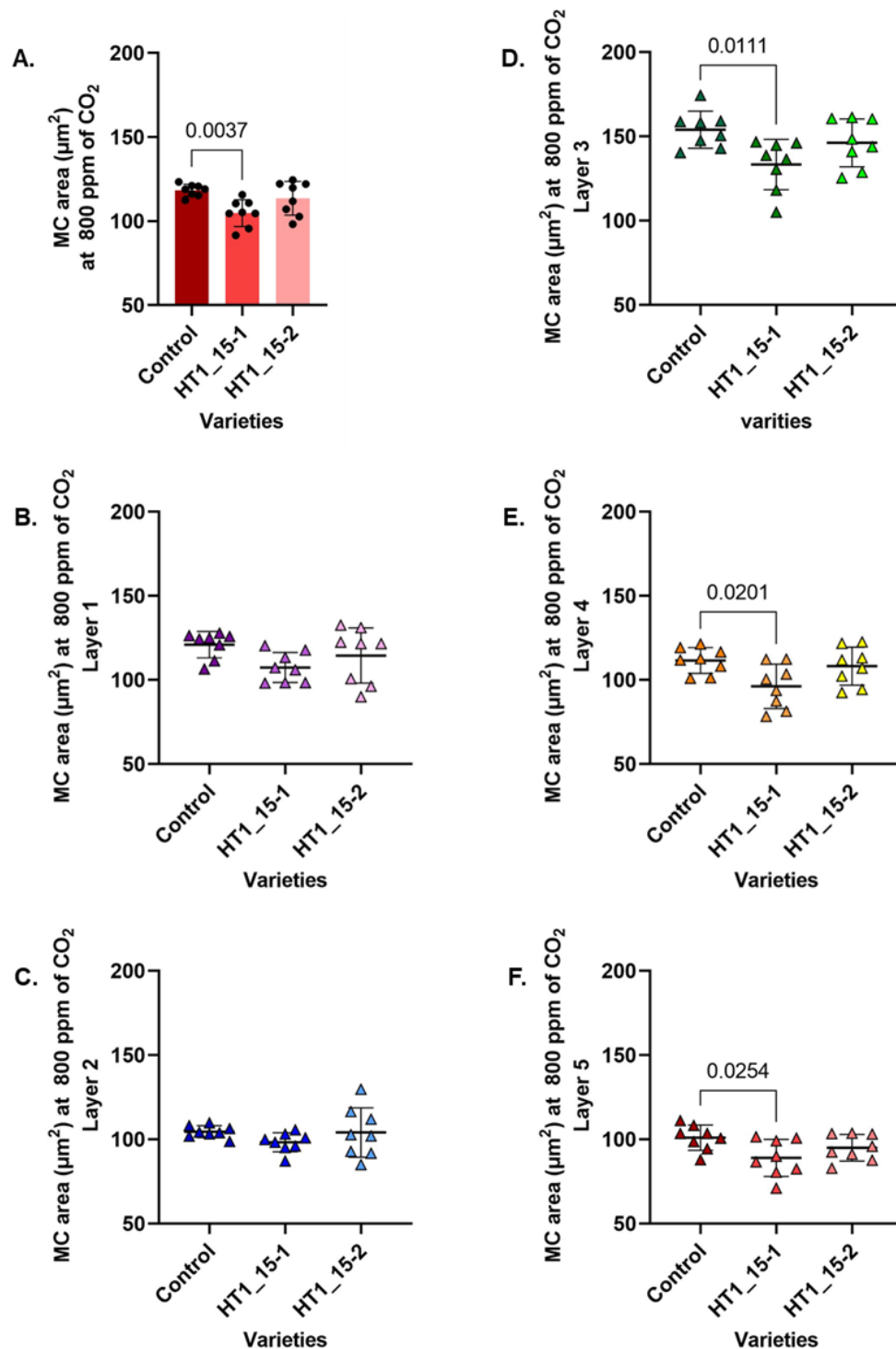
Figure 4.9. At 800 ppm, the mesophyll cell size of *HT1* mutant and non-mutant plants were measured as showed in scatter plots with mean and SD values (A-F). MC size of *HT1_15-1* displayed a significant smaller than a control (A, p = 0.0066, one-way ANOVA). Similar to mesophyll cell area of mutant lines from layer 4 (E, one-way ANOVA, p = 0.0267) and 5 (F, one-way ANOVA, p = 0.0445) was also presented a significant decrease in *HT1* mutants The data of MC area was showed in scatter plots with mean and SD values. All multiple pairwise comparisons, Dunnette, p values are shown in the plots with n = 8 plants.
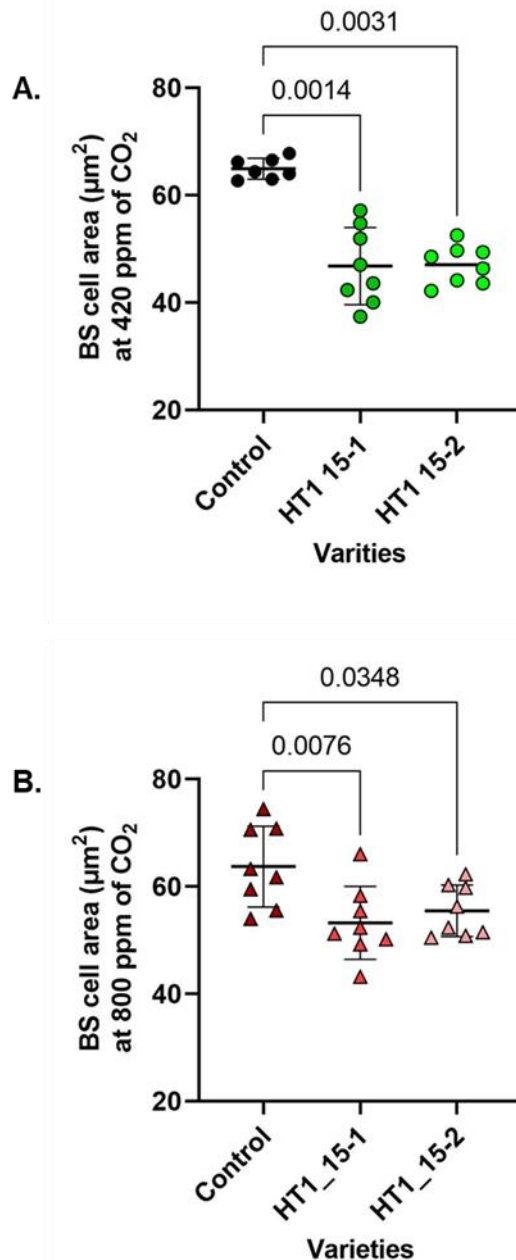
Figure 4.10. A significant decrease of BS cell size was visible in *HT1 15-1* and *15-2* mutants in both 420 ppm (A, Kruskal Wallis, p = 0.0009) and 800 ppm (B, one-way ANOVA, p = 0.0099, n = 8) of CO_2 levels. The horizontal and error bars shown mean and SD values of BS cell area. Both the p-values obtained from multiple comparisons and the corresponding numbers of plant replications were included in the plots.
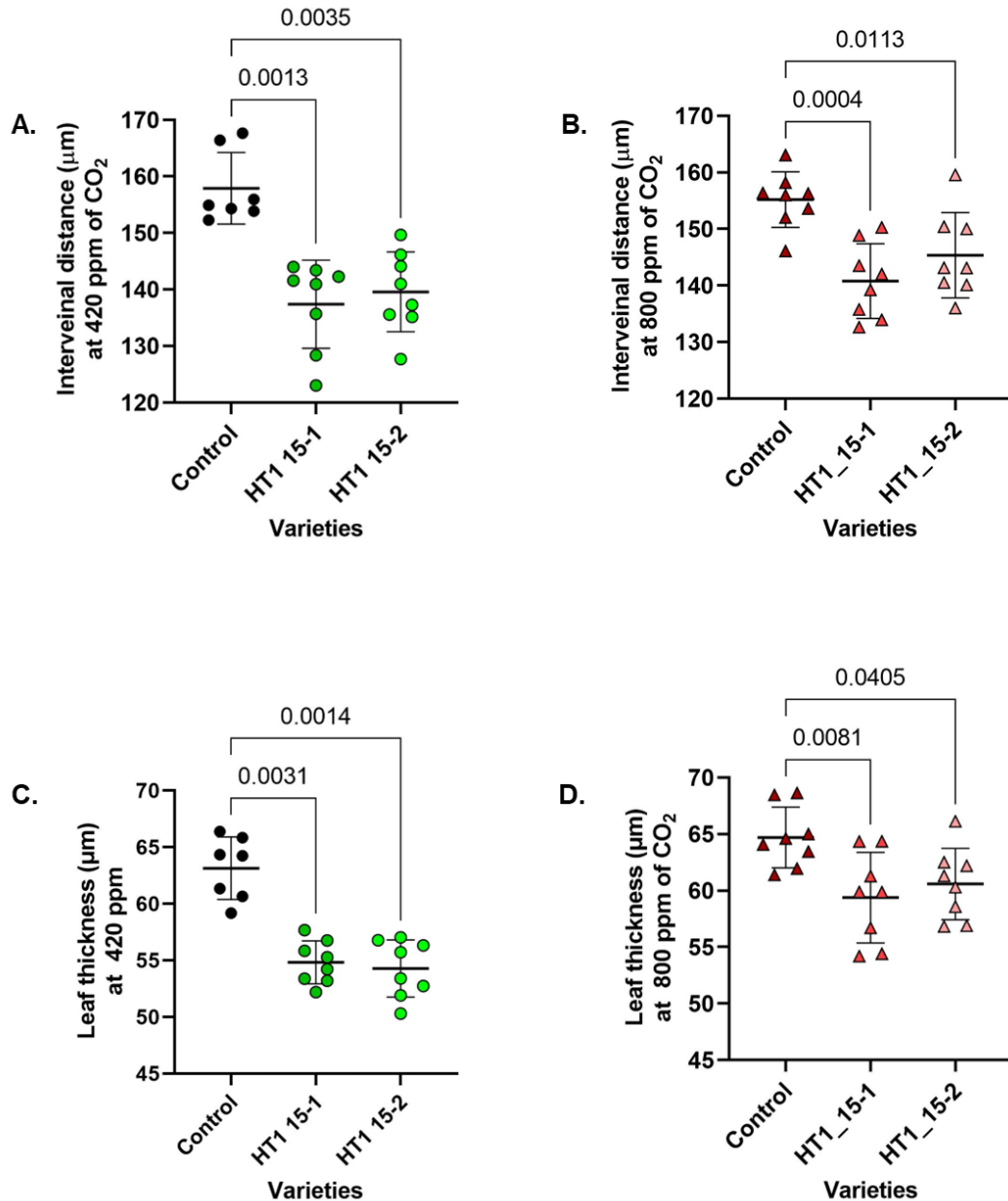
Figure 4.11. Other parameters such as IV distance between two minor cells (A and B) and leaf thickness (B and C) of *HT1* mutants and control rice plant were measured under 420 and 800 ppm of CO_2 as showed in the scatter individual plots with mean and SD. The IV distance and leaf thickness of *HT1* mutants of CO_2 decreased when compared to a control line at both ambient (Kruskal Wallis, p = 0.0009 (A and C)) and high CO_2 conditions (one-way ANOVA, p = 0.0007 (B), p = 0.0110 (D), n = 8). The plots included both the p-values derived from multiple comparisons and the numbers of plant replications.

4.7. Discussion

Results from previous chapters led to the novel observation that there was a link between stomatal density and the lobing of mesophyll cells in rice leaves. One interpretation of these data is that the altered flux of gas through stomata in these mutant lines somehow influences mesophyll cell shape, consistent with previously published data (Lundgren et al., 2019). To test this idea further, I exploited access in the group to unpublished lines of transgenic rice in which the *HT1* gene had been mutated.

HT1 encodes a kinase involved in the closure response of stomata to high CO2 in Arabidopsis (Horak et al., 2016; Hashimoto-Sugimoto et al., 2016). The gene edited lines used in this chapter were in rice and at the time of my experiments were still being characterised. The expectation was that these rice mutants would be disrupted in the stomatal response to CO_2, thus providing a tool to alter stomatal conductance without changing parameters of stomatal size or density. These lines would therefore enable me to test whether the changes in mesophyll lobing in the mutants in stomatal density (*osEPF1_oe* with low stomatal density, *osEPFL9_oe* with high stomatal density) were related to altered gas flux rather than number of stomata.

My analysis of stomata in the two *HT1* mutant lines indicated that, as expected, there was no major difference in size between mutant and control (Fig. 4.1), irrespective of whether the plants were grown under ambient or elevated CO_2. Similarly, a direct comparison of stomatal density also did not reveal a significant difference between mutant and control under either treatment (Fig.4.2A and B). However, when g_{smax}, a theoretical estimate of maximal potential stomatal conductance (Dow et a., 2014), was calculated, it was clear that both *HT1* mutants had an increased value, both under ambient and elevated CO_2 levels (Fig. 4.3A and B).

Measurement of g_s was not performed in the experiments reported here due to limited access to the relevant equipment during the pandemic, but measurements made by a colleague (Shanshan Wang, Sheffield) indicated that under standard growth conditions both *HT1* mutants displayed lower g_s than control plants. However, g_s in the mutant plants is relatively unresponsive to altered environmental conditions (ie., the

stomata do not open or close as well as controls). It is thus at present unclear whether in the experiments reported here the analysed leaves (over their lifetime) have a lower cumulative g_s. It is probable that they have g_s that varied less over the diurnal period, although this parameter was not measured. This lack of clarity on the change of g_s imposed in the *HT1* leaves should be borne in mind in the interpretation of the mesophyll cell size and shape data. Performing the experiment with regular measurement of actual g_s via, e.g, porometer measurements, would provide the data needed to clarify the actual g_s experienced by the leaf tissue.

My results also showed that both *HT1* mutant lines were characterised by a significant increase in mesophyll cell lobing, with a concomitant decrease in cell circularity. This change in cell shape was observed in essentially all cell layers of the leaf and occurred when plants were grown under both ambient and elevated CO_2. If the g_{smax} data were taken as an indicator of stomatal conductance, the data supported the hypothesis that the degree of mesophyll cell lobing was responsive to g_s, with increased gas flux being linked to increase cell lobing. The results were consistent with the data shown in the previous chapter that altered stomatal density resulted in altered mesophyll lobing. The data were also consistent with reports in the literature that gas flux through stomata influence the cellular architecture of the mesophyll in both other grasses (such as wheat) and eudicots such as Arabidopsis (Lundgren 320 et al., 2019; Wilson et al., 2021). However, there was the caveat that (as outlined above) the actual outcome of the edited *HT1* genes in rice is still under analysis. On the one hand, there was clearly an increase in g_{smax} fitting with the hypothesis of a positive link of g_s and cell lobing but a lack of clarity on whether there actually was an increase of g_s in the mutant (indeed, g_s might be less than in control). Until these points were clarified, conclusions needed to be limited.

In addition to increased lobing, mesophyll cells showed a tendency for decreased size in both *HT1* mutants. This phenotype was strongest in plants grown under ambient CO_2, but the tendency for smaller mesophyll cell size was also seen in plants grown under elevated CO_2. Bundle sheath cells were also smaller in the *HT1* mutants, with interveinal distance decreasing as well. Therefore there was a general shift in the *HT1* mutant plants towards smaller cells, resulting in thinner, smaller leaves. This changes in many aspects of leaf structure suggested that the *HT1* mutations were leading to

an overall decrease in growth, suggesting that altered gas flux was leading to decreased carbon assimilation. It was therefore possible that the altered mesophyll cell lobing observed in the *HT1* mutants was part of a larger, more complex growth response of the leaves rather than simply reflecting altered g_s. The central role of gas exchange in plant growth makes interpretation of the phenotypes involved complicated, making it difficult to resolve immediate and indirect outcomes of altered gene activity. Experiments in which altered *HT1* gene expression was targeted to specific cell types or was inducible within an otherwise wild-type background might help resolve this issue.

Chapter 5

Final discussion

5.1. The relationship between rice leaf structure and photosynthesis

Peng Wang and colleagues from the University of Oxford conducted a study to investigate the genes responsible for leaf structure in C4 plants. They created more than 50 different transgenic rice lines by introducing specific transcription factors associated with the development of Kranz anatomy in maize. Both the *Kitaake* and IR64 rice backgrounds were used for these transgenic lines, referred to as "*JL*" lines. The researchers analysed these lines to determine if any C4-like traits were observed. While no significant changes in leaf structure consistent with a more C4-like anatomy were reported, there were noticeable alterations in mesophyll cell size in certain lines. The genetic resources generated through this study offered a unique opportunity to explore the potential impact of altered mesophyll cell size and shape on photosynthesis.

CO_2 must go through several barriers and pathways before reaching the chloroplast, where photosynthesis occurs. These barriers include the leaf epidermis, stomatal pores, and leaf mesophyll cells (Flexas et al., 2012). The delivery of CO_2 to chloroplasts might be delayed, which could limit the efficiency of photosynthesis. This delay could be caused by the transport of CO_2 across multiple boundaries and pathways. The limitations on CO_2 movement are referred to as resistances and can be measured as mesophyll conductance (g_m). Studies have shown that improving gm could increase photosynthetic efficiency around 10% (South et al.,2019; Smith et al., 2023). G_m is determined by the arrangement of airspaces and other structural factors including cell wall thickness and composition of the plasma and chloroplast membranes (Evans, 2020).

In particular, the surface area of mesophyll cells exposed to airspaces is critical for mesophyll conductance, not simply the proportion of airspace in the total leaf volume (porosity) (Terashima et al., 2011). Therefore, an altered mesophyll size and shape could affect to cell surface area. For example, a decrease of MC size and lobing in JL

lines lead to decrease cell surface area for CO_2 flux. In the *osEPF1_oe* leaves there was a decrease in stomatal density and a decrease in g_{smax}. This line was expected to show a decrease in CO_2 flux into a leaf (Cain et. al.,2019). In contrast, an increased cell lobing of the *osEPFL9_oe* line (with high stomatal density) increased cell surface area for CO_2 flux.

According to the results from Chapter 2, if the mesophyll cells can sense CO_2 level or flux, then a decrease in lobing should decrease the exposed surface area for CO_2 uptake, thus the cell shape would accommodate to provide the surface area needed for CO_2 uptake and photosynthesis. How mesophyll cells might sense CO_2 is an open question. It could be via some direct CO_2 sensor or could be indirect via the influence of altered CO_2 level on, e.g., aspects of photosynthetic metabolism. The nature of the mechanism is a topic for future investigation.

5.2. The relationship between stomatal function and mesophyll structure in rice leaves

The internal structure of the mesophyll in leaves is influenced by the activity of stomata on the epidermal surfaces, as suggested by recent data in Arabidopsis, wheat, and now rice (Lundgren et al., 2019; Wilson et al., 2021). In the case of rice, manipulating the stomatal density of leaves resulted in corresponding changes in cell lobing and g_s and g_{smax}. Leaves with increased stomatal density (*osEPFL9_oe*) displayed increased cell lobing (Fig. 2.34), while leaves with decreased stomatal density (*JL* and *osEPF1_oe* lines) showed reduced cell lobing (Fig. 2.18 and Fig. 2.32). Leaves with reduced cell lobing also exhibited a decrease in cell size (Fig. 2.31A), whereas leaves with increased cell lobing did not show a concurrent increase in cell size (Fig. 2.31AB). This suggested that the change in lobing in the latter case was a true shape change, while in the former case, the effect on lobing might be indirect due to the change in cell size. Alterations in mesophyll cell size and lobing impact the surface area/volume ratio, which could affect gas flux through the mesophyll. The increased cell lobing in leaves with higher stomatal density provides a relatively larger area for gas diffusion, leading to an expected increase in gas flux. Conversely, the decreased cell lobing in leaves with lower stomatal density results in a relatively smaller area for gas diffusion, leading to an expected decrease in gas flux.

Research on mesophyll cell lobing in rice provides evidence to support the idea that it plays a role in optimizing gas flux within the plant (Sage and Sage, 2009). While progress has been made, there is still much to discover about the mechanism and regulation of mesophyll cell lobing (Lundgren and Fleming, 2020). Recent studies have provided insights into how epidermal cells within the leaf form intricate lobes, resulting in the characteristic jigsaw-like pattern. One significant finding is the involvement of the cytoskeleton, a network of protein filaments within the cell, causing localized deformations of the cell wall that contribute to the formation of lobes. (Sampathkumar et al.,2014). Additionally, it is believed that the buckling of the perimeter of these cells is part of the initial process of lobe formation (Bidhendi and Geitmann, 2019). The similarities in the molecular processes governing lobing between rice and other grass species suggests that there might be shared mechanisms for controlling the number and extent of lobing in mesophyll cells.

However, there are still many unanswered questions. The relationship between mesophyll cell lobing and gas flux, including how these processes interrelate, remained poorly understood. Additionally, the mechanisms by which the surface area-to-cell volume ratio, an important parameter for gas exchange, is sensed and linked to other physiological processes such as photosynthesis requires further investigation. This study, combined with previous research on wheat (Wilson et al., 2021), emphasizes the significance of stomatal-derived gas exchange in influencing the size and shape of mesophyll cells.

However, it is important to acknowledge that the cellular responses and underlying mechanisms might vary between the two grass species. In wheat, an increase in stomatal conductance results in larger mesophyll cell volume and more lobes. On the other hand, rice shows minimal changes in overall cell size but exhibits noticeable modifications in cell lobing and circularity. These variations indicate that different grass species utilize unique cellular strategies to maintain the surface area-to-volume ratio, which may have been a crucial trait subject to evolutionary selection pressure due to its influence on leaf photosynthetic capacity and water loss. If gas flux via stomata influences mesophyll cell lobing, this raises the question whether it modulates a process of lobing that is already occurring, or whether it might actually be involved in the initiation of the process.

As a first step to answer this question I examined when during rice leaf development mesophyll cells first become measurably lobed (Chapter 3). By comparison with the timing of other events in leaf development (e.g., stomatal differentiation) I hoped to position lobing in the process of mesophyll differentiation.

5.3. Mesophyll cell lobing initiates at an early stage of leaf development

To investigate to specific stage that MC lobing was generated, IR64 was used as a model of study. Rice leaf 6 of IR64 was harvested from day 9 to 12 to perform hand sections. Three different regions of the leaf; tip (part 1), middle (part 2), and base (part 3) were examined to observe the differentiated mesophyll lobing.

The results indicated that the longer (thus older) leaves contained a higher degree of MC lobing. Cell lobing was detect in young leaves with less than 20 mm length in most of 3 regions analysed (Fig. 3.7). Unfortunately it was difficult to measure the tip region of the smallest leaves (2 mm length) but the other parts (2 and 3) could be analysed. More advanced imaging techniques would need to be used to analyse these regions, but the time available in my covid-impacted project did not allow me to complete this analysis.

In the monocot leaf (grass leaf), at the early stage of leaf development (P0-P2), a group of cells differentiates to generate an initial leaf primordia at the flank of SAM, with the vascular bundle also appearing in this stage (Itoh et al., 2005). At the P1/P3 stage (less than 1 cm), a leaf has a specific region where cells divide at the base of the leaf. After cell division, the younger dividing cells remain at the base of the leaf whereas the older cells are displaced toward the tip (Schnyder et al., 1990; Beemster et al., 1996 and Cox, 2020) . Thus the cells located at the basal part of the leaf primordium (part 3) were smaller than the tip and middle regions., The MCs lobing in part 1 was clearly seen under the light microscope, suggesting that cell lobing was present at the very early stage of the leaf development (less than 20 mm).

In addition, stomata and 4 to 6 mesophyll cells have been reported to be presented at the P3 and P4 respectively. So, It is possible that the mesophyll lobing might be

generated between P3 and P4 stages and the mesophyll cell lobing might be modulated by stomata at these stages.

5.4. CO_2 signalling influences mesophyll cell lobing

The *HT1* gene encodes a protein kinase involved in the regulation of stomatal movement. The previous evidence showed that plants lacking the *HT1* gene lose stomatal response to CO_2 in Arabidopsis thaliana (Horak et al. 2016; Hashimoto-Sugimoto et al 2016). The function of *HT1* in rice is unknown, but colleagues in my research group had generated rice plants containing an *HT1* edited gene (*HT1 15-1* and *15-2*). The expectation (backed up by preliminary observations) was that the rice *HT1* mutants showed disruption of stomata function in response to CO_2. The *HT1* mutants could therefore be used as a tool to test the hypothesis that mesophyll lobing responds to stomatal conductance (as already tested in this thesis using the *osEPF1_oe* and *osEPFL9_oe* lines). These lines show altered g_s via altered stomatal density, whereas the H1 lines were expected to only show a change in stomatal function.

The *HT1 15-1* and *HT1 15-2* mutants showed no major difference of stomata features (size, pore length and guard cell area) in both ambient and high CO_2 levels, as shown in Fig. 4.1(A-F). Similarly, stomata density did not change significantly compared to control plants (Fig. 4.3), but the anatomical g_{smax} of the *HT1* mutants was higher than controls, both in ambient (420 ppm) and elevated (800 ppm) CO_2 .

The anatomical g_{smax} is a theoretical value to estimate the gas exchange when all stomata are fully open (Bertolino et al.,2019), which is calculated from Fig. 2.2. Although there was no difference of stomatal density between *HT1* mutants and wild type, the stomatal number of both *HT1 15-1* and *HT1 15-2* was slightly higher than a control, resulting in an increase of g_{smax}. With respect to mesophyll cell shape, both *HT1* mutant lines showed an increased degree of lobing, under both ambient and high CO_2 levels (Fig.4.2). The results of this chapter indicated that the change of g_{smax} was potentially linked to mesophyll cell shape, which supports the hypothesis that a high g_{smax} is functionally linked to a higher degree of cell lobing. The conclusion was made more complicated by the fact that the *HT1* gene in rice appears to be modulating

aspects of stomatal density and stomatal function. Since plant growth was greatly decreased in the HT1 mutants compared to control, leading to smaller leaves at the same developmental stage, the conclusions made are preliminary.

Gas exchange analysis by Infra-red gas analysis (IRGA) should be used to determine g_s value to validate the results of this research. The parameters related to gas exchange, such as carbon assimilation, stomatal conductance to water vapor, intrinsic water use efficiency, and stomatal kinetics, are influenced by anatomical traits like stomatal density (SD) and stomatal length (SL). (Nunes et al., 2022). Both SD and SL have a negative correlation and can vary depending on environmental factors such as temperature, relative humidity, carbon dioxide concentration, and light intensity (Bertolino et al., 2019; Zhang et al., 2021). As environmental conditions change throughout the seasons, the plasticity of stomatal anatomical traits can also vary within the same species. This variation can affect the performance of gas exchange and, consequently, the outcomes of long-term studies focusing on gas exchange phenotyping (Nunes et al., 2022).

5.5. Future work

Due to the COVID-19 pandemic, I had to work from home for almost 4-5 months because the university was temporary closed and it took time to allow the students to access to the laboratory and some university facilities, with limited numbers of student allowed to use the equipment. In addition, The duration time of my scholarship was limited (3.5 years) and for most of the pandemic I was in my third year, which means I had only a few months left to do experimental work. Thus it was very difficult for me to complete all the experiments planned during my PhD. Nevertheless, some interesting results have been obtained which could be the basis for future work.

For example, in future work, the measurement of gas exchange such as actual g_s, CO_2 A rate and other parameters involved in photosynthesis in the various *osEPF_oe* and *HT1* mutant lines should be performed. Together with the result of g_{smax}, leaf and stomatal characteristics in Chapter 2 and 4, this would help me to understand the relationship between the altered leaf structure, photosynthesis and gas exchange more clearly. To observe the initiation of mesophyll lobing (earlier or later than the

controls?), would be interesting, i.e., to see when mesophyll lobing starts in different mutant rice varieties such as *JL* lines, *osEPF1_oe*, *osEPFL9_oe* and *HT1* lines. This experiment might take a lot of time because rice plants have to grow to investigate the stage of leaf development (P0-P5/P6) estimated from the length of leaf 6 as shown in Cox (2020).

In addition,.further characterisation of the *HT1* mutants to identify which aspects of CO_2 response and stomatal function have been altered would help in the interpretation of the data from these experiments. Finally, it would be interesting to investigate how the altered mesophyll shape resulting from altered stomatal function influences photosynthesis. Analysis of metabolite changes during rice leaf development (Cox et al, 2020) might provide an interesting way to examine this problem, with the data available suggesting significant changes in metabolism at the P3/P4 transition, which is when mesophyll lobing and stomatal differentiation are occurring. These experiments would start to address the larger problem of how gas exchange, photosynthetic metabolism and cell size and shape are linked to provide a physiologically functional leaf.

References

Aboonajmi, M. and Faridi, H. (eds) (2016) *Proceedings of the 3rd Iranian International NDT Conference.* Olympic Hotel, Tehran, Iran, 21-22 February. Available at: https://www.ndt.net/article/IranNDT2016/papers/A13105.pdf.

Ahuja, S.C. and Ahuja, U. (eds) (2006) *2nd International Rice Congress*,. New Delhi, India:, 9-12 October. Available at: https://www.researchgate.net/profile/Subhash-Ahuja/publication/321334487_Rice_in_Religion_and_Tradition/links/5bf4de87a6fdcc 3a8de62413/Rice-in-Religion-and-Tradition.pdf.

Ainsworth, E.A. and Long, S.P.(2005) 'What have we learned from 15 years of free-air CO_2 enrichment (FACE)? A meta-analytic review of the responses of photosynthesis, canopy properties and plant production to rising CO_2' , *New Phytologist*. 165, pp. 351-371.

Ainsworth, E. A. and Rogers, A. (2007) 'The response of photosynthesis and stomatal conductance to rising [CO_2]: mechanisms and environmental interactions', *Plant Cell Environment*, 30, pp. 258–270.

Alberts, B. et at. (2002). *Molecular biology of the cell.* 4th edn. New York: Molecular Biology of the cell.

Apostolakos, P., Galatis, B. and Panteris, E. (1991) 'Microtubules in cell morphogenesis and intercellular space formation in Zea mays leaf mesophyll and Pilea cadierei epithem.' Journal of Plant Physiology, 137: pp. 591–601.

Asai, K. et al. (2002) 'A rice heterochronic mutant, mori1, is defective in the juvenile-adult phase change.', *Development,* 129(1), pp. 265–273.

Assman, S. M., Simoncini, L. and Schroeder, J. L. (1985) 'Blue light activates electrogenic ion pumping in guard cell protoplasts of *Vicia faba'*, *Nature,* 318, pp. 285–287.

Baillie, A.L. and Fleming, A.J. (2019) 'The developmental relationship between stomata and mesophyll airspace', *New Phytologist*, 225(3): pp. 1120-1125.

Bassham, J.A. and Lambers, H. (2021) 'photosynthesis'. Available at: https://www.britannica.com/science/photosynthesis (Accessed 23 February 2022).

Bertolino, L. T. , Caine, R. S. , and Gray, J. E. (2019) 'Impact of stomatal density and morphology on water-use efficiency in a changing world.' Frontiers in Plant Science, 10(225). doi: 10.3389/fpls.2019.00225.

Beemster, G.T.S., Masle, J., Williamson, R.E. and Farquhar, G.D. (1996) 'Effects of soil resistance to root penetration on leaf expansion in wheat (Triticum aestivum L): kinematic analysis of leaf elongation', Journal of Experimental Botany, 47, pp. 1663–1678.

Bidhendi, A.J. and Geitmann, A. (2019) 'Geometrical Details Matter for Mechanical Modeling of Cell Morphogenesis.', Developmental Cell, 50(1), pp. 117-125.e2.

Bielczynski, L.W. et. al. (2017) 'Leaf and plant age affects photosynthetic performance and photoprotective capacity', *Plant Physiologist*, 175(4), pp. 1634-1648.

Biology Libretexts (2022) Available at: https://bio.libretexts.org/Bookshelves/Botany (Accessed: 30 December 2022).

Brutnell, T.P. and Langdale, J.L. (1998) 'Signals in Leaf Development', *Advances in Botanical Research,* 28: pp. 161-195.

Caffarri, S., Tibiletti, T., Jennings, R.C. and Santabarbara, S. (2014) 'A Comparison between plant photosystem I and photosystem II architecture and functioning', *Current Protein & Peptide Science*, 15(4), pp, 296–331.

Caine, R.S. et al. (2019) 'Rice with reduced stomatal density conserves water and has improved drought tolerance under future climate conditions', New Phytologist, 221, pp. 371–384.

Chang, T. and Bardenas, E.A. (1965) 'Morphology of the rice plant', in Chang, T. and Bardenas, E.A. (eds) *The morphology and varietal characteristics of the rice plant.* The Philippines: International Rice Research Institute, pp.5-11.

Chatterjee, J. et al. (2016) 'The evolutionary basis of naturally diverse rice leaves anatomy', *PLOS ONE*, 11(10): e0164532. doi:10.1371/journal.pone.0164532.

Chaudhari, P.R. et al. (2018) 'Rice nutritional and medicinal properties: A review article.', *Journal of Pharmacognosy and Phytochemistry*, 7(2), pp. 150-156.

Cocaliadis, M.F.(2014) ' Increasing tomato fruit quality by enhancing fruit chloroplast function. A double-edged sword?', *Journal of Experimental Botany*, 65(16), pp. 4589–4598.

Cominelli, E. (2010) 'Transcription factors controlling stomatal movements and drought tolerance', *Landes Bioscience,* 1(1), pp. 41-54.

Conklin, P.A., Strable, J., Li , S. and Scanlon, M.J. (2019) 'On the mechanisms of development in monocot and eudicot leaves', *New Phytologist*, 221(2), pp. 706-724.

Cosgrove D.J. and Anderson C.T. (2020) 'lant cell growth: do pectins drive lobe formation in *Arabidopsis* pavement cells?', *Current Biology*, 30(11), pp R660-R662

Cox, N. (2020) A structural and molecular atlas for early leaf development in rice (Oryza sativa). PhD thesis. University of Sheffield.

Crang, R., Lyons-Sobaski, S. and Wise, R. (2018) 'Stems', *Plant Anatomy*. Switzerland: Springer, Cham, pp 355–394.

Dengler, N.G. and Nelson, T. (1999) 'Leaf structure and development in C4 plants',. in: Sage, R.F and Monson, RK. (eds.) *C4 Plant Biology.* San Diego: Academic Press, pp. 133-164.

Dima, E., Manetas, Y. And Psaras, G.K. (2006) 'Chlorophyll distribution pattern in inner stem tissues: evidence from epifluorescence microscopy and reflectance measurements in 20 woody species', *Trees*, 20, pp. 515–521.

Dow G.J, Bergmann DC, Berry JA. (2014) ,An integrated model of stomatal development and leaf physiology', *New Phytologist,* 201, pp.1218–1226.

Drisch, R.C. and Stahl, Y. (2015) 'Function and regulation of transcription factors involved in root apical meristem and stem cell maintenance', *Frontier Plant Science*, 6(505), pp. 1-8.

Dunand, R. and Saichuk, J. (2009) 'Rice growth and development', in Saichuk, J. (ed.). *Louisiana Rice Production Handbook*. 3rd edn. Los Angeles: Louisiana State University Agricultural Centre, pp. 41-53.

Earles, J.M. (2019) 'Embracing 3D complexity in leaf carbon–water exchange'. *Trends in Plant Science*, 24, pp. 15–24.

Edwards, A. and Bowling, D. J. (1985) 'Evidence for a CO_2 Inhibited Proton Extrusion Pump in the Stomatal Cells of Tradescantia virginiana Get access Arrow', *Journal of Experimental Botany*, 36 (1), pp. 91–98.

Evans, J.R. (2020) 'Gm is determined by the arrangement of airspaces and other structural factors including cell wall thickness', *New Phytologist*, 229, pp.1864–1876.

Filippis, I. et al. (2013) 'Using a periclinal chimera to unravel layer-specific gene expression in plants', *The Plant Journal,* 75(6): pp. 1039–1049.

Flexas, J. et al. (2012) 'Mesophyll diffusion conductance to CO_2: An unappreciated central player in photosynthesis', *Plant Science*, 193–194, pp. 70–84.

Feldman, A. B. et al. (2017) 'Increasing leaf vein density via mutagenesis in rice results in an enhanced rate of photosynthesis, smaller cell sizes and can reduce interveinal mesophyll Cell number', *Frontiers in Plant Science,* 8 (11), pp. 1–10.

Finch-Savage, W.E. and Leubner-Metzger, G. (2006) 'Seed dormancy and the control of germination', *New Phytologist* , 171(3), pp. 501-523.

Futakuchi, K., Sié, A. and Saito, K. (2012) 'Yield potential and physiological and morphological characteristics related to yield performance in *Oryza glaberrima* Steud.', *Plant Production Science,* 15(3), pp.151—163.

Galatis, B. (1988) 'Microtubules and epithem-cell morphogenesis in hydathodes of Pilea cadierei.', *Planta*, 176: pp. 287–297.

Gan, P. et al. (2019) 'Chloroplasts— Beyond Energy Capture and Carbon Fixation: Tuning of Photosynthesis in Response to Chilling Stress', *International Journal of Molecular Sciences*, 20(20), 5046, doi: 10.3390/ijms20205046.

Ghadirnezhad, R. and Fallah, A. (2014) 'Temperature effect on yield and yield components of different Rice cultivars in flowering stage, *International Journal of Agronomy,* 2014, 846707, doi.org/10.1155/2014/846707.

Gilbert, S.F. 'Germination' in Gilbert, S.F. (ed.) *Developmental Biology*. 6th edn. Sunderland (MA): Sinauer Associates.

Giuliani, R. et al. (2013) 'Coordination of leaf photosynthesis, transpiration, and structural traits in rice and wild relatives (Genus Oryza).', *Plant Physiol*. 162, 1632–1651.

Ha, C.M., Jun, J.H. and Fletcher, J.C. (2010) 'Shoot apical meristem form and function', *Current Topics in Developmental Biology*, 91: pp. 103-140.

Hochholdinger, F. and Feix, G. (1998) 'Early post-embryonic root formation is specifically affectedin the maize mutantlrt1', *The Plant Journal*, 16(2), pp. 247–255.

Hashimoto, J. et al. (2006) '*Arabidopsis* HT1 kinase controls stomatal movements in response to CO_2.', *Nature Cell Biology,* 8, pp. 391–397.

Helariutta, Y. et al. (2000) 'The SHORT-ROOT Gene Controls Radial Patterning of the Arabidopsis Root through Radial Signaling', *Cell,* 101(5), pp. 555-567.

Hibberd, J.M., Sheehy, J.E. and Langdale, J.A. (2008) 'Using C4 photosynthesis to increase the yield of rice-rationale and feasibility', *Current Opinion in Plant Biology*, 11(2), pp. 228-231.

Ho, Q.T. et al. (2016) 'Three-dimensional microscale modelling of CO_2 transport and light propagation in tomato leaves enlightens photosynthesis', *Plant, Cell & Environment*, 39: pp. 50–61.

Horak, H.(2016) 'A dominant mutation in the ht1 Kinase uncovers roles of MAP Kinases and GHR1 in CO_2-induced stomatal closure', The Plant Cell, 28, pp. 2493–2509.

Hu, M. et al. (2018) 'The domestication of plant architecture in African rice.', *Plant Journal*, 94(4), pp. 661-669.

Hunt, L. and Grey, J.E. (2009) 'The Signaling Peptide *EPF2* Controls Asymmetric Cell Divisions during Stomatal Development', *Current Biology,* 19(10), pp. 864-869.

John, R.E. and Caemmerer, S.V. (1996) 'Carbon dioxide diffusion inside leaves', *Plant Physiology*, 110(2), pp. 339-346.

Itoh, J.L. et. al. (2005) ' Rice plant development: from zygote to spikelet ', *Plant Cell Physiology*, 46(1), pp. 23–47.

Kajala, K. et al. (2011) 'Strategies for engineering a two-celled C4 photosynthetic pathway into rice', *Journal of Experimental Botany*, 62 (9), pp. 3001–3010.

Kaldenhoff, R. (2012) 'Mechanisms underlying CO_2 diffusion in leaves', Current Opinion in Plant Biology, 15, pp. 276-81.

Kamiya, N. et al. (2003) ' The SCARECROW gene's role in asymmetric cell divisions in rice plants', *Plant Journal,* 36, pp. 45-54.

Kwan, S.J. et al.(2006) 'O. sativa is a diploid species with 24 chromosomes and the genetic code AA.', *Genes & Genetic Systems,* 81, pp. 93-101.

Kwiatkowska, D. (2008) 'Flowering and apical meristem growth dynamics' , *Journal of Experimental Botany*, 59(2), pp. 187–201.

Lee, D.G. et al. (2009) 'Chilling stress-induced proteomic changes in rice roots', *Journal of Plant Physiology*, 166(1), pp. 1-11.

Li, G. et al. (2021) 'Genetic control of panicle architecture in rice', *The Crop Journal,* 9(3), pp. 590-597.

Lin, C.H. et al. (2020). 'A Partial C4 photosynthetic biochemical pathway in rice', *Front Plant Science*, 11, 564463, pp. 1-12.

Linares, O. (2002) 'African rice (Oryza glaberrima): history and future potential ', *PNAS.* 99 (25), pp. 16360-16365.

Liu, J and Iersel, W.V. (2021) ' Photosynthetic physiology of blue, green, and red Light: light intensity effects and underlying mechanisms ', *Frontiers in Plant Science*, 12, pp. 1-14.

Lodish, H. et al. (2000) 'Molecular Cell Biology', 4th edn. New York: WH Freeman.

Long, S. P., Marshall-Colon, A. and Zhu, X.G. (2015) ' Meeting the global food demand of the future by engineering crop photosynthesis and yield potential ', *Cell*, 161, pp. 56-66.

Lopez, F.B. and Barclay, G.F. (2017) 'Plant Anatomy and Physiology', in Badal, S. and Delgoda, R. (ed.). *Pharmacognosy.* United States: Academic Press, pp. 45-60.

Lui, S. et al. (2019) 'Overexpression of a CPYC-Type Glutaredoxin, OsGrxC2.2, causes abnormal embryos and an increased grain weight in rice', *Frontiers in Plant Science*, 10, pp.1-12.

Lundgren, M.R. et al. (2019) 'Mesophyll porosity is modulated by the presence of functional stomata', Nature Communications, 10, 2825.

Maai, E., Miyake, H. and Taniguchi, M. (2011) 'Differential positioning of chloroplasts in C4 mesophyll and bundle sheath cells', *Plant Signal and Behavior,* 6(8), pp. 1111–1113.

Martin, E.M. and Harris, W.M. (1976) 'Adventitious root development from the coleoptilar node in Zea mays L. Am', *American Journal of Botany*, 63, pp. 890-897.

Maylani, ED., Yuniati, R. and Wardhana, W. (2020) *The Effect of leaf surface character on the ability of water hyacinth, Eichhornia crassipes (Mart.) Solms. to transpire water, 4th International Symposium on Current Progress in Functional Materials 2019*. Bali, Indonesia, 6-7 November. Bristol: IOP Publishing Ltd. Volume 902.

McDowell, N. et al. (2008) 'Mechanisms of plant survival and mortality during drought: why do some plants survive while others succumb to drought?', *New Phytologist*, 178(4), pp. 719-739.

McElrone, A. et. al. (2013) 'Water Uptake and Transport in Vascular Plants', *Nature Education Knowledge,* 4(5), 6.

Meeker, E.W. et al. (2021) 'Modification of a gas exchange system to measure active and passive chlorophyll fluorescence simultaneously under field conditions', *AoB Plant*, 13(1), pp. plaa066. doi: https://doi.org/10.1093/aobpla/plaa066.

Menke, F.L.H. and Scheres, B. (2009) 'Plant Asymmetric Cell Division, Vive la Différence!', *Cell*, 137(7) : pp. 1189-1192.

Mitchell, P. and Sheehy, J.E. (2006) 'Supercharging rice photosynthesis to increase yield', *New Phytologist*, 171(4), pp. 688-171.

Misra, B.B. et al. (2015) 'The guard cell metabolome: functions in stomatal movement and global food security', *Frontiers in Plant Science*, 6(334).

Miwa, H. et al. (2009) 'Plant meristems: CLAVATA3/ESR-related signaling in the shoot apical meristem and the root apical meristem', *Journal of Plant Research*, 122: pp. 31–39.

Miya, M. et al. (2021) 'Genome-wide analysis of spatiotemporal expression patterns during rice leaf.', *BMC Genomics*, 22(169). doi: 10.1186/s12864-021-07494-5. PMID: 33750294; PMCID: PMC7941727.

Moldenhauer, K. E. W. C. and Slaton, N. (2001) 'Rice growth and development'. *Rice production handbook*, 192, pp. 7-14.

Moshe, L.S. and Brady, S.M. (2022) 'SHORT-ROOT and SCARECROW homologs regulate patterning of diverse cell types within and between species', *New Phytologist*, 237(5), pp. 1542-1549.

Nadal, M. and Flexas, J. (2018) 'Mesophyll conductance to CO_2 diffusion: effects of drought and opportunities for improvement', in Tejero I.F.G., Hugo, V. and Zuazo, D. *Water Scarcity and Sustainable Agriculture in Semiarid Environment*. US: Academic Press, pp. 403-438.

Nishad, A.et. al. (2018) ' Effect of temperature on growth and yield of rice (Oryza sativa L.) cultivars', *International Journal of Chemical Studies 2018*, 6(5), pp. 1381-1383.

Nishimura, A. et al. (2002) 'OsPNH1 regulates leaf development and maintenance of the shoot apical meristem in rice', *The Plant Journal.* 30(2), pp. 189-201.

Nunes, T.D.G. et al. (2022) 'Quantitative effects of environmental variation on stomatal anatomy and gas exchange in a grass model', Quantitative Plant Biology, 3(e6), pp. 1-13.

Oguchi, R., Hikosaka, K. and Hirose, T. (2003) 'Does the photosynthetic light-acclimation need change in leaf anatomy?', *Plant, Cell & Environment,* 26(4), pp. 505-512.

Panteris, E, Apostolakos, P. and Galatis, B. (1993) 'Microtubule organization, mesophyll cell morphogenesis and intercellular space formation in Adiantum capillus-veneris leaflets.' *Protoplasma*, 172: pp. 97–110.

Panteris, E., Apostolakos, P. and Galatis, B. (1993c) 'Microtubule organization and cell morphogenesis in two semi-lobed cell types of Adiantum capillus-veneris L. leaflets.' , *New Phytologist,* 125: pp. 509–520.

Pyke, K. (2012) 'Mesophyll.', *eLS.* doi:10.1002/9780470015902.a0002081.pub2.

Rahman, M.A. et. al. (2013) 'Correlation analysis of flag leaf with yield in several rice cultivars', *Journal of Life and Earth Science*, 8, pp. 49-54.

Rancourt, G.T. et al. (2021) 'Maximum CO_2 diffusion inside leaves is limited by the scaling of cell size and genome size', *Royal Society*, 288 (1945), pp.1-9.

Raschke, K., Shabahang, M. and Wolf, R (2003). 'The slow and the quick anion conductance in whole guard cells: their voltage-dependent alternation, and the modulation of their activities by abscisic acid and CO_2.', *Planta journal*, 217, pp. 639–650.

Rebouillat, J. et al. (2009) 'Molecular Genetics of Rice Root Development', *Rice*, 2, pp. 15-34.

Roddy, A.B. et al. (2020) 'The scaling of genome size and cell size limits maximum rates of photosynthesis with implications for ecological strategies', *Journal Plant Sciences*, 181, pp. 75-87.

Roderick, M.L. et al. (1999) 'Morphology with the function of leaves', *Functional Ecology,* 13 (5), pp. 683-695.

Rochaix, J.D. (2011) 'Regulation of photosynthetic electron transport, *Biochimica et Biophysica Acta (BBA) – Bioenergetics'*, 1807(3), pp. 375-383.

Rohr, K.S., and Nelson, B.J. (2021) 'O_2 and other high-energy molecules in photosynthesis: why plants need two photosystems', *Life (Basel)'*, 11(11), 1191.

Rossini, L. et al. (2001) 'The maize g olden2 gene defines a novel class of transcriptional regulators in Plants', *Plant Cell*, 13(5), pp. 1231–1244.

Sage, R. F., Khoshravesh, R. and Sage, T.L. (2014) 'From Proto-Kranz to C4 Kranz: building the bridge to C4 Photosynthesis', *Journal of Experimental Botany*, 65(13), pp. 3341–3356.

Sage, T.L. and Sage, R.F. (2009) 'The functional anatomy of rice leaves: Implications for refixation of photorespiratory CO_2 and efforts to engineer C4 photosynthesis into rice.', Plant and Cell Physiology, 50(4), pp. 756–772.

Sage, R.F. and Zhu, X.G. (2011) 'Exploiting the engine of C4 photosynthesis', *Journal of Experimental Botany,* 62(9), pp. 2989–3000.

Sampathkumar, A. et al. (2014) 'Subcellular and supracellular mechanical stress prescribes cytoskeleton behaviour in Arabidopsis cotyledon pavement cells', eLife, eLife Sciences Publications, Ltd 3. https://doi.org/10.7554/eLife.01967.

Saathoff, A.J. and Welles, J. (2021) 'Gas exchange measurements in the unsteady state', *Plant, Cell & Environment*, 44(11), pp. 3471-3700.

Schnyder, H., Seo, S., Rademacher, I.F. and Kuhbauch, W.(1990) 'Spatial distribution of growth rates and of epidermal cell lengths in the elongating zone during leaf development in Lolium perenne L', Planta, 181, pp 423–431.

Schroeder, J.I., Hedrich, R. and Fernandez, J.M. (1984) 'Potassium-selective single channels in guard cell protoplasts of *Vicia faba*', *Nature,* 312, pp. 361–362.

Sharkey T.D., Bernacchi C.J., Farquhar G.D., Singsaas E.L. (2007) ' Fitting photosynthetic carbon dioxide response curves for C3 leaves. Plant', *Cell &Environment*, 30, pp.1035–1040.

Shah, S.H. and Fahim, M. (2020) 'Physiological modification of plants through small RNA. in plant small RNA' in Guleria, P. and Kumar, V. (eds) *Plant Small RNA.* USA: Academic Press, pp. 493–519.

Sheehy, J.E., Mitchell, P.L. and Hardy, B. (eds) (2000). Proceedings of the workshop on the quest to reduce hunger: redesigning rice photosynthesis. Los Banos, Philippines, 30 November - 3 December 1999. Amsterdam, The Netherlands: International Rice Research Institute

Shieh, Y.J. et al. (1982) 'Photosynthetic Metabolism of Aspartate in Mesophyll and Bundle Sheath Cells Isolated from Digitaria sanguinalis (L.) Scop., a NADP+-Malic Enzyme C4 Plant', *Plant Physiology.* 69(4), pp. 776–780.

Shimakawa, G. and Miyake, C. (2018) 'Oxidation of P700 Ensures Robust Photosynthesis', *Frontiers in Plant Science*, 9, 1617.

Shimazaki, K.I., Doi, M., Assmann, S.M. and Kinoshita, T. (2007) ' Light regulation of stomatal movement', *Annual Review of Plant Biology*, 58, pp. 219–247.

Slewinski, T.L. et. al. (2012) 'Scarecrow plays a role in establishing Kranz anatomy in maize leaves', *Plant Cell Physiology*. 53, pp. 2030–2037.

Smith, E.N. et al. (2023) 'Improving photosynthetic efficiency toward food security: Strategies, advances, and perspectives', *Molecular Plant*, 16(10), pp. 1547-1563.

Sohn, S.I. et al. (2021) 'Seed dormancy and pre-harvest sprouting in rice—an updated overview', *International Journal of Molecular Sciences,* 22(21), 11804*.* doi: https://doi.org/10.3390/ijms222111804.

South, P.F et al. (2019) 'Synthetic glycolate metabolism pathways stimulate crop growth andproductivity in the field', *Science,* 363(6422), pp. 1-9.

Steffens, B. and Rasmussen, A. (2016) 'The Physiology of Adventitious Roots', *Plant Physiologyl*, 170(2), pp. 603–617.

Sudhakar, K. and Mamat, R. (2019) 'Artificial leaves: towards bio-inspired solar Energy converters', *Reference Module in Earth Systems and Environmental Sciences.* Amsterdam: Elsevier.

Sugimoto, H.M., Negi, J., Monda, K., Higaki, T., Isogai, Y., Nakano, T., Hasezawa, S. and Iba, K. (2016) ' Dominant and recessive mutations in the Raf-like kinase HT1 gene completely disrupt stomatal responses to CO_2 in Arabidopsis', Journal of Experimental Botany, 67(11), pp. 3251–3261.

Takahashi et al. (2022) 'Stomatal CO_2/bicarbonate sensor consists of two interacting protein kinases, Raf-like HT1 and non-kinase-activity requiring MPK12/MPK4', *SCIENCE ADVANCES,* 8(49).

Taiz, L. et. al. (2015) *Plant physiology and development*, 6th edn. Massachusetts: Sinauer Associates, pp 761.

Tardieu, F. and Granier, C. (2000) 'Quantitative analysis of cell division in leaves: methods, developmental patterns and effects of environmental conditions.', *Plant Mol Biol*, 43(5-6): pp. 555-567.

Taub, D.R. (2010). 'Effects of rising atmos0pheric concentrations of carbon dioxide on plants', *Nature Education Knowledge*, 3(10):21.

Terashima, I. et al. (2011) 'Leaf functional anatomy in relation to photosynthesis', Plant Physiology, 155, pp. 108-116.

Tholen, D., Zhu and X.G. (2011) 'The mechanistic basis of internal conductance: a theoretical analysis of mesophyll cell photosynthesis and CO_2 diffusion', *Plant Physiology*. 156, pp. 90-105.

Tholen, D., Booma, C. and Zhu, X.G. (2012) 'Opinion: prospects for improving photosynthesis by altering leaf anatomy', *Plant Science,* 197, pp. 92-101.

Tõldsepp, K. et al. (2018) 'Mitogen-activated protein kinases MPK_4 and MPK12 are key components mediating CO_2-induced stomatal movements.', *Plant Journal,* 96: pp. 1018–1035.

Vatén, A. and Bergmann, D.C. (2012) 'Mechanisms of stomatal development: an evolutionary view', *EvoDevo,* 3(11), pp.1-9.

Vo, T.Q. et al. (2022) 'Temporal Analysis for Multi-hazard Risk Assessment of Rice Cultivation in Coastal Areas: A Case Study of Soc Trang, Vietnam', *2nd International Conference on Civil and Environmental Engineering (ICCEE 2022)*. Malaysia, 6-7 January. France: EDP Sciences, pp. 1-12.

Veit, B. (2003) 'Cell division and differentiation', in Thomas, B. (ed) *Encyclopedia of Applied Plant Sciences.* Netherlands: Elsevier, pp. 532-539.

Vernon, L.P. and Seely, G.R. (eds) (1965) *The Chlorophylls*. 1st edn. New York: Academic Press.

Wang, C. et al. (2019).'The smaller the leaf is, the faster the leaf water loses in a temperate', *Frontiers in Plant Science*, 10(58), pp. 1-12.

Wang, P. et. al. (2017) 'Re-creation of a Key Step in the Evolutionary Switch from C-3 to C-4 Leaf Anatomy', *Current Biology,* 27(21), 3278-3287.

Wang, P. et. al. (2013) 'Genome-wide transcript analysis of early maize leaf development reveals gene cohorts associated with the differentiation of C4 Kranz anatomy', *The Plant Journal*, 75(4), pp. 656-670.

Wang, P., Vlad, D. and Langdale, J.A. (2016) 'Finding the genes to build C4 rice', *Plant Biology,* 31, pp. 44-50.

Watson, J.E.M. et. al. (2014) 'The performance and potential of protected areas' *Nature*, 515, pp. 67–73.

Weber, A.P. and von Caemmerer S. (2010) 'Plastid transport and metabolism of C3 and C4 plants —comparative analysis and possible biotechnological exploitation', *Current Opinion in Plant Biology*, 13, 256–264.

Wei, X. et al. (2012) 'Origin of Oryza sativa in China Inferred by Nucleotide Polymorphisms of Organelle DNA', *Plos One*, 7(11), pp.1-9.

Wernicke, W and Jung, G. (1992) 'Role of cytoskeleton in cell shaping of developing mesophyll of wheat (Triticum aestivum L.).', *European Journal of Cell Biology*, 57, pp. 88–94.

Wernicke, W. Gunther, P. and Jung, G. (1993) 'Microtubules and cell shaping in the mesophyll of Nigella damascena L.', *Protoplasma*, 173, pp. 8–12.

Wilson, M.J. et al. (2021) 'Ploidy influences wheat mesophyll cell geometry, packing and leaf function', Plant Direct, 5(4), e00314, doi.org/10.1002/pld3.314.

Wopereis, M.C.S. et. al. (2008) 'Participatory Learning and Action Research (PLAR) for Integrated Rice Management (IRM) in Inland Valleys of Sub-Saharan Africa: Technical Manual' WARDA Training Series. Cotonou, Benin: Africa Rice Center, pp. 128.

Wright, I. et al. (2004).'The worldwide leaf economics spectrum', *Nature*, 428, pp. 821–827.

Xiao, Y., Tholen, D., Zhu, XG. (2016) 'The influence of leaf anatomy on the internal light environment and photosynthetic electron transport rate: exploration with a new leaf ray tracing model', *Journal of Experimental Botany,* 67: pp. 6021–6035.

Xue, S. et al. (2011) 'Central functions of bicarbonate in S-type anion channel activation and OST1 protein kinase in CO_2 signal transduction in guard cell.', *The EMBO Journal,* 30, pp. 1645–1658.

Yahia, E.M. et al. (2019) 'Photosynthesis' in Yahia, E.M (Ed) *Postharvest Physiology and Biochemistry of Fruits and Vegetables*. Sawston, United Kingdom: Woodhead Publishing, pp. 47-72.

Yamaguchi, T. et al. (2004) 'The YABBY gene DROOPING LEAF regulates carpel specification and midrib development in *Oryza sativa', Plant Cell,* 16(2), pp. 500-509.

Yang, W. et al. (2013) 'Control of Rice Embryo Development, Shoot Apical Meristem Maintenance, and Grain Yield by a Novel Cytochrome P450', *Molecular Plant,* 6(6), pp. 1945-1960.

Yi, X. et al. (2022) 'Defining the scope for altering rice leaf anatomy to improve photosynthesis: a modelling approach', *New Phytologist,* 237(2), pp. 441-453.

Ying, L. et. al.,(2018) 'Factors Influencing Leaf Chlorophyll Content in Natural Forests at the Biome Scale', *Frontiers in Ecology and Evolution,* 6(64), pp. 1-10.

Zhang, L. et al. (2021) 'An intrinsic geometric constraint on morphological stomatal traits.' *Frontiers in Plant Science*, 12(628). doi:10.3389/fpls.2021.658702.

Zhu, X. G., Long, S.P. and Ort, D.R. (2010) 'Improving photosynthetic efficiency for greater yield', *Annual Review of Plant Biology*, 61, pp. 235-261.

Zoulias, N. et al. (2018) 'Molecular control of stomatal development ', *Biochemical Journal,* 475(2), pp. 441-454.